Essays on Charitable Fundraising, Optimal Health Policy and Economic Inequality

By Haokun Pang

Department of Economics
University of Birmingham

Thesis submitted in accordance with the requirements of the University of Birmingham for the degree of Doctor of Philosophy in Economics

Supervisors: Prof. Aditya Goenka
Prof. Kimberley Scharf

Declaration

I declare that the thesis has been composed by myself and that the work has not be submitted for any other degree or professional qualification. I confirm that the work submitted is my own, except where work which has formed part of jointly-authored papers has been included. My contribution and those of the other authors to this work have been explicitly indicated within the authorship declaration forms attached at the end of the thesis. I confirm that appropriate credit has been given within this thesis where reference has been made to the work of others.

Introduction

Haokun Pang *

December 7, 2024

Abstract

The thesis consists of three chapters, each of which is an independent paper. Chapter 1 is an empirical paper focusing on charitable fundraising during pandemics. Using Chinese data, I discuss whether charitable organizations react in response to a natural disaster or to co-existing government initiatives. Chapters 2 and 3 both delve into epidemiological macroeconomics. In Chapter 2, we apply deep-learning dynamic programming to solve epidemiological economic models under a representative agent framework. We address the question of whether the choice of epidemiological model matters in policymaking. We compare the optimal health policy functions and the dynamics between models with different assumptions on epidemiological dynamics. Chapter 3 is the main contributing paper in this thesis. We drop the representative agent assumption in the canonical epidemiological economic model and focus on the inequality problem during pandemics. A SIRS model is integrated into the Heterogeneous Agent Continuous Time Framework (HACT) to study the optimal precautionary and recuperative behaviours for individuals and the dynamics of wealth-health distribution during pandemics. This extends the canonical heterogeneous agent framework to include partial insurance against productivity shocks. The analysis of the joint evolution of infection rates and economic variables allows us to see how health, income, and wealth inequalities change during pandemics.

Keywords: Covid-19 pandemic, infectious diseases, economic epidemiology, charities in China, charitable fundraising, government collaborative advocacy, optimal policies, SIRS, SIR, NPI, growth model, value function, policy function, neural networks, heterogeneous-agent model, wealth and health Heterogeneity, HACT

*Department of Economics, University of Birmingham, Email: h.pang.1@bham.ac.uk

INFECTIOUS diseases pose a significant threat to humanity, impacting both individual well-being and broader societal outcomes. The morbidity and mortality resulting from infections have profound negative effects on the economy, affecting not only individual quality of life, behaviour, and productivity but also aggregate growth and equality. Despite lessons learned from historical pandemics such as Influenza and SARS, the global community still faced considerable challenges in mitigating health and economic losses during the SARS-CoV-2 (hereafter referred to as Covid-19) pandemic, a major global health event that began in late 2019. This pandemic has underscored the need to critically evaluate our learned experiences and address the complex trade-offs between health and economic consequences during such crises. Developed during the Covid-19 pandemic, this thesis primarily aims to explore and elucidate the economic effects of pandemics and the formulation of optimal health policies using both empirical and modeling approaches.

The study of the economic impacts of infectious diseases has begun early prior to the Covid-19 pandemic.[1] The recent global outbreak of Covid-19 has spurred a surge in economic literature related to the pandemic, enhancing both the empirical study of infectious diseases[2] and research through epidemiological economic models.[3] This thesis contributes significantly to this body of literature and includes three independent papers (chapters). The first paper empirically investigates how charitable organizations adjust their fundraising behaviour in response to pandemics and government interventions. The second and third papers revisit economic epidemiology models from two distinct perspectives. Chapter Two applies Deep Learning Neural Networks to solve dynamic programming problems in a representative-agent neoclassical growth model that includes infectious diseases. Chapter Three integrates infectious disease dynamics into a heterogeneous-agent general equilibrium model following the approach of Aiyagari (1994); Achdou et al. (2022). These two chapters contribute to recent advancements in the application of machine learning in macroeconomics[4] and in the heterogeneous-agent macroeconomic models.[5] The remainder of this introduction will provide overviews of each paper in this thesis.

This thesis begins with an empirical paper. **Chapter 1** *What does Charitable Fundraising Respond to: Disaster or the Government?* examines the charitable sector in China during the Covid-19 pandemic. This study is motivated by the observation that in economies with emerging and less developed philanthropic sectors,

[1]See, e.g., contributions by Gersovitz and Hammer (2004); Goenka and Liu (2012); Achdou et al. (2013); Goenka, Liu and Nguyen (2014) that integrate well-established compartmental epidemiological models into economic models to rigorously evaluate disease dynamics.

[2]See, e.g., Chetty et al. (2023).

[3]See, e.g., Acemoglu et al. (2021); Goenka, Liu and Nguyen (2022); Calvia et al. (2023).

[4]See, e.g., Fernandez-Villaverde et al. (2020); Fernández-Villaverde, Hurtado and Nuno (2023).

[5]See, e.g., Achdou et al. (2013); Kaplan, Moll and Violante (2018); Achdou et al. (2022).

such as China, charities often do not operate independently but are subject to various political interventions by the government. However, during disasters like the Covid-19 pandemic, when the net benefit of charitable fundraising could be diminished, it may conflict with the interests of charitable organizations if the government signals them to raise funds to support disaster relief projects. It is unclear how charitable organizations behave during pandemics and whether they comply with government directives. From the unique perspective of charitable fundraising, this paper sheds light on the charity-government relationship in China by evaluating how charitable organizations target their fundraising efforts when faced with both pandemic and government interventions. This paper also makes a contribution by studying the unresearched policy tool of top-down collaborative advocacy, which is considered a political signal to the charitable sector.

The analysis begins by developing a theoretical model, which generates several predictions about how a charitable organization decides to fundraise during pandemics and government interventions. In this model, fundraising behaviour is influenced by donor preferences, income, and the cost of fundraising. To empirically test these predictions, I collect a unique dataset on public fundraising activities and merged it with data on the Covid-19 pandemic and government advocacy. A difference-in-differences framework is used to evaluate changes in fundraising effort subject to pandemic and advocacy shocks. I find that charitable organizations decrease their fundraising efforts during local pandemic outbreaks and increase their efforts when governments advocate for fundraising. The timing of these effects varies: advocacy boosts fundraising efforts only temporarily, while the impact of the pandemic is more persistent. The short-term effect of advocacy may be due to organizations strategically shifting future efforts forward to align with government interests.

Chapter 2 *Does Epidemiology Matter? Policy Functions in Economic Epidemiological Models of Covid* explores the optimal health policies a social planner might employ under different epidemiological models. Early in the Covid-19 pandemic, economic epidemiological modeling typically relied on the SIR model, which assumes permanent immunity post-infection. However, with growing evidence of reinfection, the SIRS model, allowing for temporary immunity, became more pertinent. This chapter investigates how changes in epidemiological assumptions influence a social planner's optimal health policies and the implications of misrepresenting the epidemiology model.

In our approach, we integrate a standard continuous-time neoclassical growth model with both the SIR and SIRS models to compare differences in optimal policies for reducing consumption and increasing health expenditures to control infection.

To offer deeper policy insights, we transition from analyzing steady-state outcomes to exploring transitional dynamics by determining the optimal policy as a function of state variables. We solve the model using the Pontryagin minimization principle through the Hamiltonian approach and dynamic programming via the Hamiltonian-Bellman-Jacobian Equation (HJB). To address the non-linearity and the "curse of dimensionality" inherent in our model, we employ a Deep Learning Neural Network to globally approximate the HJB equation. The neural network's approximation aligns well with the theoretical solution derived from the Pontryagin principle in steady state.

By visualizing the policy functions and phase diagrams, we observe that although the optimal health policies recommended by different epidemiological models appear qualitatively similar—indicating increased health expenditure with rising susceptible and infection rates—the magnitude and dynamics of these policies vary significantly. Our findings suggest that social planners would benefit from adopting the SIRS model-based health policy when the pathogen's immune evasion capabilities remain uncertain. This approach minimizes the potential losses from misrepresenting the epidemiological model, as the consequences of inaccurately specifying a SIRS model are more severe than those of an SIR model.

Chapter 3 *Health and Economic Inequality during Pandemics* is the main contributing part of this thesis. This paper is motivated by the empirical observation that the economic inequality of both income and wealth was worsened during the Covid-19 pandemic; the wealthier people are better protected from infection. However, the mechanism driving these changes are not fully understood. We focus on the role of optimal health and economic decisions in determining the joint evolution of inequality in health and economic outcomes. The purpose of the paper is two-fold: (1) to model the inequality dynamics during the pandemic; (2) to model the behaviour responses for individuals with different wealth/income level. In application of the model, we further discuss the effects of government income support scheme and government fiscal constraint.

The model in our paper integrates a heterogeneous-agent macroeconomic model *à la* Aiyagari (1994) and Achdou et al. (2022) with an epidemiological model with *SIRS* dynamics. Specifically, we assume there are infinite number of non-atomic individuals following a continuous wealth distribution. Each individual is labelled with their health status of either *Susceptible*, *Infected*, or *Recovered*. The health status is endogenous by the epidemiological model with *SIRS* dynamics. When individuals meet in the economy, susceptible individuals can be infected with some probability if they are in contact with the infected. Infected individuals recover with temporary immunity at some rate. The epidemiological side of the model interacts with the economic side by the following assumptions: The first assumption is that labour productivity of the infected individuals is reduced so that it acts like a productivity shock. We also allow a direct welfare loss of being infected. This assumption makes infection induces not only income loss but also health loss (well-being loss) for individuals. Secondly, we assume that the Poisson intensities for health status transition can be affected by two types of consumption-reduction health expenditures. Infection probability could be lowered by more precautionary preventive expenditure, while recovery time could be shortened by more treatment (recuperative) expenditure. Individual choose their optimal precautionary and ex-post behaviour against pandemic, while pandemic, in turn, is affected by the aggregation of individuals' choice. This extends the canonical heterogeneous agent framework by allowing optimal choices that partially insure against the productivity, which in this case is health, shock.

The key contribution of this paper is extending the canonical epidemiological economic model with representative agent assumption[6] to a Heterogeneous Agent Continuous Time Framework (HACT). The framework is essentially formulated as a Mean Field Game (MFG). The Nash equilibrium of the MFG finds the joint distribution of individual state variables, such that infinitesimal agents in the model takes the mean outcomes, aggregated by the distribution, as given when optimizing their own behaviours, while the distribution is exactly generated by individuals' optimal controls. This paper also contributes that we endogenize the idiosyncratic shocks by individuals' choice variables. The risk is hence insured that individuals with higher wealth levels have lower probability of productivity loss. This differs from Aiyagari (1994) where the idiosyncratic shocks are exogenous.

We use continuous-time dynamic programming to solve the model. The solution of the model is classified by three parts: the Hamiltonian-Jacobian-Bellman Equation (HJB) to characterize individuals' the individuals' optimization problem; the Kolmogorov Forward Equation (KF) to characterize the dynamics of the state variables; and the market clearing conditions (MC) to characterize the equilibrium. We numerically solve the stationary equilibrium and the transitional dynamics of the model by the Finite Differencing Method (FDM). We calibrate the model to the later evidence of Covid pandemic. Our model matches the basic reproduction number R_0 of the Omicron variant as well as the infection dynamics of the Omicron B.A.1 outbreak.

The outcomes of the model primarily match the empirical findings that the wealthier individuals spend more in both prevention and treatment to the disease, and are consequently associated with lower infection rate. The health expenditures insure against the infection risk in our model. We find the insurance mechanism

[6] See e.g. Goenka and Liu (2012); Goenka, Liu and Nguyen (2014, 2022) etc..

actually worsens the equality as wealthier people spend more on health to be better insured from infection which induces income loss. In the simulation of transitional dynamics, we find the income and wealth Gini index both increase but with different pace. The income Gini is procyclical to infection rate such that it peaks and drops back within 3 months. The wealth Gini index, however, adjusts much more slowly with its increase being persistent for several years. Furthermore, the government income support scheme could mitigate the negative effect on equality. However, we also identify the trade-off that subsidizing the infected group could demote individual health expenditure and lead to higher infection rate and lower output in the aggregate level.

References

Acemoglu, Daron, Victor Chernozhukov, Iván Werning, and Michael D Whinston. 2021. "Optimal targeted lockdowns in a multigroup SIR model." American Economic Review: Insights, 3(4): 487–502.

Achdou, Yves, Guy Barles, Hitoshi Ishii, Grigory L Litvinov, and Yves Achdou. 2013. "Finite difference methods for mean field games." Hamilton-Jacobi Equations: Approximations, Numerical Analysis and Applications: Cetraro, Italy 2011, Editors: Paola Loreti, Nicoletta Anna Tchou, 1–47.

Achdou, Yves, Jiequn Han, Jean-Michel Lasry, Pierre-Louis Lions, and Benjamin Moll. 2022. "Income and wealth distribution in macroeconomics: A continuous-time approach." The review of economic studies, 89(1): 45–86.

Aiyagari, S Rao. 1994. "Uninsured idiosyncratic risk and aggregate saving." The Quarterly Journal of Economics, 109(3): 659–684.

Calvia, Alessandro, Fausto Gozzi, Francesco Lippi, and Giovanni Zanco. 2023. "A simple planning problem for COVID-19 lockdown: a dynamic programming approach." Economic Theory, 1–28.

Chetty, Raj, John N Friedman, Michael Stepner, and Opportunity Insights Team. 2023. "The Economic Impacts of Covid-19: Evidence from a New Public Database Built Using Private Sector Data." The Quarterly Journal of Economics, qjad048.

Fernandez-Villaverde, Jesus, Galo Nuno, George Sorg-Langhans, and Maximilian Vogler. 2020. "Solving high-dimensional dynamic programming problems using deep learning." Unpublished working paper.

Fernández-Villaverde, Jesús, Samuel Hurtado, and Galo Nuno. 2023. "Financial frictions and the wealth distribution." Econometrica, 91(3): 869–901.

Gersovitz, Mark, and Jeffrey S Hammer. 2004. "The economical control of infectious diseases." The Economic Journal, 114(492): 1–27.

Goenka, Aditya, and Lin Liu. 2012. "Infectious diseases and endogenous fluctuations." Economic Theory, 50: 125–149.

Goenka, Aditya, Lin Liu, and Manh-Hung Nguyen. 2014. "Infectious diseases and economic growth." Journal of Mathematical Economics, 50: 34–53.

Goenka, Aditya, Lin Liu, and Manh-Hung Nguyen. 2022. "Modelling optimal lockdowns with waning immunity." Economic theory, 1–38.

Kaplan, Greg, Benjamin Moll, and Giovanni L Violante. 2018. "Monetary policy according to HANK." American Economic Review, 108(3): 697–743.

Contents **Page No.**

What does Charitable Fundraising Respond to: Disaster or the Government? *

Haokun Pang †

December 7, 2024

Abstract

Natural disasters, such as the COVID-19 pandemic, may reshape the relationship between charities and the government. This paper investigates the organizational behaviour of charitable fundraiser, focusing on the binary decision-making process regarding whether to initiate fundraising activities in response to pandemic shocks and government interventions through collaborative advocacy. We begin by developing a partial equilibrium model to generate several theoretical predictions. Then, we provide empirical evidence using the data of *Charity in China*. We apply a Difference-in-Difference framework to capture the treatment effect from both pandemic and government shocks. Consistent with our theoretical predictions, we identify a significant negative impact from the local outbreaks of pandemics and a positive effect from government advocacies on the likelihood of initiating fundraising activities. Moreover, we observe that the duration of these effects varies: government advocacy impacts are temporary, whereas the effects of pandemic outbreaks are more enduring.

Keywords: Covid-19; Charitable Fundraising; Government Advocacy; Charitable Organization in China
JEL Classification: *D64; H00; H12; H32; H50; H41; L31*

*We thank 35th China Economic Association (CEA, UK) Annual Conference, University of Birmingham, University of Bristol, Zhongnan University of Economics and Law, especially Kimberley Scharf, Aditya Goenka, Liu Lin, Mingyao (Derrick) Xu, Yuanping Lu and Yaohong Zhao for their helpful comments. The usual disclaimer applies.

†Department of Economics, University of Birmingham, Email: h.pang.1@bham.ac.uk

I. INTRODUCTION

Charitable organizations play an active role in disaster relief. In developed economies, it is generally accepted that the charitable sector should function independently of the government to improve the efficiency of public good provision (Fitch-Fleischmann and Kresch, 2021). However, in less marketized economies, such as China, the charitable sector and the government are often politically intertwined that the behaviour for charitable organizations could be affected by government's political interventions. For example, charitable organizations in these countries may collect donations to support government-led disaster relief. To provide insights into the government-charity relationship, this paper explores whether charitable organizations respond directly to disasters or to the directives of government.

The focus of this paper is the fundraising behaviour of charitable organizations, which has been less explored in the economic literature.[1] Specifically, I analyze the behaviour of charitable organizations in holding fundraising activities (campaigns).[2] Why is this action significant? First, fundraising is important because potential donors often have a latent demand to donate that they may not give unless prompted to do so. Fundraising activities are often regarded as a "necessary evil" (Andreoni and Payne, 2011) due to their effectiveness in attracting donations, particularly for disaster relief. Second, from the government's perspective, directly encouraging individual donations could be ethically inappropriate, as it might be perceived as a tax-financed donation rather than voluntary giving. Encouraging charitable organizations to invest greater effort into fundraising, therefore, serves as an effective policy tool for mobilizing the philanthropic sector to boost social donations.

However, although government may have strong incentive to mobilize charitable sector during disaster[3], it might conflict with the interests of charitable organizations, as they may not view such activities as optimal due to the reducing returns of fundraising. This effect arises because, while public attention could naturally shift towards disaster-related causes and increase the pool of donors, the negative income effect, particularly during events like the COVID-19 pandemic, could on the contrast reduce people's willingness to donate and the amount of donation (Cinnamon, 2020). In this context, how the returns of fundraising change during disasters,

[1] Typical research on fundraising behaviour includes Andreoni and Payne (2003, 2011).

[2] Referred to hereafter as "fundraising activities." In China, according to the 2015 Charity Law, holding fundraising activities is one of the main tasks for charitable organizations. This will be discussed in detail later.

[3] Especially during Covid pandemics when the mismatch between increasing demand for public spending (Leslie and Wilson, 2020) with destroyed fiscal income (Clemens and Veuger, 2020) brought large financial burden to the government, private philanthropy could be a potential funding source for the large-scale disaster relief/economic stimulus projects.

how charitable organizations respond to these changes, as well as the effectiveness of government interventions remain unclear. This paper investigates whether charitable fundraising activities are conducted in response to disasters or primarily to align with government initiatives.

My paper examines a special form of policy tool — collaborative advocacy, where the government proposes a partnership with the charitable sector to enhance public good or service provision. I focus on a typical practice in China during the COVID-19 pandemic. At the onset of the pandemic, the Chinese central government, followed by some local governments, issued collaborative advocacies encouraging charitable organizations within their jurisdictions to initiate fundraising activities and collect social donations in support of government-led disaster relief projects. Unlike other intensively studied policy tools, such as taxation and grants (Andreoni and Payne, 2003, 2011; Andreoni, Payne and Smith, 2014), which directly affect government budgets, advocacy functions as a low-cost political signal, leaving receivers with the autonomy to decide whether to comply. Thus, such a policy could be particularly appealing to economies facing tighter fiscal constraints.[4]

Although this paper focuses on Chinese practices during the COVID-19 pandemic, it is worth noting that government signaling of partnerships with the charitable sector is not unique to this context. This strategy has appeared across different historical periods, such as the *Chinese Poverty Alleviation Project*, where Chinese government referred to the charitable sector as the "right hand" of this government-led project (Xinhua News Agency, 2016); as well as in different economies, such as the "*Third Way*" politics of British New Labour,[5] during which the UK government highlighted the charitable sector as instrumental in providing goods and services that were otherwise unavailable or unaffordable through either the private or public sectors (Haugh and Kitson, 2007). Therefore, understanding the economic mechanisms of such political signal, as well as potential distortions it may introduce, is crucial for the government sector.

After reviewing the institutional background, my analysis begins by developing a static partial equilibrium model. In this model, a mass of donors optimizes their instantaneous utility by choosing consumption and donation. There is also a representative charitable organization that collects funds from these donors. The donors differ in their preferences for charitable activities, which are unknown to the fundraiser. However, the distribution of these preferences is assumed to be com-

[4] During the COVID-19 pandemic, charity-government collaboration was notably implemented in some East Asian economies. Cai et al. (2021) reviews government-charity policies during the COVID-19 pandemic, including information sharing in South Korea, collaborative advocacies in China, and government contracts in Japan. Few countries, such as the UK (Gov.UK, 2021), directly subsidized the charitable sector.

[5] The period from the mid-1990s to 2010 under the leadership of Tony Blair and Gordon Brown.

mon knowledge. The charitable organization seeks to maximize the net funds it can collect by tailoring the "version" of its charitable activities to align with donors' preferences. In equilibrium, the charitable organization's optimal strategy for starting an activity depends on the distribution of donors' preferences, their income, and the cost of fundraising.

I incorporate pandemic shocks and government advocacy shocks into the model through several comparative experiments. For the pandemic shocks, we distinguish between the aggregate effect and the local effect. This distinction is important because the COVID-19 pandemic, as a widely recognized global health event, exposed all charitable organizations and donors to news about the pandemic. However, there was significant geographical variation in infection rates, with some cities experiencing severe local outbreaks while others were less affected.[6] The income effect was also more pronounced in the affected areas. Consequently, donors' behaviour may have varied based on their distance to disaster areas (Deryugina and Marx, 2021), leading to different responses from fundraisers.

The theoretical predictions first indicate that a national outbreak of the pandemic could increase the overall likelihood of holding fundraising activities. This is because the COVID-19 pandemic significantly captured public attention. In the model, when donors' preferences for different charitable activities become less diverse, the benefits of initiating a new fundraising activity increase. In contrast, local outbreaks of the pandemic reduce donors' income and, consequently, their donation amounts. The model predicts that charitable organizations would respond to these conditions by lowering their fundraising activity probability. Finally, government advocacy mainly affects fundraising through the channel of fundraising costs. If the government provides implicit political advantages or shares useful information with organizations that comply with the advocacy, the fundraising costs for these organizations would decrease. As a result, charitable organizations may respond positively to government advocacy.

Next, to empirically evaluate the differential response of charitable organizations to the COVID-19 pandemic and subsequent government advocacies, I collect data on fundraising activities for all qualified charitable organizations in China from a government-administered cloud platform, *Charity in China*. This data is transformed into a daily panel at the organization level and merged with COVID-19 infection data and government advocacy data. I applied a Logit regression to explain the binary decision of initiating fundraising activities. The regressions capture the marginal effect on the log odds ratio, which increases if a charitable organization be-

[6] At the onset of the Alpha/Beta variants and the early Delta variant of COVID-19 in China, the government imposed a strict Zero-COVID policy. Non-Pharmaceutical Interventions (NPIs) like lockdowns kept the pandemic at a city-level endemic stage, with infections detected in only certain cities at any given time.

comes more likely to start fundraising. This can be interpreted as the organization's fundraising effort. A Difference-in-Differences (Diff-in-Diff) framework is applied to identify the impact of local pandemic outbreaks and local government advocacies. The identification strategy exploits city-by-time variation. By treating cities that experienced a pandemic outbreak or published government advocacy as the treated groups, we conducted an event study to examine the dynamics of fundraising effort around the days these shocks occurred. The empirical results align with our theoretical predictions. Our estimation suggests that, on average, charitable organizations targeted a lower fundraising probability—about 1 unit of log-odds ratio lower—when subjected to pandemic shocks, and about 0.74 units higher when subjected to government advocacies.

The political connections between charitable organizations and the government may play a significant role in interpreting our empirical findings. However, our data does not allow us to precisely identify organizations with such connections. Therefore, we consider two proxies for political connections. The first proxy is an indicator for the Charity Federation and the Red Cross Society, whose branches are key components of Government-organized Charitable Organizations (GOCOs). The second proxy is the physical distance to local governments. We exploit the fact that organizations located closer to their administrative governments may be subject to more supervision. These organizations could also be GOCOs that were privatized or split off from government departments.[7] Our empirical evidence shows that organizations with stronger political connections are more responsive to government collaborative advocacies, and local pandemic outbreaks have a less negative impact on their fundraising behaviour.

The next question I explore is the persistence of the effects from pandemics and government advocacy. By extending the event windows of these shocks, we find that the positive impact of local government advocacy is temporary, with its cumulative effect diminishing to insignificance around 200 days later. This suggests that advocacy interventions may prompt strategic responses from charitable organizations.[8] These organizations might expedite their planned activities to align with government interests, leading to no long-term change in overall fundraising probability. In contrast, the impact of pandemic outbreaks proves to be persistent, with the negative effects enduring for more than a year.

Finally, the Difference-in-Differences (DID) framework captures the effect of local

[7]As we will introduce later, philanthropic activities were initially conducted directly by local government departments. Between 2008 and 2015, many charitable organizations were privatized from these government departments, and they may still be located near the government entities from which they separated.

[8]Strategic philanthropy is a global phenomenon. See, e.g., Bertrand et al. (2020) for firms' strategic donations; Bertrand et al. (2021) for decision-making in nonprofit organizations.

shocks, while the aggregate change in fundraising is absorbed by the time-fixed effect. We close the empirical part of our paper by examining the nationwide behaviour following the outbreak of the COVID-19 pandemic. The specification leverages time series variation to capture the aggregate change. Unlike the negative impact observed from local pandemic outbreaks, we identify a significant "lifting effect" on fundraising efforts at the national level. The probability of initiating fundraising activities increases, aligning with our theoretical predictions. Additionally, we observe a significant "shifting effect," where fundraising for causes unrelated to the COVID-19 pandemic is squeezed out.[9]

This paper makes several contributions to the literature on disaster relief. Studies such as those by Muller and Kräussl (2011); Scharf and Smith (2015); Scharf, Smith and Wilhelm (2017); Tiefenbach and Kohlbacher (2015) highlight a lifting effect on total donations following national natural disasters. Conversely, when disasters vary in magnitude across regions, the local effect can differ, with donations in directly impacted areas remaining unaffected, as noted by Deryugina and Marx (2021). The COVID-19 pandemic, extending beyond a typical natural disaster, has had significant economic impacts. Online reports and news indicate that the income effect predominates, leading to reductions in charitable giving (Cinnamon, 2020; Kess, 2020). Experimental evidence supports this finding (Branas-Garza et al., 2020), with declines in willingness to donate linked to social distancing (Whitehead, 2021), event cancellations (CAF, 2021; Butler, 2021), and economic uncertainty (Hargrave, 2021). Diverging from existing studies on changes in charitable donations, our paper provides new insights from the angle of charitable fundraising. We support findings from Saleh, Lehmann and Medford (2021), who observed a significant increase in web-based crowdfunding post-pandemic. This paper goes further by discussing the distinctions between local and national effects, and temporal versus persistent impacts.

My research also contributes to the growing body of literature on government intervention in the charitable sector. Early research by Roberts (1984); Bergstrom, Blume and Varian (1986) suggested that government grants could completely crowd out charitable donations, though later studies with the impure altruism assumption showed only partial crowding out (Andreoni and Payne, 2003; Andreoni, Payne and Smith, 2014).[10] The literature also explores the role of taxation, including tax incentives (Duquette, 2016; Almunia et al., 2020), tax rebates (Scharf and Smith, 2015; Hungerman and Ottoni-Wilhelm, 2021), and tax credits (Chatterjee et al.,

[9] Scharf, Smith and Wilhelm (2017) finds a lifting and shifting effect on donations after natural disasters. Our study extends this by identifying a similar effect in the organizational response to fundraising efforts.

[10] There is also a possibility of a crowd-in effect on social donations. See, e.g., Andreoni, Payne and Smith (2014).

2020; Fack and Landais, 2010). Differing from traditional mechanisms like grants and taxes, recent papers examine political interference, where charitable donations can serve as political resources (Chan and Feng, 2019) or "tax-exempted" lobbying (Bertrand et al., 2020). During natural disasters, charitable and political giving can be substitutes (Petrova et al., 2020). Our study adds to this discussion by examining a less-researched form of government interference through collaborative advocacy, demonstrating that, especially in economies with a less-developed charitable sector like China, political signaling can effectively, albeit temporarily, crowd in charitable fundraising.

Finally, this paper add to the discussion on Chinese charitable sector. The majority of paper for this strand of literature focuses on corporate philanthropy. Factors like political intervention (Gao and Hafsi, 2015; Chan and Feng, 2019), media attention (Zheng, 2009; Hurtado and Agudelo, 2013), internationalization (Liu, Luo and Cui, 2018) etc. may have significant impact on firms' decision on donation. For papers on charitable organizations, transparency of charitable foundation is discussed (Xu et al., 2020; Hua, 2021). However, the China Foundation Centre Data (CFC)[11] applied in these papers is a subsample of for charitable organizations in China. A large fraction of government-organized charitable organizations like Charity Federation and the Red Cross Society is omitted in the CFC data. Our paper complement this strand of literature by applying a more complete data consisting of charitable organizations with different level of political connection to the government.

The rest of my paper is organized as below. Following the introduction, section II. reviews the institutional background of Chinese charitable sector and government's response to Covid-19 pandemic. Then, we build a partial equilibrium model and generate some theoretical predictions in section III.. Next, in section IV., we describe the data we use in our paper. section V. demonstrates the empirical specifications and the corresponding results. Finally, section VI. concludes.

II. Institutional Background

A. Charitable Sector in China

Market Structure and History. We begin by reviewing the structure of the Chinese charitable sector, which can be categorized into three types based on the characteristics of their organizers:

(1) Government-organized Charitable Organizations (GOCOs): These are typically established directly by government bodies and include major entities like the

[11] The CFC data is no longer publicly available from 2018.

Charity Federation and the Red Cross Society, which have branches across numerous Chinese cities.

(2) Corporate-organized Charitable Organizations (COCOs): Formed by corporations or corporate executives, usually by large firms.

(3) Grass-Root Charitable Organizations (GRCOs): Founded by individuals or social groups lacking significant political or financial resources.

Historically, charitable organizations in China have been closely tied to the government, regardless of type. During the initial stages of adopting Western-style charity, the concept of private, donative-style charity was largely unfamiliar to the public, and thus, charitable donations were sustained primarily through government credibility.[12] Strict regulations, enforced through "Regulation by Registration", impose high political costs for registration, allowing governments considerable autonomy over the process. This led to philanthropy activities being primarily conducted by GOCOs, with some local governments even operating specific departments to run their own charitable activities. In contrast, most COCOs and GRCOs remained unregistered, and those that were registered often had significant governmental ties or shared interests.[13]

The government-dominated philanthropy landscape began to shift following the 2008 Sichuan Earthquake. The disaster revealed inefficiencies in distributing the relief resources[14], prompting a reevaluation of the role of non-governmental organizations in disaster response. The subsequent relaxation of registration and regulation restrictions marked 2008 as the "Year of Civil Society" (Shieh and Deng, 2011). By 2014, many GOCOs were privatized or became nominally independent from government departments, signaling a significant transformation in the operation of government-dominated charities.[15]

Charity Law and Fundraising Activity. The 2015 Charity Law was a pivotal development in the Chinese charitable sector, significantly lowering the barriers to registration for charitable organizations.[16] According to this law, all

[12] Hsu (2008) reviews the origins of Western-style charity in China with Project Hope in 2002, led by the China Youth Development Foundation, an affiliate of the Communist Party's Youth League. The project's legitimacy, derived from its political affiliation, attracted donors.

[13] Hildebrandt (2013) discusses the challenges faced by unregistered organizations and notes that charities geographically closer to the political center are more likely to get registered.

[14] During the disaster relief for this earthquake, the participation of charitable sector, especially for those COCOs and GRCOs, is very limited. Only a few GOCOs had Public Fundraising Authority, and regulations prohibited NGOs from establishing or holding activities outside their registered areas (Shieh and Deng, 2011).

[15] The "Suggestion on Promoting Charitable Activity" (NDRC [2014] No.61) encouraged local governments to promote charitable activities.

[16] The Law covers definitions of charitable activities, the establishment of charitable organizations, qualifications for public fundraising, charitable trusts, information disclosure, and government promotion of charitable activities.

charitable organizations must register with the civil affairs departments of central or local governments. This formalization reduced local government autonomy in registration, diminishing the previously prevalent political relationships.

The law mandates that charitable organizations engage in Fundraising Activities, including Public and Targeted Fundraising Activities.[17] However, as data on targeted fundraising activities is not publicly available, our study focuses on public fundraising behaviours. Organizations seeking to conduct public fundraising must obtain Public Fundraising Certificates (PFCs). Interestingly, organizations without PFCs can still participate in public fundraising by collaborating with those holding PFCs, such as web-based charitable platforms like the Tencent and Alibaba foundations, which, despite often lacking PFCs, can effectively attract donations through their advanced telecommunication technologies. Appendix Figure D1 shows the basic structure of Chinese charity market.

B. Government Response to Covid-19

Chinese government imposed strict social restriction at the beginning of the pandemic. These policies have been intensively reviewed by Fang, Wang and Yang (2020); Almond, Du and Zhang (2020); Fisman et al. (2021) etc.. Similar to 2008 Sichuan Earthquake, charitable sector again operated under the shadow of the government that their contribution is marginalized (Dong and Lu, 2020). The Chinese government set up a special committee to lead the national response and the task of resource transportation was given to the Military rather than charities or other NGOs, NPOs. Furthermore, the charitable organization had limited autonomy in distributing their resource that large part of the donation fund served the government deployment. Therefore, charitable sector was not mobilized as an independent powerful force during the Covid relief.

Instead, it was mobilized as a complementary funding body for the government-led relief project to provide additional public goods and services. To boost charitable fundraising efforts, the Chinese central government published the **collaborative advocacy** (Cai et al., 2021). On 26$^{\text{th}}$ Jan. 2020, the Ministry of Civil Affairs issued the *Announcement of Advocating Charitable Sector to Participate in the Prevention and Control of Covid-19* [Minister of Civil Affairs, Issue 476].[18] Following the central government policy, local governments subsequently issued their own policies during January and February 2020. The main content of these local policies aligns with the central advocacy, serving as local implementations of the central government

[17] Public fundraising activities raise funds from the general society, while targeted fundraising activities collect funds directly from specified targets.

[18] 《民政部关于动员慈善力量依法有序参与新型冠状病毒感染的肺炎疫情防控工作的公告》[民政部公告第 476 号] http://www.mca.gov.cn/article/xw/tzgg/202001/20200100023667.shtml.

directive.[19]

The advocacies primarily suggested that

> *charitable organizations initiate public fundraising activities to mobilize social donation to assist in the government-led disaster relief plan.*

Throughout these advocacies, there is no enforcement by law or executive order from the government. Therefore, they function as a political signal, allowing charitable organizations autonomy in deciding whether to comply. A detailed introduction to government advocacy is provided in Appendix A.

III. THE MODEL

Our paper studies the fundraising behaviour for charitable organizations subjected to the pandemic shocks and the government collaborative policy. In this section, we build a simple partial equilibrium model to generate possible reactions for organizations. As mentioned in section II., holding fundraising activity is the main endeavour for charitable organizations. We thus study the binary decision of initiating fundraising activity in our model. In equilibrium, the optimal decision is driven by donor preference, income and organization's cost of holding activity. These factors are changed by pandemic shocks and the collaborative policy from the government.

A. Model Setup

There are two sectors in the model — donors indexed by i and a representative charitable organization. Donors are assumed to be warm-glowed, maximizing their utility by choosing the amount of consumption and givings. Donors are also heterogeneous on their own preferences, or "tastes" , for charities. The tastes are private information for donors and is unknown for charitable organization. However, the distribution of tastes could be known, either by market survey or news. If donor gives g_i^t unit of money, he derives his utility in the following quasi-linear form,

$$\begin{aligned} \max_{c_i^t, g_i^t} \quad & \ln(c_i^t - \gamma) + \frac{1}{(\beta_i^t - x^t)^2} g_i^t, \\ s.t. \quad & c_i^t + g_i^t = w_i^t, \\ & g_i^t \geq 0. \end{aligned} \tag{1}$$

c_i^t denotes donor's consumption; γ is the minimum living cost; w_i^t denotes income. For the second part of the utility function, β_i^t is the taste of charity for donor,

[19]The primary focus of our empirical estimations is on evaluating charitable organizations' responses to local advocacies while controlling for the national policy.

while x^t is version of charity held by charitable organization. $(\beta_i^t - x^t)^2$ evaluates the squared distance between donor's taste and the version of charity he gives to. This term captures the utility weight between warm glow effect and consumption. Intuitively, "giving to who I want to give" implies smaller distance and hence a higher utility weight for givings. By Lagrangian, the optimal donation would be

$$g_i^t = \max\left\{w_i^t - \gamma - (\beta_i^t - x^t)^2, 0\right\}. \tag{2}$$

For charitable organization, the expected fund raised would be $\mathbb{E}\sum_i g_i^t$. Therefore, its maximin strategy[20] on charity version would be the solution of the following expression

$$\arg\max_{x^t} \quad \sum_i \max\left\{\mathbb{E}^t(w_i^t - \gamma) - \mathbb{E}^t(\beta_i^t - x^t)^2, 0\right\}. \tag{4}$$

Equation 4 implies that the organization picks the version of their charity to maximize the aggregate donation collected. This objective function is essentially consistent with Andreoni and Payne (2003) where charitable organization maximizes the social service provided, which equals the net fund received. Differently, the fundraising cost in Andreoni and Payne (2003) is associated with the difficulty of soliciting donors, while we assume a lump-sum cost for targeting the version x^t, which will be introduced shortly. In our context, it is straightforward that the optimal version would be $x^t = \mathbb{E}^t(\beta_i^t)$. This implies that charitable organization would target the version at the average level of donors' tastes.

Before we proceed to the discussion of organization's optimal strategy, we draw some assumptions on the distribution of β_i^t to simplify the derivation. Specifically, we let

$$\begin{aligned} &\beta_i^t = \mu^t + \eta_i, \\ \text{where} \quad & \\ &\mu^t = \mu^{t-1} + v^t, \\ &v^t \sim N(0, \sigma_v^2); \quad \eta_i \sim N(0, \sigma_\eta^2). \end{aligned} \tag{5}$$

This expression decomposes the evolution of donors' tastes into a time-series component μ^t and a donor-specific component η_i. The first component, μ^t, captures the average taste of donors, which varies over time. This term is used to model changes

[20] Here we assume the representative charitable organization is risk-adverse. This assumption allows us to give the close-form solution without solving the truncated joint distribution of w_i^t and β_i^t. The lower bound of expected donation collected is

$$\mathbb{E}\sum_i \max\left\{w_i^t - \gamma - (\beta_i^t - x^t)^2, 0\right\} \geq \quad \sum_i \max\left\{\mathbb{E}(w_i^t - \gamma) - \mathbb{E}(\beta_i^t - x^t)^2, 0\right\}. \tag{3}$$

in public attention over time and provides incentives for charitable organizations to re-optimize their version x^t. For simplicity, we assume that the average taste evolves as a random walk process.[21] A higher variance in this process (σ_v^2) indicates more volatile changes in public attention. The second component, η_i, captures deviations of individual donors' preferences from the social average. This term introduces heterogeneity into individual preferences. A higher variance in this component (σ_η^2) implies a more diverse distribution of individual preferences at any given time. Under these assumptions, the optimal version of charity for a fundraiser at period t is simply $\mathbb{E}^t(\beta_i^t) = \mu^t$.

For the distribution of income w_i^t, we assume a log normal distribution that

$$\ln(w_i^t) = \ln(\bar{w}^t) + \varepsilon_i; \quad \varepsilon_i \sim N(0, \sigma_\varepsilon^2), \tag{6}$$

where $\bar{w}^t$ is the average income. Then, without loss of reasonability, I just let the living cost be proportional to the average income, that is $\gamma = m\bar{w}^t$. So, we have components in Equation 4 that $w_i^t - \gamma = \bar{w}^t(e^{\varepsilon_i} - m)$ and $\mathbb{E}^t(w_i^t - \gamma) = \bar{w}^t(e^{\frac{1}{2}\sigma_\varepsilon^2} - m)$.

Optimal Choice for Fundraising. Suppose at period t, the fundraiser targets the optimal version μ^t. At period $t+1$, the distribution for donors' taste is changed. The organization thus faces a choice on whether to initiate a new charitable activity in order to meet donors' preference.[22] Denote the binary choice using

$$d = \begin{cases} 1 & \text{Initiate a New Activity} \\ 0 & \text{Keep the Old One} \end{cases}. \tag{7}$$

For the new activity, charitable organization can re-target its version to the optimal level, i.e. μ^{t+1}. However, those do not re-optimize would inherit the previous versions from the last period, i.e. μ^t. We further let R to be the lump-sum cost of holding a new fundraising activity. The cost could arise not only by managing and holding fundraising activity, but also by investigating the market, i.e. the distribution of donors' preferences. As mentioned earlier, the optimal version of charity would be the mean of donors' preferences. One could think of R to be the cost to obtain this information. Denote $V(d)$ as the value function, the optimal strategy for holding new activity would be

[21] The random walk assumption is adopted to simplify the subsequent derivation. It can be easily generalized to an autoregressive process.

[22] We are interested in this binary choice because the strategy of initiating new fundraising activities is observable in our empirical data. In the next part of the empirical analysis, we model this decision using a binary-dependent-variable regression to examine the timing of initiation behavior.

$$d = \arg \max_{d=\{0,1\}} \quad dV(1) + (1-d)V(0),$$

where

$$\begin{aligned} V(1) &= \max\left\{\mathbb{E}^{t+1}(w_i^{t+1} - \gamma) - \mathbb{E}^{t+1}(\beta_i^{t+1} - \mu^{t+1})^2, 0\right\} - R, \\ V(0) &= \max\left\{\mathbb{E}^{t+1}(w_i^{t+\tau} - \gamma) - \mathbb{E}^{t+1}(\beta_i^{t+1} - \mu^{t})^2, 0\right\}. \end{aligned} \tag{8}$$

By drawing our assumption on β_i^t and w_i^t, we can have expressions

$$\begin{aligned} V(1) &= \max\left\{\bar{w}^t(e^{\frac{1}{2}\sigma_\varepsilon^2} - m) - \sigma_\eta^2 - R, -R\right\}, \\ V(0) &= \max\left\{\bar{w}^t(e^{\frac{1}{2}\sigma_\varepsilon^2} - m) - \sigma_\eta^2 - \sigma_v^2, 0\right\}. \end{aligned} \tag{9}$$

The implications of the expressions above are straightforward. First, the value for a charitable organization is negatively affected by the heterogeneity of donors' preferences, σ_η^2. When donors' tastes are more diverse, fewer donors align with the version of the charity, leading to lower donations. Second, if the organization initiates a new activity (i.e., $d = 1$), it incurs a cost R. However, if it continues the activity from the previous period (i.e., $d = 0$), the organization's value instead is decreased by the volatility of public attention, σ_v^2. For instance, in the case of the Covid-19 pandemic, as donors become more inclined to support health-related charities, organizations that do not update their version risk receiving fewer donations. The trade-off between the initiation cost and the opportunity cost from time-varying public attention determines the optimal choice for initiating a new fundraising activity. The optimal fundraising strategy can be expressed as:

Proposition 1: *The representative charitable organization begins new fundraising activity if $\bar{w}^t(e^{\frac{1}{2}\sigma_\varepsilon^2} - m) - \sigma_\eta^2 - R > 0$ and $\sigma_v^2 > R$.*[23]

The optimal conditions for organization's strategy are two folded. The first part $\bar{w}^t(e^{\frac{1}{2}\sigma_\varepsilon^2} - m) - \sigma_\eta^2 - R > 0$ implies that the funds collected by the new activity should at least cover its initiation cost. The second part $\sigma_v^2 > R$ requires that the initiation cost should not exceed the potential loss from of doing nothing, which incurs because of donors' time-varying average taste.

[23]The proof of this proposition is very simple. To prove the first condition that $\bar{w}^t(e^{\frac{1}{2}\sigma_\varepsilon^2} - m) - \sigma_\eta^2 - R > 0$, if conversely $\bar{w}^t(e^{\frac{1}{2}\sigma_\varepsilon^2} - m) - \sigma_\eta^2 - R < 0$ then $V(1) < 0$. As $V(0) > 0$, we have $V(1) < V(0)$ that organization will choose not to start a new fundraising activity. Therefore, the first condition must hold.

Now we turn to the second condition. If the first condition holds, $V(1) > 0$. There are two possible cases for $V(0)$, the first one is $\bar{w}^t(e^{\frac{1}{2}\sigma_\varepsilon^2} - m) - \sigma_\eta^2 - \sigma_v^2 \leq 0$ such that $V(0) = 0$. In this case, organization will choose $d = 1$. The second one is $\bar{w}^t(e^{\frac{1}{2}\sigma_\varepsilon^2} - m) - \sigma_\eta^2 - \sigma_v^2 > 0$ such that $V(0) > 0$. In this case organization will choose $d = 1$ if $\sigma_v^2 > R$. To summarize, the sufficient condition for $d = 1$ would be $\bar{w}^t(e^{\frac{1}{2}\sigma_\varepsilon^2} - m) - \sigma_\eta^2 - R > 0$ and $\sigma_v^2 > R$.

Figure 1. Optimal Choice Set

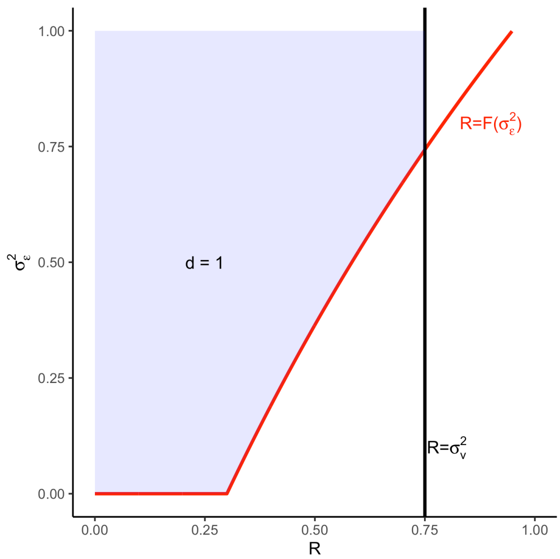

Notes: (i) This Figures plots the optimal policy for charitable organizations. The horizontal axis denotes the fundraising cost of initiating new charitable activities. The vertical axis denotes the variance for donors' income. (ii) The red line denote the bundles with $R = \bar{w}^t(e^{\frac{1}{2}\sigma^2_\varepsilon} - m) - \sigma^2_\eta$. The black line denotes the bundles with $R = \sigma^2_v$. Charitable organizations with bundles in the shadowed area optimally initiate fundraising activity.

Figure 1 shows the optimal choice set for the representative charitable organization. We standardize R, σ^2_ε, σ^2_η and σ^2_v to the range [0,1] and denote $F(\sigma^2_\varepsilon) = \bar{w}^t(e^{\frac{1}{2}\sigma^2_\varepsilon} - m) - \sigma^2_\eta$. The horizontal and vertical axis denote cost R and income variance σ^2_ε respectively. Following Proposition.1, any bundles above $F(\sigma^2_\varepsilon) = R$ and left to $R = \sigma^2_v$ would choose to initiate fundraising activities, i.e. the shadowed area.

B. Comparative Analysis

To link the theoretical model with the context of the Covid-19 pandemic, we apply the model to explore potential changes in charitable organizations' decisions through comparative analysis. We propose several scenarios as follows.

1. Effect of Social Attention. When Covid-19 hit the economy, non-Covid-related news was largely squeezed out of social media, causing donors' attention to centralize around the pandemic. As a result, donors became more willing to give to charities with Covid-related causes. In our model, this concentration of donors' preferences implies a reduction in the diversity of donors' tastes, σ_η. This change shifts the curve $R = F(\sigma^2_\epsilon)$ rightward, expanding the fundraising area and indicating a higher likelihood of initiating fundraising activities.

2. Effect of Income Drop. The income effect during the pandemic would reduce fundraising. Strict social restrictions were imposed in cities experiencing local outbreaks, such as Wuhan, where lockdown policies required citizens to stay at home to limit viral spread. These restrictions negatively affected donor incomes, particularly for those employed in the retail or restaurant industries (Alfaro, Becerra and Eslava, 2020; Chetty et al., 2023). Additionally, the spread of infection directly incapacitated workers, reducing their labor income (Goenka, Liu and Pang, 2024). We therefore expect $\bar{w}^t$ to decrease more significantly in cities with local outbreaks, while it would remain unchanged or decrease less in unaffected or less affected cities. Correspondingly, the curve $R = F(\sigma_\varepsilon^2)$ would shift leftward, reducing the likelihood of fundraising in affected areas.

3. Effect of Fundraising Cost. The probability of initiating fundraising is negatively correlated with the cost of holding fundraising activities. In our model, an increase in cost shifts the black line ($R = \sigma_v^2$) leftward, decreasing the probability of fundraising, and vice versa.

We link the effect of government collaborative advocacies to a decrease in fundraising costs. Local governments may provide political conveniences or share market information, reducing the fundraising costs for charitable organizations that comply with their advocacies. One could interpret this as the government, acting as a social planner, having knowledge of the distribution of donor preferences. By sharing this market information with compliant organizations, the government lowers their cost of investigating the market (e.g., obtaining μ in our model), making them more likely to initiate fundraising activities.

Furthermore, during pandemic outbreaks, the cost of holding in-person activities may increase due to administrative challenges. For example, fundraisers might need to provide additional guidance and support, such as ensuring social distancing, sanitizer availability, and facial masks, for donors during pandemics, which could discourage fundraising. However, there is no evidence suggesting that the costs of online charitable activities increase significantly.[24]

4. Summary. Our model has the following implications for organizations' fundraising decision:

(1) The nationwide fundraising probability could increase because the pandemic induces concentration of donors' preferences.

(2) The negative income effect by local outbreaks reduces the expected donation. Charitable organization hence becomes less likely to start fundraising.

(3) Government advocacies mitigated part of the income effect and boost fundraising effort by lowering the fundraising costs.

[24]In our empirical studies, we cannot distinguish whether the activities were held in person, online, or as a hybrid. However, given the context of China, it is more likely that activities were conducted online during pandemic outbreaks due to strict social restrictions.

In the next several sections, we would empirically test these predictions and channels by a unique data of Chinese charitable sector.

IV. The Data

Charity in China Data. We now begin testing the predictions from our model empirically. The main data set we apply comes from Charity in China[25] which is a governmental administration platform for Chinese charitable organizations. The data consists of two parts. The first part of the data records all the 1,0304[26] registered charitable organizations in China. It provides us with a detailed cross-sectional registration information, including their registered government; set-up date; geographical location; whether have public fundraising authorities; mission statement etc. Figure 2 presents the geographical distribution of Chinese charitable organizations at the county level.[27] It could be viewed that the geographical distribution is east-biased that there are more charitable organizations located in the eastern provinces.

The second part of the data records all public fundraising activities held by the organizations. The quality of the record data is reliable after the year of 2016. In each record, we can find detailed information about the fundraising activities, including their beginning and ending date; mission statements; main usages; and beneficiary groups etc.. In our paper, we distinguish the Covid-related activities by the following criteria: *The fundraising activity is Covid-related if Covid related words*[28] *are mentioned in its title, mission statements, main usages, or beneficiary groups.*. We plot the number of charitable activities hold in each month in Figure 3. One could easily find that charitable organizations have strong seasonal preferences in holding activities. Within each year, the number of activities usually peaks at September.[29] However, we find that Covid-related activities, denoted by the red connected dots, created another big bunch at the beginning of 2020, which is not a usual pattern for any years before.

Moreover, we notice that part of the public fundraising activities publish their financial records on the platform. This gives us the third part of the data. It tracks

[25] The data is publicly available in `http://cishan.chinanpo.gov.cn/platform/login.html`.. This data set is similar to the Charity Commission Data in the UK.

[26] Updated at 9^{th} May 2021.

[27] To reduce the variance, we use the percentile of the number of charitable organizations in each county.

[28] In Chinese, we define the Covid-related words as 新冠 (Covid), 肺炎 (Infection), 抗疫 (Fighting Pandemic), 战疫 (Fighting Pandemic), 防疫 (Preventing Pandemic), 疫情 (Pandemic), 病毒 (Virals), 驰援湖北 (Helping Hubei), 驰援武汉 (Helping Wuhan), 援鄂 (Helping Hubei)

[29] This because 5-Sept is the Chinese Day of Charity by the *Charity Law*. This is to be in lined with the International Day of Charity by UN. The Day of Charity would crowd-in donation and fundraising.

Figure 2. Geographical Distribution of Chinese Charitable Organizations

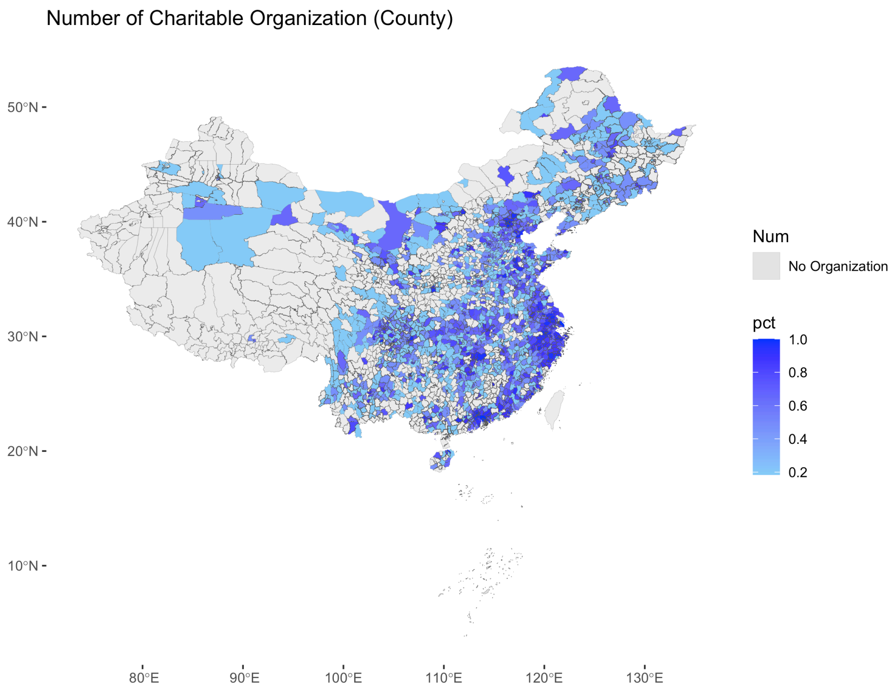

Notes: (i) This Figure shows the geographical distribution of Chinese charitable organization. (ii) We solve the distribution for the number of charitable organizations in each county. The colours in the map represent the percentile for counties in the distribution.

the donation received and the administration costs for those activities. Unfortunately, these records are not well disclosed every month. For example, some activities update their donation records every month, while some of them only publish the records at the end of the activity. We notice that there is also a potential "selective disclosure problem" in the financial records. Therefore, our empirical strategy would be relied on the timing of holding fundraising activities. The financial record data are used for mechanism and further study.

Pandemics and Government Data. It is not difficult to obtain the data of the pandemic because Chinese government built powerful Covid trackers and publish their records. We download a city-by-date level panel data from the China Stock Market & Accounting Research Database (CSMAR). This data is also abundant in time and geographical variation that it tracks the number of infected and death cases in each city each date after the time when the first infected case was found in Wuhan, Hubei province.

We now introduce how we identify the periods of pandemic outbreak using the Covid trackers data. Suppose there are two types of episodes in the pandemic dynamics: {Outbreak, Break}. The first type of the episodes may generate high

Figure 3. Total Number of Charitable Fundraising Activities

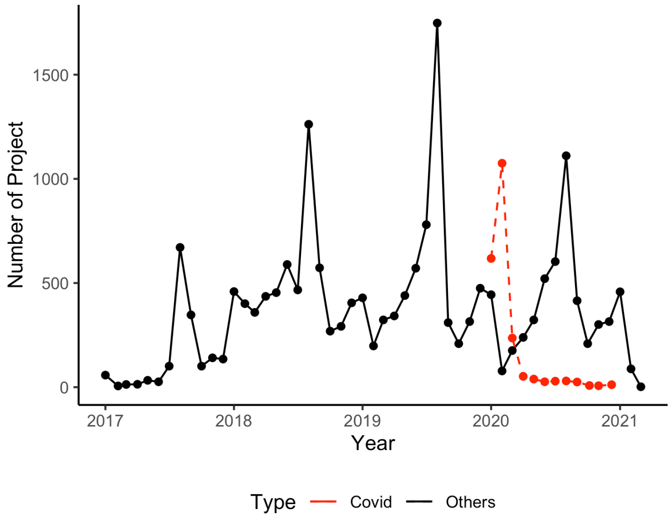

Notes: (i) This Figure shows the time series for number of charitable activities initiated in monthly frequency. (i) The red dash represents the number of activities related to Covid-19 pandemic.

spikes of infection case, for example, the onset periods. In contrast, during the Break episode, there were no new local confirmed cases[30]. We build the following criteria to identify the outbreak periods: *City j on date t is classified as Outbreak Episode, if the number of local confirmed cases $I_{j,t}$ satisfies any conditions in*:

(1) $I_{j,t} > 0$;

(2) $I_{j,t} = 0$, but date $t-1$ is classified as outbreak and $I_{j,t+\tau} > 0$, where $0 < \tau \leq 14$.

The first condition indicates that if there is any new infection, the period should be classified as Outbreak. The second condition is to identify the scenario that there is no infection detected at date t but it shows some new infection in the coming 2 weeks.[31]

We show two related examples in the Panel A of Figure 4 where we plot the cumulative confirmed cases over time in two typical cities. For sensitivity, we hide the names of the cities. The red and blue thick lines denote the Outbreak episodes, while the black lines indicate the Break episode. It could be viewed that the city in red line experienced only one outbreak of pandemic, with the cumulative confirmed cases climbed dramatically during the onset. For the blue line, Covid-19 did not bring too much infection at the onset period. However, in July of 2020, this city experienced another outbreak, with more than 200 additional infected cases.

[30] The sample periods of our data is at the early stage of Covid-19 pandemic when Chinese government imposed zero-infection policy by intensive lockdown. The pandemic was thus kept well in the endemic stage with part of the cities having new cases.

[31] This is due to the finding that it may take up 2 weeks for the infection to be detected. Thus, the confirmed cases could be connected to the infection 14 days earlier.

Figure 4. Classification of Outbreak Episode and Advocacy Arrival Dates

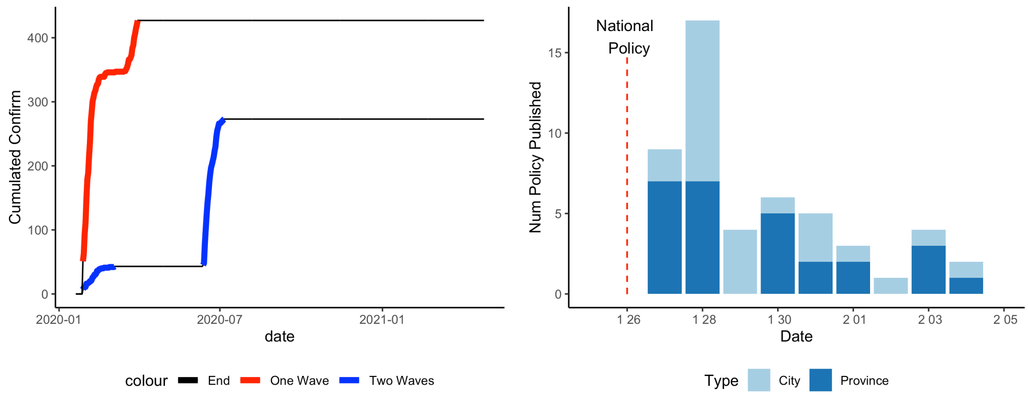

(a) Example of Outbreak Episode **(b)** Advocacy Arrival Dates

Notes: (i) Panel (a) shows two examples for our classification of outbreak episode. The thicker parts represent periods that classified as outbreak. The horizontal axis denotes the cumulated cases of infection. (ii) In these two samples, the cities in red and blue experienced one and two waves of local outbreaks. (iii) Panel (b) shows the number of government advocacies published over time. The red dash line is the time when national advocacy was published. The dark and light blue denote city-level and provice-level policies respectively.

For government shocks, we search and download all the Covid-related policy documents from the law database by Peking University (Beida Fabao[32].). Then, we manually read and filter those policies that advocate charitable organizations to raise fund for Covid-19 relief. The national advocacy was published on 26 Jan 2020. We also find 35 provincial level policies and 27 city level policies. Panel (b) of Figure 4 plots the distribution of advocacy arrival date. We can see that all the provincial and city-level advocacies were published after the national policy came into effect. The rest of data about economic, demographic, geographic information are obtained from the Economic Prediction Platform (EPS), which is a new and complete database on Chinese economy.

Merge and Summary Statistics. The datasets we adopt have different frequencies and cross-sectional levels. To link these datasets together, we firstly reshape the public fundraising data into an organization-by-date level balanced panel data. The generated variable is the number of activities initiate each date. Then, the reshaped data can be merged with the Covid data and the government advocacy data by the keys of city and date. Then, we drop the samples before 01-Jan-2017 due to the limited number of fundraising activities, and the samples after 01-Apr-2021 to remove the effects from virus mutation of Delta/Omicron variants.[33] We also drop the charitable organizations located in the Tibet province because there is

[32] http://www.pkulaw.cn

[33] Another reason for dropping samples after Delta mutation is that the *Charity in China* website upgrades its anti-crawling technique. The data becomes difficult to update.

only one organization with public-fundraising authority in our sample. The cleaning process would leave us with a daily panel with 3,498,208 observations.

For the financial record data, due to the low data quality, we aggregate the data into a cross-section of fundraising activities. We generate the average daily donation received and fundraising cost for each activity record. After dropping records before 01-Jan-2017, after 01-Apr-2021 and those ongoing activities, we have only 8,186 activity records left in the sample. The financial record data is linked with the Covid and government panel data by the keys of city and time. Different from the fundraising data, the time dimension for the financial record data is referred to the date of initialization. Our coming empirical specifications using this dataset mainly compares the activities with different initiation times.

Table I presents some summary statistics of the data. In Panel A, we define the event window of Covid-19 to be period from 01-Jan-2020 to 01-Apr-2020[34]. In the first two rows, it could be viewed that the intensive margin (fundraising or not) and the extensive margin (number of activities initiate) for fundraising during the event window is much greater than the other time. The differences are statistically significant. However, for those not-for-Covid activities, as shown in the third and forth row, are negatively affected during the event window. This implies a potential crowd-out effect for fundraising activities with not-for-Covid causes. Panel B shows the summary statistics for the financial records of the charitable activities. It could be viewed that the average donation received was increased while the average fundraising cost was decreased during the event window. Finally, in Panel C, we show the cross-sectional composition of organizations in our dataset. Around 23% of charitable organizations in our sample are branches of the Charity Federation, while 39% are branches of the Red-cross Society. Regarding to the treatment group, there are around 41% and 54% of organizations in our sample were affected by pandemic and advocacy shocks respectively.

[34]This is just for convenience. In our following empirical part, we will formally identify the event windows for Covid-19 shocks and government advocacy shocks.

Table I. Summary Statistics

	(1)	(2)	(3)
Panel A: Fundraising Num.Obs = 3,498,208			
	Event Window	Rest of Date	Diff
Fundraising or Not	0.012	0.003	0.008 (2e-04)
Number of Activity	0.013	0.006	0.007 (3e-04)
Fundraising or Not (Not-for-Covid)	0.002	0.003	-0.001 (1e-04)
Number of Activity (Not-for-Covid)	0.003	0.006	-0.002 (3e-04)
Panel B: Financial Record Num.Obs = 8,186			
Average Donation (in log)	8.037	4.367	3.67 (0.141)
Average Cost (in log)	0.567	0.953	-0.386 (0.0613)
Panel C: Sample Composition			
	Fraction		
Charity Federation	0.232		
Red-cross Society	0.39		
Treatment Group (Covid Shock)	0.417		
Treatment Group (Policy Shock)	0.544		

Notes: (i) This table summarizes the main data set we employ. For illustration, we simply define the event window for Covid pandemics as the periods between 2020-01-01 to 2020-04-01. The numbers in the parentheses denote standard error. (ii) Panel A summarizes the key variables of fundraising behaviour in the fundraising data. Panel B compares the average daily donation received and daily cost of holding activity in the financial record data. Panel C displays the sample composition.

V. EMPIRICAL ESTIMATION

This section presents the empirical strategies and the results of our paper. Our empirical strategy is aimed at capturing the treatment effects on fundraising from the outbreaks of Covid-19 pandemics and the subsequent government advocacies. To identify the effects, we exploit the treatment variation in city level and assume that charitable organizations would not be affected by infection or governments in other cities[35]. Specifically, we define the cities that ever experienced one or more than one waves of Outbreak Episodes as the treatment group for the pandemic shock. At the same time, we let the cities where their governments ever published advocacies as the treatment group for the government shock.[36]

We apply a staggered DID framework to compare the fundraising behaviour between the treatment and control groups before and after the shocks occurred. Recall that in our theoretical model, the charitable organization decides whether

[35]This assumption rules out the spatial spillover effect. This is because the local advocacies restrict that the donation collected should be used in the jurisdiction, as we mentioned earlier. Nevertheless, we will empirically test this assumption later in our paper.

[36]We assume that all the cities in the province are advocated by the provincial government. Thus, the treatment date for advocacy shock would be the earlier time for the city and province advocacies.

to initiate a new fundraising activity and match the "version" of the activity with donors' preferences. The latter behaviour is challenging to measure with our data as preferences are unobservable. Therefore, in this section, we focus on evaluating organizations' behaviour in starting new activities. Specifically, in our data, we define a dummy variable $F_{i,j(p),t}$, which equals 1 if charitable organization i in city j of province p initiated a new public fundraising activity on date t. Our empirical model evaluates the probability $\mathbb{P}(F_{i,j(p),t} = 1)$.

A. Event Study

One important preliminary of using DID specification is the parallel trend assumption. It requests probability of fundraising evolved similarly for the treated and controlled charitable organizations before treatment. To empirically test this assumption, we employ a canonical event-study approach as in equation Equation 10.

$$
\begin{aligned}
F_{i,j(p),t} =& \theta_i + \lambda_t + \phi_{p,y} + \psi_{p,w} + \rho_{p,d} \\
&+ \sum_{\substack{-10\leq\tau\leq 10 \\ \tau\neq 0}} \alpha^{\tau} C^{\tau}_{j(p),t} + \sum_{\substack{-10\leq\tau\leq 10 \\ \tau\neq 0}} \beta^{\tau} G^{\tau}_{j(p),t} + \varepsilon_{i,j(p),t}.
\end{aligned} \tag{10}
$$

$F_{i,j(p),t}$ is a binary explained variable as introduced before. Because it is hard to find control variables for the daily panel data[37], we absorb various high-dimensional fixed effects to rule out some potential endogeneity caused by unobservable factors. We firstly control the organization fixed effect θ_i and the time fixed effect λ_t so that all the individual- and date-invariant unobservable factors would be absorbed by these terms. $\phi_{p,y}$ is the province-by-year fixed effect. It captures all annual provincial variation (e.g. annual GDP, annual population growth etc.). We also absorb the interactive fixed effect at the level of province by week ($\psi_{p,w}$) and province by day of week ($\rho_{p,d}$). We use them to address the heterogeneous fundraising preference during a year (or week) for different provinces.

The remaining variation of organization-by-date level would be explained by two sets of DID style dummies. In the summation parts of Equation 10, τ is the indicator for periods with the duration of 10 days. Specifically, if the samples are 0 - 10 days after the shocks arrive, $\tau = 1$; 11 - 20 days after, $\tau = 2$ etc.. Vice versa, $\tau \leq 0$ indicate the periods before the shocks arrive. Variable $C^{\tau}_{j(p),t}$ is a family of dummies which take value of 1 if the samples are τ periods before or after the pandemic local outbreak. It captures the impact from pandemic outbreak. Similarly, $G^{\tau}_{j(p),t}$ captures the policy shocks. It equals 1 if the observation is τ periods before or after the time when city j advocated charitable organizations to raise fund. Finally,

[37]We will introduce some interaction-type control variables later in our Diff-in-Diff specification later.

Figure 5. Event Study

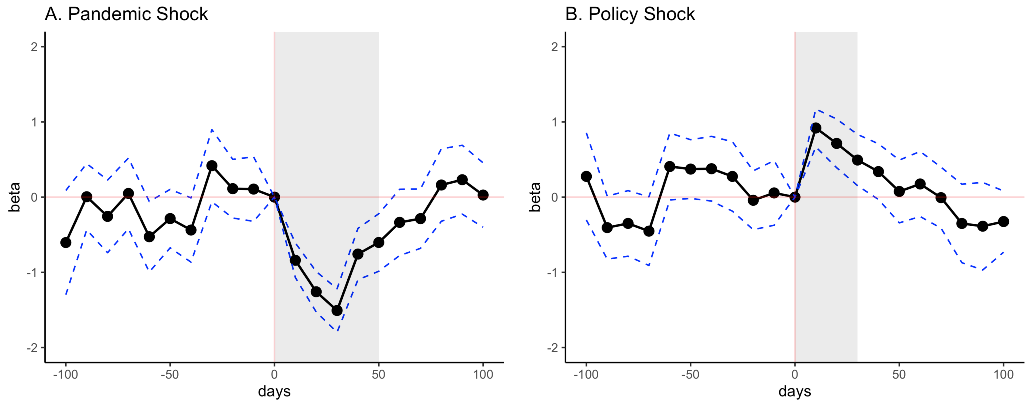

Notes: (i) This Figure shows the estimation results for event study. Panel (a) shows the results for pandemic shock while Panel (B) shows the results for advocacy shock. (ii) The black solid lines are the value of estimators. The blue dash lines denote the 95% confidential interval.

$\varepsilon_{i,j(p),t}$ is the random error clustered at the city level.

We use the C.D.F of Logit distribution as the joint function for the generalized linear model. Therefore, the parameters $\{\alpha^\tau, \beta^\tau\}$ should be interpreted as the marginal effects on the log odd ratio of fundraising, i.e. $\log \frac{\mathbb{P}(F=1)}{\mathbb{P}(F=0)}$. We set the reference period as 1 to 10 days before shocks arrived by excluding $\tau = 0$ out of the summation parts. Therefore, the coefficients $\{\alpha^\tau, \beta^\tau\}$ estimate the difference in log odd ratio between the treated and the controlled group, related to the referenced period.

The corresponding estimation result is documented in Column (1) of Appendix Table C1. In the main text, we plot the estimated coefficients with 99% confidence interval in Figure 5. Panel (a) shows the result for pandemic shock. Before the Covid-19 outbreak, the log odd ratio for fundraising did not change significantly related to the reference period. However, after the pandemic shock arrived, the value of α^τ reduces sharply to be negatively significant for around 50 days. This implies that the pandemic outbreak brought negative impact for local charitable fundraising. Charitable organizations which were affected would be less likely to start fundraising activities in response to the pandemic shock. As for the policy shocks in the Panel (b), on the contrast, it could be viewed that the government advocacies encourage fundraising, with the coefficients for β^τ being positively significant for around 40 days.

From Figure 5, we find that the parallel trend assumption is roughly satisfied, with most of the pre-treatment coefficients being insignificant. We statistically test the joint significance by χ^2 test. We cannot reject the null hypothesis that $\alpha^\tau = 0$, $\beta^\tau = 0$ for all $\tau < 0$, with the test statistics of 2.08 and 15.265, $p - value$ of 0.203 and 0.123. Therefore, we could subsequently implement a restricted estimation as

Figure 6. Restricted Specification

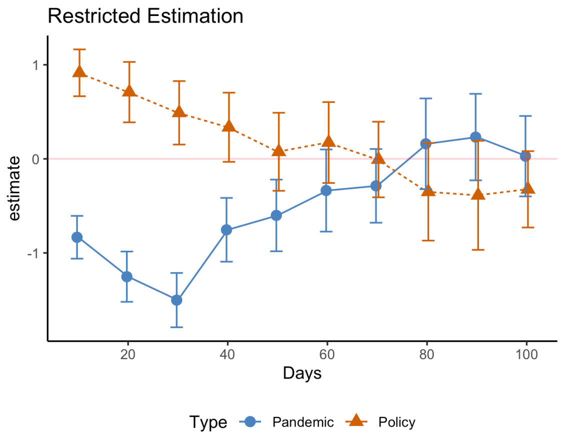

Notes: (i) This Figure shows the results for the restricted estimation, where we let the coefficients before shocks arrive to be 0. (ii) The red and blue lines denote estimators for pandemic and policy shocks respectively. The little bars denote the 95% confidential intervals.

Equation 11 to capture the Average Treatment Effect on the Treated Group (ATT) each period after the shocks arrive by restricting α^τ and β^τ to be 0, for $\tau \leq 0$.

$$F_{i,j(p),t} = \theta_i + \lambda_t + \phi_{p,y} + \psi_{p,w} + \rho_{p,d} + \sum_{\tau=1}^{10} \alpha^\tau C^\tau_{j(p),t} + \sum_{\tau=1}^{10} \beta^\tau G^\tau_{j(p),t} + \varepsilon_{i,j(p),t}. \quad (11)$$

We show the corresponding estimation table in Column (2) of Appendix Table C1. Figure 6 visualizes the result for the restricted estimation. The blue and orange connected lines indicate the effects from pandemic and policy shocks respectively. Consistent with our previous findings, the negative impact on fundraising from local pandemic outbreaks lasted for 50 days. The effective period for government advocacies is less persistent, with the coefficients for G^τ dropping back to the insignificant level at 30 days after the advocacy.

B. DID Estimation

After evaluating the dynamic effect from pandemic outbreaks and government advocacies, we now turn to our main DID specification. Given the parallel trend assumption hold and the effective treatment period presented above, we could write the DID specification as Equation 12. The explained variable and the high-dimensional fixed effects are identical to our previous specifications. $Covid_{j(p),t}$ is the DID variable for pandemic shocks. It is a binary variable which takes value 1 if the treated samples are of 0 to 50 days after the Covid-19 local outbreaks. Here, we apply our findings of effective treatment period in Figure 6. Similarly, $Policy_{j(p),t}$ equals 1 if city j is of 0 to 30 days after the government advocacies were published. By this setting, coefficients β_1 and β_2 estimate the ATT during the effective treatment periods of Covid-19 shocks and government advocacy shocks.

$$F_{i,j(p),t} = \theta_i + \lambda_t + \phi_{p,y} + \psi_{p,w} + \rho_{p,d} + \beta_1 Covid_{j(p),t} + \beta_2 Policy_{j(p),t} + \varepsilon_{i,j(p),t}. \tag{12}$$

Table II presents the estimation results for Equation 12. We keep the organization and the date fixed effects in all regressions to ensure that the specification is DID. The estimators for the direct effect (β_1 and β_2) is shown in the first panel. In Column (1) and (2), we display the results with or without province by time fixed effects. The estimators are significant with only small difference in their magnitudes. When all the interactive fixed effects are controlled, we find that $Covid_{j(p),t}$ is estimated to negatively significant, with the coefficients of -1. This implies that the log odd ratio of initiating new public fundraising activities is reduced by 1 unit on average during 0 - 50 days after the Covid-19 local outbreaks. At the same time, the coefficient for $Policy_{j(p),t}$ is estimated to be 0.734, significant at the level of 0.001. This parameter indicates that the government advocacy could increase the log-odd ratio of fundraising by 0.734 unit on average during its effective treatment period.

The Effect of Political Connection. The information about political connection for charitable organizations is unavailable in our dataset. Therefore, to study the effect from political connection, we consider two proxy variables of cross-sectional variation. The first one is the indicator for the branches of Charity Federation and Red-cross Society. As mentioned earlier, most of these charities are GOGOs. They are established and managed by the local governments. The second proxy makes use of the geographical information. We label organizations as political-connected if the geographical distance between the organization with its registered government is less than 100 metre. The intuition behind this setting is three folded. Firstly, as hinted by (Hildebrandt, 2011), Chinese government apply a "regulation by registration" policy to charitable sector before the publication of 2015 Charity Law. Organizations closer to the political centre are easier get registered. Secondly, if the organization lies sufficiently close to the government, it is more likely that this organization is privatized or split from the charity department of the government after 2008. Also, organizations that geographically close to their registered governments are naturally under stronger supervision or impact from governments.

We interact the proxy variables with our main DID variables in Equation 12 and show the corresponding results in the second panel of Table II. We find the interactive terms are all significantly positive. This implies that the negative effect

Table II. Baseline Result

	(1) Logit	(2) Logit	(3) Logit	(4) Logit
Baseline Effect				
Covid	-0.727***	-1.00***	-1.38***	-1.07***
	(0.124)	(0.111)	(0.124)	(0.114)
Policy	0.733***	0.734***	0.075	0.628***
	(0.119)	(0.135)	(0.144)	(0.137)
Political Connection				
Covid × Fed. & Red Cross			1.01***	
			(0.172)	
Policy × Fed. & Red Cross			1.03***	
			(0.181)	
Covid × $\mathbb{1}$(Dist.<100m)				0.585**
				(0.241)
Policy × $\mathbb{1}$(Dist.<100m)				0.573***
				(0.184)
Observations	3,094,248	2,873,685	2,873,567	2,873,573
Pseudo R^2	0.289	0.312	0.314	0.312
θ_i	✓	✓	✓	✓
λ_t	✓	✓	✓	✓
$\phi_{p,y}$		✓	✓	✓
$\psi_{p,w}$		✓	✓	✓
$\rho_{p,d}$		✓	✓	✓

Notes: (i) Standard error in the parentheses. Same for the rest of the tables. (ii) Column (1) and (2) of this table show the estimation results for the DID specification Equation 12. All the fixed effects are included in the Column (2). (iii) In Column (3) and (4), we include the interactive term of DID variable with the proxy variables for political connection with governments. Fed. & Red Cross is the indicator for the branches of Charity Federation and Red-cross Society. $\mathbb{1}$(Dist.<100m) is the indicator for organizations that geographically located within 100 metres from its registered governments.

from pandemic outbreak is mitigated, while the positive effect from government advocacy is amplified by political connection. Organizations with higher connection with government target higher (lower) fundraising probability subjected to pandemic (government) shocks. Furthermore, notice in the Column (3), the estimator for regressor $Policy_{j(p),t}$ positive but insignificant. Hence, government advocacies mainly motivate fundraising activity by the branches of Charity Federation and Red-cross Society, while other organizations are less responsive.

Specification and Robustness Checks. To further validate our DID results, various specification checks and robustness tests are conducted Appendix B. We firstly consider the effect of spatial spillover. We concern that charitable organizations could either precautionarily or altruistically respond to pandemic outbreaks in their neighbourhood cities. We find the effect is not statistically significant, the main regressors remain significant when the spillover effect is taken into account, with trivial change in their magnitudes.

Secondly, we implement the placebo tests by leading/lagging the treatment time or randomizing both treatment period and treatment group. The t-statistics for the placebo estimators are normally distributed around 0. Next, we control the confounding effects from some economic factors. We include the interaction between the economic variables of cross-sectional variance with the time-series indicators for the treatment periods as control variables. The main regressors remain statistically significant with little change in the magnitudes. We also rule out the effect from co-existing events including other natural disasters, the matching rescue policy and the poverty alleviation project. Our main results persist.

For the robustness of our regressions, we further estimate our DID specification by Linear Probability Model; change the explained variable; control more fixed effects; change level of the cluster standard error. Our main findings are not sensitive to these alterations.

Taken together, the estimation results are consistent with the predictions of the theoretical model in section III.. Charitable organizations at cities with local outbreak of pandemic are less likely to initiate fundraising activities, compared to the controlled organizations at the unaffected cities. On the other hand, the collaboration advocacies from government reversely encourage charitable fundraising. We also notice that the magnitude for the coefficient for $Covid_{j,t}$ is larger than that for $Policy_{j,t}$ after controlling all the fixed effects. Therefore, we believe that the negative impact brought by pandemics outweighs the effect by government advocacy.

Similar to Deryugina and Marx (2021) which also follows DID approach to evaluate effect on donation from natural disaster, we must be careful when interpreting our result. The DID estimator is local that it implies nothing on the national change in fundraising level. All the organization-homogeneous but time-varying shocks would be partial out. The ATTs we evaluate only capture the difference change between the treatment and control group. That is, we cannot claim that cities under Covid-19 outbreak would reduce their overall fundraising effort.[38] Instead, our result only suggests that charitable organizations that experienced local outbreaks of pandemic (for the same reasoning, government advocacy) would target relatively lower (higher) fundraising efforts, compared with their counterparts that received no treatments. Second, our DID estimations evaluate the relative change during the effective treatment period. The overall change could be different as the

[38]For the national response of fundraising, as shown in our descriptive evidence Figure 3 and Table I, the aggregate fundraising effort was increased during the pandemic that there exists an additional bunch at Feb of 2020. The overall increase of fundraising is similar to the lifting effect in Muller and Kräussl (2011); Scharf and Smith (2015); Tiefenbach and Kohlbacher (2015). We will explore more on this later.

out-of-event-window effect could be of the opposite direction (Cengiz et al., 2019). We will further discuss this problem in the subsequent part of the paper.

C. Overall Effect and National Shocks

In this section, we will complement our analysis in two directions. Firstly, the treatment effects in the last section is short-run as we manually assign 50 and 30 days of effective treatment periods to the pandemic and government shocks. However, the overall effect could be different from the local effect (Cengiz et al., 2019). In the long run, the time-cumulative response to shocks could be different due to the out-of-event-window impact. Secondly, the treatment effects in the last session only estimate the difference in fundraising efforts between the treated and controlled cities. The national response to shocks is unevaluated as it is absorbed by the date fixed effects. We will further our studies in these two aspects.

Overall Effect. To examine the treatment effects in a relatively longer run, we gradually extend the effective treatment periods by estimating Equation 13. The notation for the explained variable and fixed effects are identical to our previous specifications. Differently, $\tilde{C}^{\tau}_{j(p),t}$ are dummies which take value of 1 if the observations are of 0 to τ days after the Covid-19 local outbreaks. The same logic applies for the government advocacy shocks $\tilde{G}^{\tau}_{j(p),t}$. We let τ goes through every 10 days after the treatment date. The coefficients reflect the running-sum effect on fundraising efforts for k days after the shocks arrive. The coefficients α and β captures the running-sum effects in τ days after the treatments.

$$\begin{aligned} F_{i,j(p),t} =& \theta_i + \lambda_t + \phi_{p,y} + \psi_{p,w} + \rho_{p,d} + \alpha \tilde{C}^{\tau}_{j(p),t} + \beta \tilde{G}^{\tau}_{j(p),t} + \varepsilon_{i,j(p),t}, \\ & \text{for } \tau \in \{10, 20, 30, 40...\}. \end{aligned} \tag{13}$$

Next, to obtain the overall effect, we regress

$$F_{i,j(p),t} = \theta_i + \lambda_t + \phi_{p,y} + \psi_{p,w} + \rho_{p,d} + \alpha C\tilde{ovid}_{j(p),t} + \beta Po\tilde{licy}_{j(p),t} + \varepsilon_{i,j(p),t}, \tag{14}$$

where $C\tilde{ovid}_{j(p),t}$ and $Po\tilde{licy}_{j(p),t}$ are dummies which for all the samples observed after the shocks arrive.

In Panel (a) of Figure 7, we show the running-sum effect obtained by Equation 13. The green bars denote the 99% confidential intervals for local pandemic shocks. The effects decrease in the first 30 days. Then, the coefficients remain negatively significant at around -0.5 while we extend the treatment periods. For government advocacy shock in blue bars, the running-sum effect is positive during the first 200 days after the treatment. However, the coefficients become insignificant from 200 days onward.

Figure 7. Overall Effect

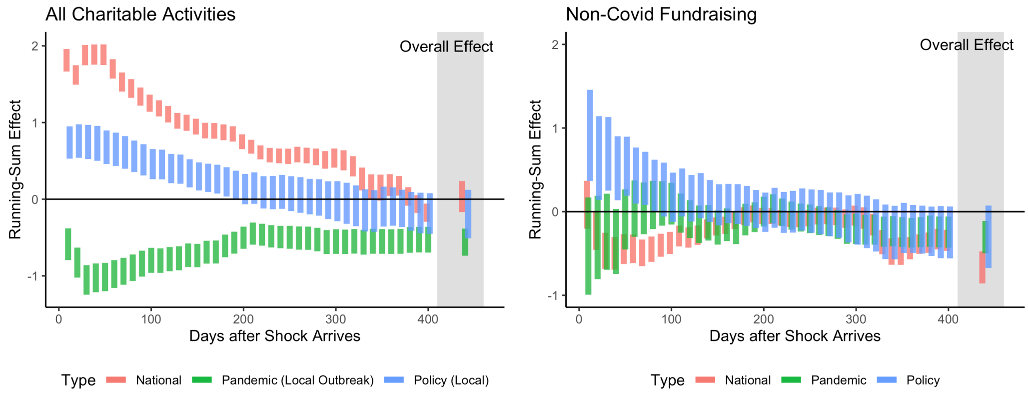

(a) **(b)**

Notes: (i) This Figure plots the effect on fundraising efforts when we extend the event window. (ii) The red bars represent the 95% confidential intervals for the aggregate effect from national outbreak of pandemic. The blue and green bars represent the effects from local outbreaks and government advocacies. (iii) The bars in the shadowed area are the overall effect, obtained by letting the event window to be all periods after the shocks arrived. (iv) Panel (B) replicates the estimations for those no-for-Covid activities.

The estimation result for overall effect by Equation 14 is displayed in Column (1) of Table III and plot in the shadowed area of Figure 7. It could be viewed that the negative impact from pandemic shocks is persistently negative, with its overall effect estimated to be -0.56. However, for the policy shocks, the effect is not long-lasting that the overall coefficient is estimated to be insignificant. This implies that the political advocacies could only boost fundraising efforts temporarily. In the long run, they are not effective. The results might arise because charitable organizations shift their future fundraising activities forward just to meet government's request. That is, the organizations may target a lower fundraising effort subsequently after they fulfil governments' suggestion. The total number of fundraising activities during a long period, however, remains nearly unchanged.

National Response. The second pitfall for our previous research is that the DID strategy does not capture any national-aggregate response of fundraising, which is partialed out by the time fixed effect. We now evaluate the impact on aggregate fundraising probability from Covid-19 outbreak by Equation 15. Here, our main explanatory variable $National_t^\tau$ exploits the time-series variation. It indicates the observations during period from 2020-01-20 to τ days later.[39] Technically, to estimate the coefficient of this variable, we need to exclude the time fixed effect λ_t.

[39] We let 2020-01-20 as the begin date of national pandemic. On this day, Dr. Nanshan Zhong, the most famous pulmonologist in China, announced that the Covid-19 was proved to be transmissive among human being. From this date, Chinese people began to understand the infection of this disease.

Table III. Overall Effect

	ProbCharity		ProbCharity_other	
	(1)	(2)	(3)	(4)
	Logit	Logit	Logit	Logit
$\tilde{Covid}$	-0.560***		-0.304***	
	(0.108)		(0.117)	
$\tilde{Policy}$	-0.194		-0.300	
	(0.192)		(0.227)	
$NationalShock$		0.034		-0.666***
		(0.123)		(0.116)
Observations	2,873,583	3,234,513	1,516,437	1,726,476
Pseudo R^2	0.311	0.287	0.292	0.278
θ_i	✓	✓	✓	✓
λ_t	✓		✓	
$\phi_{p,y}$	✓	✓	✓	✓
$\psi_{p,w}$	✓	✓	✓	✓
$\rho_{p,d}$	✓	✓	✓	✓

Notes: (i) Column (1) and (2) use whether organization hold charitable activities as the explained variable. In Column (3) and (4), we restrict our attention on charities that are uncorrelated to Cvoid-19. (ii) In Column (1) and (3), we evaluate the overall effect from the local outbreaks of Covid-19 and government advocacy. Variables $\tilde{Covid}$ and $\tilde{Policy}$ are dummies that assign value 1 to the treated samples after the shocks arrived. (iii) In Column (2) and (4), we omit the date fixed effect to capture the national response of fundraising. $NationalShock$ is dummy indicating all observations after the date of 2020-01-20.

$$\begin{aligned} F_{i,j(p),t} =& \theta_i + \phi_{p,y} + \psi_{p,w} + \rho_{p,d} + \delta National_t^{\tau} + \varepsilon_{i,j(p),t}, \\ & \text{for } \tau \in \{10, 20, 30, 40...\}. \end{aligned} \tag{15}$$

The red bars in Panel (a) of Figure 7 shows the estimation results for δ. The national change gives different picture from our previous estimations for the local effects. On average, the nationwide fundraising probability increased after the Covid-19 shocks arrived. Then, the effect decayed gradually. We also estimate the overall effect of national shock in Column (2) of Table III, where $NationalShock$ indicates all the samples after the date 2020-01-20. We find that the national increase in the fundraising efforts is not persistent, with the coefficient being statistically insignificant.

Finally, to study the potential shifting (crowd-out) effect among different causes of charitable activities, we follow a similar strategy to check the change of those not-for-Covid charitable fundraising activities. We replace the explained variable by $\tilde{F}_{i,j(p),t}$, which is a dummy that equals 1 if organization i initiated new not-for-Covid fundraising activities at date t. The results are demonstrated in Panel (b) of Figure 7 and Column (3) to (4) of Table III. We find that the national change in not-for-Covid activity was reduced after the pandemic outbreak. Such effect persists in a relatively longer run.

Taken all together, for the nationwide change in fundraising, our empirical evidence detect a temporary lifting effect and a persistent shifting effect. In the short run. Charitable organizations might respond to the Covid-19 by holding more fundraising activities (lifting). Such increase of fundraising activity was mainly contributed by Covid-directed activities. Those not-for-Covid activities, on the other hand, were crowded out (shifting). This indicates that fundraising for Covid-19 indeed came to a cost for other types of fundraising activities. In the long run, the change in total fundraising is insignificant, while the negative impact on not-for-Covid fundraising persists.

D. Mechanism

In the theoretical model in section III., the change of fundraising behaviour is induced by the income effect for the local outbreaks of pandemics and by the cost effect for the government advocacy. We now provide some supportive evidence for these mechanisms.

Income Effect. For the income effect, our model indicates that charitable organizations are less likely to initiate fundraising activities during outbreaks of pandemics because donors give less, which reduces the total donation collected. However, because the monthly or daily panel data for residence income is generally not available in China, we consider two proxy variables for donors' income loss. The first one is the severity index of infection. Here we actually assume that people live in cities higher infection rate would lose more income on average. This assumption is widely adopted in the epidemiological economic models (see e.g. Goenka, Liu and Nguyen (2014); Goenka, Liu and Pang (2024) etc.). This index is calculated using Equation 16. We count the total number of infection in each wave outbreak where $I_{j,t}$ is the number of infection and $\mathcal{T}_j$ is the set for outbreak episode defined in section IV.. We mark that this index is of the panel variation because cities could experienced multiple waves of outbreaks.

$$WaveInc_{j,t} = \begin{cases} \log(\sum_{t\in\mathcal{T}_j} I_{j,t}) & \text{if outbreak} \\ 0 & \text{else.} \end{cases} \tag{16}$$

Secondly, notice that the Chinese government imposed very strict lock-down during the Covid pandemics. Residences in the cities with pandemic outbreaks are restricted from working in the workplace. Workers for the service sector or small business enterprises may lose large part of their income. Thus, the second proxy for the income effect we consider is the lockdown intensity index. We apply the data of

Baidu Mobility Intensity from the China Data Lab of Harvard University. Appendix Figure D7 shows the evolution of mobility intensity in each city. We accordingly let the period from 01-Jan-2020 to 20-Jan-2020 to be the pre-lockdown period; from 01-Feb-2020 to 01-Mar-2020 to be the lockdown period. We calculate the lockdown intensity of each city by

$$LockDown_j = \frac{-(M_j^{Lock} - M_j^{Pre})}{M_j^{Pre}}, \tag{17}$$

where M_j^{Pre} and M_j^{Lock} denotes the average mobility intensity of city j during the pre-lockdown and lockdown period.[40] This expression evaluates the fractional change on average mobility intensity before and during the lockdown

We interact the proxy variables $WaveInc$ and $LockDown$ with our DID variables in our baseline DID specification. Column (1) and (2) of Table IV show the corresponding results. It can be viewed that the estimators for the interactive terms are negatively significant. This implies that fundraising is more vulnerable to pandemic if the city is subjected to larger income drop. The government advocacy, on the other hand, becomes less effective in motivating charitable organization to hold fundraising activities.

To provide further supplemental evidences for the income effect, we employ the financial record data for charitable activities to evaluate the impact for donation received. We regress the average daily donation received[41] on the DID variables. As the financial record data is linked with the Covid and government data by the key of initiation time, the coefficients estimated for our DID variables measure the change in difference between the activities that initiated during the treatment period with others. The result is shown in Column (3) of Table IV. The estimator for $Covid$ is not significantly different from 0, with its significance level of 0.17 being close to 1%. The insignificance could be result from the low quality of financial record data. However, the negative sign of the estimator for $Covid$ supports our theoretical prediction that the total donation collected is lower if the fundraising activities are initiated during the local outbreaks of pandemics.

Cost Effect. When it comes the mechanism for government advocacy, our model proposes that the governments may provide political convenience or other support for organizations that follow the advocacies. This could reduce the politi-

[40]The lockdown intensity index does not vary across waves of outbreaks as the severity index $WaveInc$. We don't calculate different index for different waves of outbreaks. This is because the mobility index remains low after the onset outbreak. The change for the mobility index across waves is small.

[41]We use the average donation instead of total donation to get rid of the impact from different duration of fundraising activities. The donation received is naturally higher if the activity last for a longer period. We drop all the records for ongoing fundraising activities. The average daily donation received is calculated by the ratio of total donation over duration of fundraising activity.

Table IV. Mechanism

	ProbCharity (1) Logit	ProbCharity (2) Logit	Donation (3) OLS	Cost (4) OLS
Covid	-0.624***	1.69***	-1.33	0.888
	(0.151)	(0.530)	(0.968)	(0.628)
Policy	1.13***	2.69***	0.244	-1.22**
	(0.164)	(0.409)	(0.863)	(0.485)
$Covid \times WaveInc$	-0.071***			
	(0.027)			
$Policy \times WaveInc$	-0.096***			
	(0.028)			
$Covid \times LockDown$		-4.45***		
		(0.876)		
$Policy \times LockDown$		-3.76***		
		(0.672)		
Observations	2,873,579	2,380,551	8,129	8,165
Pseudo R^2	0.312	0.305	0.202	0.205
θ_i	✓	✓	✓	✓
λ_t	✓	✓	✓	✓
$\phi_{p,y}$	✓	✓	✓	✓
$\psi_{p,w}$	✓	✓	✓	✓
$\rho_{p,d}$	✓	✓	✓	✓

Notes: (i) Column (1) and (2) use our main data set of charitable fundraising. We include the interactive terms between DID variables with the infection severity $WaveInc$ and the lockdown intensity $LockDown$. (ii) Column (3) and (4) use the dataset of financial records for fundraising activities. The explained variables are the average daily donation received and the average daily cost of the activities.

cal or management cost for holding fundraising activities. To empirically test this channel, we stay with the financial record data and regress the daily cost of activity on the DID variables, as in Column (4) of Table IV. It could be viewed that the estimator for *Policy* is significantly negative as anticipated, while the estimator for *Covid* remains insignificant. This implies that the fundraising cost for activities held in response to the publication of government advocacies is relatively smaller.

E. Discussion

Our paper evaluates the fundraising behavior of charitable organizations. Now we return to the question posed at the outset: does charitable fundraising respond to disasters, or to corresponding government initiatives? According to our empirical studies from China, the answer is both, though the responses vary in direction. Collectively, charitable organizations increase their fundraising efforts to the disasters. However, when disasters impact donor income domestically, charitable fundraising responses are negative. Conversely, government advocacy effectively boosts short-run fundraising efforts. Fundraising during local pandemic outbreaks tends to react more to government initiatives, an effect underscored by the political connections within the charitable sector. These organizations act as instruments for the government, providing extra public goods or services in exchange for political convenience.

Given that charitable organizations may comply with government advocacy, this leads us to another fundamental question: are non-profit organizations, such as charities in China, truly non-profitable and charitable? Economically speaking, our answer is likely not. A key criterion for charities to be considered truly charitable in our analysis is their ability to internalize the externality of disaster. During the Covid pandemic, this externality is evident as the demand for private support in disaster relief increases, while supply diminishes due to the income effect. Ideally, the social benefit would be enhanced if charitable organizations aimed to increase fundraising efforts, thereby attracting more social donations for redistribution. However, our empirical evidence contradicts this narrative. Further reviewing the underlying assumptions in our theoretical model, we find that charitable organizations aim to maximize net benefits, aligning generally with the profit maximization problem of a firm, even though their "revenue" is total donations, which are interpreted as social impact (Andreoni and Payne, 2003). Fundraising behavior during pandemics is driven by factors that alter the organization's cost and benefit, while social benefit is not included in their objective function.

In this context, political intervention by the government may not necessarily distort public good provision by the charitable sector. This contrasts with the findings of Bertrand et al. (2020); Petrova et al. (2020), where political intervention could crowd-out charitable donations to disasters. Instead, the collaborative policy we evaluate in our paper could be a viable method to internalize the externality by crowding-in charitable fundraising. However, this approach is sustained by political connections, and its effects may be short-lived. Whether this approach is more effective than others, such as direct subsidies like those in the UK (Gov.UK, 2021), remains to be discussed.

VI. Concluding Remarks

In this article, we examine the organizational response of charitable fundraising to large-scale public health crisis and political interference. We evaluate the shocks of Covid-19 and the collaboration advocacies from governments. We firstly build a partial equilibrium model to generate several theoretical predictions. We then employ the data of Chinese charitable organizations to empirically test the predictions.

Our paper yields following suggestive conclusions. First, at the aggregate level, we find the national outbreak of pandemic lifts the nationwide fundraising probability. This might arise that the national public health event attracts donors' attention, bringing a reduction for the diversity of preference for donors and hence increase the marginal benefit of fundraising.

However, when it comes to the local impact from Covid-19 outbreak, we find that charitable organizations in the outbreak cities would target relatively lower probability of initiating fundraising activities, compared with their referenced cities without new infections. We find the drop is statistically significant and persistent. It might due to the negative income effect brought by infection and social restrictions. Donors' may hence give less, implying a reduction in the expected fund collected by charitable organizations. Organizations hence target lower fundraising efforts.

Finally, we find the collaboration advocacies from governments, on the other hand, motivate charitable organizations to hold fundraising activities. As a mechanism, we suggest that governmental advocacy as a political signal could decrease the expected fundraising cost. Charitable organizations may believe that government would provide political convenience or release useful market information for the conformers. However, we mark that the direct political interference via advocacy may not be a sustainable tool for governments. The effect is shown to be less persistent that organizations might just shift their future fundraising effort forward, leaving the overall effort unchanged.

References

Alfaro, Laura, Oscar Becerra, and Marcela Eslava. 2020. "EMEs and Covid-19: shutting down in a world of informal and tiny firms." National Bureau of Economic Research.

Almond, Douglas, Xinming Du, and Shuang Zhang. 2020. "Ambiguous pollution response to Covid-19 in China." National Bureau of Economic Research.

Almunia, Miguel, Irem Guceri, Ben Lockwood, and Kimberley Scharf. 2020. "More giving or more givers? The effects of tax incentives on charitable donations in the UK." Journal of Public Economics, 183: 104114.

Andreoni, James, Abigail Payne, and Sarah Smith. 2014. "Do grants to charities crowd out other income? Evidence from the UK." Journal of Public Economics, 114: 75–86.

Andreoni, James, and A Abigail Payne. 2003. "Do government grants to private charities crowd out giving or fund-raising?" American Economic Review, 93(3): 792–812.

Andreoni, James, and A Abigail Payne. 2011. "Is crowding out due entirely to fundraising? Evidence from a panel of charities." Journal of public Economics, 95(5-6): 334–343.

Benmelech, Efraim, and Nitzan Tzur-Ilan. 2020. "The determinants of fiscal and monetary policies during the Covid-19 crisis." National Bureau of Economic Research.

Bergstrom, Theodore, Lawrence Blume, and Hal Varian. 1986. "On the private provision of public goods." Journal of public economics, 29(1): 25–49.

Bertrand, Marianne, Matilde Bombardini, Raymond Fisman, and Francesco Trebbi. 2020. "Tax-exempt lobbying: Corporate philanthropy as a tool for political influence." American Economic Review, 110(7): 2065–2102.

Bertrand, Marianne, Matilde Bombardini, Raymond Fisman, Brad Hackinen, and Francesco Trebbi. 2021. "Hall of mirrors: Corporate philanthropy and strategic advocacy." The Quarterly Journal of Economics, 136(4): 2413–2465.

Branas-Garza, Pablo, Diego Jorrat, Antonio Alfonso-Costillo, Antonio M Espin, Teresa García, and Jaromír Kovářík. 2020. "Exposure to the Covid-19 pandemic and generosity."

Butler, Patrick. 2021. "Charities face cash crisis as virus fears hit fundraising."

CAF. 2021. "Charities likely to reduce services as lockdown bites."

Cai, Qihai, Aya Okada, Bok Gyo Jeong, and Sung-Ju Kim. 2021. "Civil Society Responses to the Covid-19 Pandemic." China Review, 21(1): 107–138.

Cengiz, Doruk, Arindrajit Dube, Attila Lindner, and Ben Zipperer. 2019. "The effect of minimum wages on low-wage jobs." The Quarterly Journal of Economics, 134(3): 1405–1454.

Chan, Kam C, and Xunan Feng. 2019. "Corporate philanthropy in a politically uncertain environment: does it bring tangible benefits to a firm? Evidence from China." The European Journal of Finance, 25(3): 256–278.

Chatterjee, Chandrayee, James C Cox, Michael K Price, and Florian Rundhammer. 2020. "Robbing Peter to Pay Paul: Understanding How State Tax Credits Impact Charitable Giving." National Bureau of Economic Research.

Chetty, Raj, John N Friedman, Michael Stepner, and Opportunity Insights Team. 2023. "The Economic Impacts of Covid-19: Evidence from a New Public Database Built Using Private Sector Data." The Quarterly Journal of Economics, qjad048.

Cinnamon, Jonathan. 2020. "Platform philanthropy,'public value', and the Covid-19 pandemic moment." Dialogues in Human Geography, 2043820620933860.

Clemens, Jeffrey, and Stan Veuger. 2020. "Implications of the Covid-19 pandemic for state government tax revenues." National Bureau of Economic Research.

Deryugina, Tatyana, and Benjamin M Marx. 2021. "Is the supply of charitable donations fixed? Evidence from deadly tornadoes." American Economic Review: Insights, 3(3): 383–98.

Dong, Qiang, and Jiahuan Lu. 2020. "In the shadow of the government: The Chinese nonprofit sector in the Covid-19 crisis." The American Review of Public Administration, 50(6-7): 784–789.

Duquette, Nicolas J. 2016. "Do tax incentives affect charitable contributions? Evidence from public charities' reported revenues." Journal of Public Economics, 137: 51–69.

Fack, Gabrielle, and Camille Landais. 2010. "Are tax incentives for charitable giving efficient? Evidence from France." American Economic Journal: Economic Policy, 2(2): 117–41.

Fang, Hanming, Long Wang, and Yang Yang. 2020. "Human mobility restrictions and the spread of the novel coronavirus (2019-ncov) in china." Journal of Public Economics, 191: 104272.

Fisman, Raymond, Hui Lin, Cong Sun, Yongxiang Wang, and Daxuan Zhao. 2021. "What motivates non-democratic leadership: Evidence from Covid-19 reopenings in China." Journal of Public Economics, 196: 104389.

Fitch-Fleischmann, Benjamin, and Evan Plous Kresch. 2021. "Story of the hurricane: Government, NGOs, and the difference in disaster relief targeting." Journal of Development Economics, 152: 102702.

Gao, Yongqiang, and Taïeb Hafsi. 2015. "Government intervention, peers' giving and corporate philanthropy: Evidence from Chinese private SMEs." Journal of Business Ethics, 132(2): 433–447.

Goenka, Aditya, Lin Liu, and Haokun Pang. 2024. "Health and income inequality during pandemics." working paper.

Goenka, Aditya, Lin Liu, and Manh-Hung Nguyen. 2014. "Infectious diseases and economic growth." Journal of Mathematical Economics, 50: 34–53.

Gov.UK. 2021. "Financial support for voluntary, community and social enterprise (VCSE) organisations to respond to coronavirus (Covid-19)."

Hale, Thomas, Samuel Webster, Anna Petherick, Toby Phillips, and B Kira. 2022. "Oxford COVID-19 government response tracker (OxCGRT)." Last updated, 8: 30.

Hargrave, Russell. 2021. "Economic uncertainty may lead to lower giving, warns NPC."

Haugh, Helen, and Michael Kitson. 2007. "The Third Way and the third sector: New Labour's economic policy and the social economy." Cambridge journal of economics, 31(6): 973–994.

Hildebrandt, Timothy. 2011. "The political economy of social organization registration in China." China Q., 970.

Hildebrandt, Timothy. 2013. Social organizations and the authoritarian state in China. Cambridge University Press.

Hsu, Carolyn L. 2008. " 'Rehabilitating charity' in China: the case of Project Hope and the rise of non-profit organizations." Journal of Civil Society, 4(2): 81–96.

Hua, Ruoyun. 2021. "Political Label and Selective Information Disclosure: Evidence from Charity Foundations in China." VOLUNTAS: International Journal of Voluntary and Nonprofit Organizations, 1–18.

Hungerman, Daniel M, and Mark Ottoni-Wilhelm. 2021. "Impure impact giving: Theory and evidence." Journal of Political Economy, 129(5): 1553–1614.

Hurtado, S, and J Agudelo. 2013. "The continuity and stability of corporate philanthropy donation: Evidence from Chinese Firms' Response to Disaster Relief." International journal of business and management, 8(2): 10–18.

Kess, Sidney. 2020. "Covid-19 and Charitable Contributions by Individuals and Businesses." The CPA Journal, 90(6): 10–11.

Leslie, Emily, and Riley Wilson. 2020. "Sheltering in place and domestic violence: Evidence from calls for service during Covid-19." Journal of Public Economics, 189: 104241.

Liu, Heng, Jin-hui Luo, and Victor Cui. 2018. "The impact of internationalization on home country charitable donation: Evidence from Chinese firms." Management International Review, 58(2): 313–335.

Muller, Alan, and Roman Kräussl. 2011. "Doing good deeds in times of need: A strategic perspective on corporate disaster donations." Strategic Management Journal, 32(9): 911–929.

Petrova, Maria, Ricardo Perez-Truglia, Andrei Simonov, and Pinar Yildirim. 2020. "Are Political and Charitable Giving Substitutes? Evidence from the United States." National Bureau of Economic Research.

Roberts, Russell D. 1984. "A positive model of private charity and public transfers." Journal of political Economy, 92(1): 136–148.

Saleh, Sameh Nagui, Christoph U Lehmann, and Richard J Medford. 2021. "Early crowdfunding response to the Covid-19 pandemic: Cross-sectional study." Journal of medical Internet research, 23(2): e25429.

Scharf, Kimberley, and Sarah Smith. 2015. "The price elasticity of charitable giving: does the form of tax relief matter?" International Tax and Public Finance, 22(2): 330–352.

Scharf, Kimberley A, Sarah Smith, and Mark Wilhelm. 2017. "Lift and shift: the effect of fundraising interventions in charity space and time."

Shieh, Shawn, and Guosheng Deng. 2011. "An emerging civil society: The impact of the 2008 Sichuan earthquake on grass-roots associations in China." The China Journal, , (65): 181–194.

Tiefenbach, Tim, and Florian Kohlbacher. 2015. "Disasters, donations, and tax law changes: Disentangling effects on subjective well-being by exploiting a natural experiment." Journal of Economic Psychology, 50: 94–112.

Whitehead, Harriet. 2021. "Charity retail income fell by 90start of the pandemic."

Xinhua News Agency. 2016. "Charitable Activities Make the Poverty Alleviation more Precise."

Xu, Qing, Tim K Mackey, Raphael E Cuomo, and Bryan A Liang. 2020. "An Analysis of China Health Charity Credibility Before and After the 2016 Charity Law of the People' s Republic of China." Asian Journal of Criminology, 1–36.

Zheng, Yuanchang. 2009. "Wenchuan earthquake civic donation and the inspiration of modern philanthropy within China." The China Nonprofit Review, 1(2): 247–262.

Appendices

A Government Advocacy during Covid Pandemics

At the onset of the Covid-19 pandemic, the Chinese government mobilized charitable organizations through **Collaborative Advocacy**. Both the central government and local governments issued advocacies:

(1) 26$^{\text{th}}$ Jan. 2020: Advocacy by the central government: *Announcement of Advocating Charitable Sector to Participate in the Prevention and Control of Covid-19* [Minister of Civil Affairs, Issue 476].

(2) 27$^{\text{th}}$ Jan. 2020 to 04$^{\text{th}}$ Feb. 2020: Local governments published their local advocacies.

We searched and downloaded these advocacies from the legal database by Peking University (Beida Fabao). To compile a more compact set of advocacies, we began with the central government advocacy (MCF 476) and directed our search toward all documents citing MCF 476. This approach could efficiently locate local government advocacies.

To ensure completeness by locating advocacies that not cite MCF 476, we also manually searched for documents with titles containing keywords such as {Charity, Pandemic, Covid, Donation}. Finally, we manually reviewed these documents to confirm their relevance for advocating fundraising activities. These steps yielded 62 advocacies. Two examples of these advocacies are shown in Appendix Figure D8.

MCF 476. The central government advocacy primarily encouraged charitable organizations to raise funds or public goods to assist in the government-led relief plan. The advocacy was not enforceable. The main content of the document is as follows:

(1) Charitable organizations are suggested to mobilize social donations to assist government efforts.

(2) Donations should primarily support disaster relief efforts in Wuhan, Hubei Province,[42] and prioritize the collection of Covid-related public goods, such as facial masks, ventilators, and sanitizers.

(3) Fundraising activities should comply with the 2015 Charity Law. Charitable organizations are encouraged to enhance the efficiency and transparency of managing charitable funds.

[42] This focus reflects the timing of the MCF's publication, which was at the onset of the pandemic when the outbreaks had not spread beyond Hubei Province.

(4) List the bank detail for some GOCO charitable organizations in Hubei Province, such as the Hubei Charity Federation and the Hubei Red Cross Society.

Other Local Government Advocacies. Local governments issued their own advocacies shortly after the release of MCF 476. These local advocacies can be interpreted as implementations of the central government policy, as their main content aligns with the central advocacy's goal of encouraging charitable organizations to actively participate in government-led disaster relief plans. However, we observe that local government advocacies emphasize domestic needs for charitable donations. For instance, unlike MCF 476, which prioritizes disaster relief in Hubei Province, local advocacies often recommend charitable organizations prioritize addressing domestic needs within their own jurisdictions. Specifically, we summarize the main ideas in the local government advocacies as follow:

(1) Address the high demand for public goods within the jurisdictions and emphasize the leadership of the government during the pandemic and relief efforts.

(2) Charitable organizations are encouraged to mobilize social donations to assist <u>local</u> government initiatives.

(3) Donations should primarily support <u>local</u> disaster relief efforts and prioritize the collection of Covid-related public goods, such as facial masks, ventilators, and sanitizers.

(4) Fundraising activities must comply with the 2015 Charity Law. Charitable organizations are encouraged to enhance the efficiency and transparency in managing charitable funds.

(5) List the bank details for some local GOCO charitable organizations, such as the local branches of the Charity Federation and Red Cross Society within their jurisdictions.

B Specification Checks and Robustness Checks

Specification Checks

Spatial Spillover Effect. We now apply several specification checks to further validate the causality of our main regressions. First of all Covid-19 is a highly transmissive virus. Infections in other cities could be easily spread through city boundaries. One could therefore be concerned that the spatial spillover effect may affect our estimations. That is, charitable organizations could either precautionarily or altruistically respond to pandemic outbreaks in their neighborhood cities. We concern that charitable organizations may raise fund in preparedness for future outbreaks or as reliefs for the outbreak cities. We address this problem by re-defining our pandemic shocks as follow: *a city is under contiguous outbreak if*

(1) *This city does not experience outbreak*

(2) *At least one of its contiguous cities are under Covid-19 outbreak*

We present the corresponding results for event study and the corresponding DID estimation at Appendix Figure D4 and Appendix Table C8. Column (1) and (2) define the neighborhood city by Queen contiguous. Column (3) and (4) define the neighborhood city by Rook contiguous. It could be viewed that the geographical spillover effect is not statistically significant. The main regressors remain significant when the spillover effect is taken into account, with trivial change in their magnitudes.

Placebo Tests. We implementing two placebo tests. We firstly alter the treatment period. We fix the composition of the treatment and control groups but lead and lag the treatment period for 10, 20, 30 days and so on. Then, we re-estimate our baseline model Equation 12 using the imaginary treatment period.

Recall that the effective treatment period is 50 days for the pandemic shocks and 30 days for the advocacy shocks. Thus, if we lag or lead the treatment times for more than 50 and 30 days respectively, there would not be any overlaps between the imaginary treatment periods with the real treatment periods. The imaginary ATT should therefore be insignificant if the change in fundraising probability was indeed caused by the COVID-19 and advocacy shocks.

Appendix Figure D3 shows the corresponding coefficient plot. The horizontal axis is the days of lag or lead while the vertical axis denotes the estimator with 95% confidence interval. The blue areas shadow the estimations where the imaginary treatment periods overlap with the real treatment periods. Outside the blue area, most of the estimators are not statistically significant different from 0 or have smaller magnitude. These figures lend further support to the parallel trend assumption outside the event window.

The second placebo test randomizes both treatment period and treatment group. We randomly draw 70 cities and 20 provinces[43] as the treatment group for the pandemic and policy shocks. Correspondingly, we randomly re-assign windows of 50 and 30 days as the treatment period. Then, we estimate the baseline DID specification. These steps are repeated for 1000 times. Appendix Figure D2 plots the density of the t-statistics for the placebo estimators, which are distributed around 0. It is hard to obtain the significance level of our baseline regression, denoted by the dash line. This reveals that our previous findings are unlikely to be caused by coincidence or the large observations of our data set.

Economic Factors. In the DID specification, we do not request the treatment group selection to be strictly exogenous as long as the parallel trend assumption is satisfied. But, we are still interested in introducing some control variables to reduce the economic difference between the treatment and control groups. However, it is hard to find proper controls for our daily panel data. For example, the annual GDP or population are absorbed by the fixed effects. Therefore, in our subsequent specification checks, we control some economic factors by interacting the cross-sectional variation with the time-series variation.

We firstly select the control variables by picking up factors that significantly contribute to the difference between the treated and control groups. Specifically, we regress

$$TG_j = \beta_0 + X_j\gamma + \varepsilon_j, \tag{18}$$

where the explained variables are dummies indicating the treatment groups for COVID-19 and advocacy shocks. X_j is the pool of control variables, including log population (Pop); log population growth ($PopGrowth$); log of GDP per capita ($GDPper$); growth of log GDP per capita ($GDPGrowth$); fiscal expenditure to GDP ratio ($FracFisc$); fiscal expenditure to fiscal income ratio ($FracInc$); log of passenger flow ($Transp$); and distance to Wuhan ($DistWuhan$). All these variables are collapsed into cross-sectional variables by 5-year average during 2015-2019.

Appendix Table C2 shows the selection result. In Column (1) and (2), the explained variable is the dummy variable for the treatment group of COVID-19 shocks. We find that variables Pop, $GDPper$, $FracFisc$, $Transp$, $DistWuhan$ significantly explain the economic difference between the treated cities and controlled cities. Similarly, in Column (3) and (4) where the explained variable is the dummy for the treatment group of policy shocks. There exist significant difference in $PopGrowth$ and $DistWuhan$ between the treatment and control group. Then, by selecting the significant variables, denoted by $X_j^{(Covid)}$ and $X_j^{(Policy)}$ respectively, we regress

[43] We have 70 cities and 20 provinces as treated group in our baseline specification.

Equation 19.

$$F_{i,j,p,t} = \theta_i + \lambda_t + \phi_{p,y} + \psi_{p,w} + \rho_{p,d} + \beta_1 Covid_{j,t} + \beta_2 Policy_{j,t} + Post_t \times \tilde{X}_j^{(Covid)} \gamma_1 + Post_t \times \tilde{X}_j^{(Policy)} \gamma_2 + \varepsilon_{i,j,p,t}. \tag{19}$$

In this regression, we interact the selected variables with $Post_t$, which is dummy variable indicating the treatment periods. Specifically, we let it equals 1 for periods during 2020-01-28 to 2020-02-27.

Column (1) to (3) of Appendix Table C3 shows the result for regressions controlling economic factors. Compared with our baseline coefficient, the introduction of economic control variables have negligible impact on the significance and magnitude of our core explanatory variables. It could be viewed that the treatment effect for Covid-19 outbreak is slightly reduced by 0.042, while the effect for government advocacy shock is increased by 0.048. Hence, the change in fundraising we detected is not caused by economic difference between the treated and controlled group.

Simultaneous Event. Another potential threat to our DID specification is the events that simultaneously took place with our main events. The first simultaneous event we would like to get rid of is the natural disasters, except Covid-19. Bunch of previous literature indicate that philanthropy would response to disasters (Scharf, Smith and Wilhelm, 2017; Deryugina and Marx, 2021). Hence, we merge our main data set with the domestic disaster data[44]. This data set lists the information for all the domestic natural disasters in China, including the disaster happen date, affected cities, economic loss etc.. We control the disaster shocks as an DID-style variable, setting a 30-days effective treatment period after the disaster declare date[45].

Another important confounding policy is the matching rescue policy. This form of rescue is famous and was repeatedly applied in Chinese disaster relief[46]. During the Covid pandemic, on 11 Feb of 2020, the central government matched several provinces to assist cities in Hubei at the beginning of the pandemic[47]. Such match asked the supporter provinces to send medical team, medical facilities to the recipient cities. This policy did not impose any request on charitable organizations. However, charitable sectors may respond to this policy. Appendix Table C5 shows the detail about the supporter and recipient of the match. Similarly, we control it as an DID event.

We finally consider the confounding impact by the Poverty Alleviation Programme. On 2012, the central government listed 832 National Poor Counties (NPC). As we show in the Appendix Figure D5, most of these NPC are located in the south

[44]National Disaster Reduction Center of China: `http://www.ndrcc.org.cn`.

[45]The governments usually report and declare the detail information about the disasters in the media after the disasters end.

[46]For example, the 2008 earthquake in Wenchuan; 2002 SARS pandemic etc.

[47]http://www.gov.cn/xinwen/2020-02/11/content_5477116.htm

west China. From 2015[48], Chinese government had a fierce combat with poverty and announced a victory at September of 2020 that all the listed National Poor County exited the poverty stage. Social philanthropy played an active role here that 11% of our sampled charitable activities are targeted in poverty alleviation. This could confound our finding that charitable organizations may raise their fundraising effort in response to the pressure of meeting the target of poverty alleviation rather than rather than to the Covid-19 or government advocacy.

We control this simultaneous event by following ways. We download the list of NPC from the Chinese Poverty Alleviation Database[49]. As shown in the Appendix Table C4, we have 52 counties in 7 provinces remained in NPC series at the beginning of 2020. We firstly include the interaction $PoorCounty_i \times Post_t$ into our baseline regression, where $PoorCounty_i = 1$ if organization i is located in the NPC. In this way, the difference in the change of fundraising between the NPC and the rest of counties is partialled out during the treatment periods. Alternatively, we consider the province-level interference that we control $Num.County_p \times Post_t$ where $Num.County$ is the number of NPC in province p at the beginning of the 2020.

Column (2) of Appendix Table C3 shows the results controlling the natural disaster shocks. In Column (3), we restrict the disasters to those brought massive economic loss of more than 25 million RMB. We additionally include the DID shock for the matching rescue policy in Column (4). Moreover, in Column (5) and (6), we control the confounding event of poverty alleviation. The coefficients for the Covid-19 and government advocacy shocks remain highly significant. Comparing magnitude with our baseline regressions, we find only negligible drop in the coefficient of $Covid_{j,t}$ while the effect from government advocacy become even larger. Therefore, the negative impact on fundraising brought by pandemic outbreak and the positive effect from government advocacy are not induced by the simultaneous events.

Robustness Check

We further subject our baseline results to several robustness checks. Firstly, recall that our explained variation is a dummy variable of whether holding new fundraising activities, so that our previous regressions are estimated by Logitistic model. Now we adapt this setting by using a Linear Probability Model in Column (1) of Table C6. Our findings persist that the DID coefficients are still statistically significant[50]. In Column (2) and (3), we change the explained variable to the number

[48] On 29 Sept 2015, the central government published *A Decision of Combating Poverty*

[49] https://www.jianpincn.com

[50] We also estimate the event study specification using the LPM in the Appendix Figure D6 and Column (3) and (4) of the Appendix Table C1. General patterns persist.

of activity held. Here, the explained variation becomes integers. Thus, we employ a Poisson estimation in Column (3). It could be shown that our baseline findings persist. Finally, in Column (4), we reduce the pre-treatment period by dropping observations before 2019-01-01. The coefficients for the main variables remain highly significant.

Furthermore, recall that in our baseline regression, we control the province $\times$ year, province $\times$ week, and province $\times$ day of week fixed effect to address the endogeneity that our estimation could be driven by the province-specified trend. In the Appendix Table C7, we partial out more variations by controlling the (City, County, Organization) $\times$ (Year, Week, Day of Week) fixed effects. The magnitude of our treatment effects are reduced. Nonetheless, the estimators remain significant that our baseline results are largely robust. Finally, in Column (4) and (5) of Appendix Table C7, we show that the significance of the estimators are not sensitive to altering the level of clustered standard error.

C Table

Table C1. Event Study

	ProbCharity			
	(1) Logit	(2) Logit	(3) OLS	(4) OLS
Pandemic_b10	-0.604 (0.421)		-0.003*** (0.0006)	
Pandemic_b9	0.005 (0.268)		-8.11×10^{-5} (0.0008)	
Pandemic_b8	-0.256 (0.293)		-0.0008 (0.0009)	
Pandemic_b7	0.049 (0.286)		0.0006 (0.001)	
Pandemic_b6	-0.527* (0.284)		-0.001 (0.0009)	
Pandemic_b5	-0.286 (0.236)		0.0007 (0.001)	
Pandemic_b4	-0.438* (0.260)		-0.0008 (0.001)	
Pandemic_b3	0.418 (0.292)		0.002 (0.001)	
Pandemic_b2	0.112 (0.237)		0.002* (0.001)	
Pandemic_b1	0.107 (0.261)		0.001 (0.001)	
Pandemic_a1	-0.840*** (0.140)	-0.834*** (0.138)	0.003 (0.002)	0.002 (0.002)
Pandemic_a2	-1.26*** (0.163)	-1.25*** (0.163)	-0.004** (0.002)	-0.004** (0.002)
Pandemic_a3	-1.51*** (0.176)	-1.50*** (0.176)	-0.006*** (0.002)	-0.006*** (0.002)
Pandemic_a4	-0.757*** (0.208)	-0.754*** (0.206)	-0.0004 (0.001)	-0.0004 (0.001)
Pandemic_a5	-0.603*** (0.232)	-0.601*** (0.232)	-0.0009 (0.001)	-0.0010 (0.001)
Pandemic_a6	-0.336 (0.268)	-0.337 (0.265)	-0.0009 (0.001)	-0.0009 (0.001)
Pandemic_a7	-0.286 (0.240)	-0.287 (0.238)	-0.001 (0.0009)	-0.001 (0.0009)
Pandemic_a8	0.161 (0.293)	0.160 (0.293)	-0.0004 (0.0009)	-0.0004 (0.0009)
Pandemic_a9	0.231 (0.278)	0.231 (0.280)	0.0005 (0.0010)	0.0005 (0.0010)
Pandemic_a10	0.028 (0.260)	0.028 (0.260)	0.001 (0.001)	0.0010 (0.001)
Policy_b10	0.276 (0.352)		0.0009 (0.0007)	
Policy_b9	-0.406 (0.255)		-0.0005 (0.0008)	
Policy_b8	-0.350 (0.265)		-0.0008 (0.0009)	
Policy_b7	-0.452 (0.278)		-0.0008 (0.0009)	
Policy_b6	0.407 (0.270)		0.001 (0.0009)	
Policy_b5	0.373 (0.237)		0.002* (0.001)	
Policy_b4	0.377 (0.261)		0.002* (0.001)	
Policy_b3	0.275 (0.281)		0.001 (0.001)	
Policy_b2	-0.042 (0.238)		-0.0002 (0.001)	
Policy_b1	0.055 (0.261)		-0.0003 (0.001)	
Policy_a1	0.919*** (0.153)	0.915*** (0.151)	0.009*** (0.002)	0.010*** (0.002)
Policy_a2	0.714*** (0.197)	0.709*** (0.195)	0.004** (0.002)	0.004** (0.002)
Policy_a3	0.493** (0.207)	0.489** (0.205)	0.0004 (0.001)	0.0004 (0.001)
Policy_a4	0.339 (0.225)	0.336 (0.224)	2.64×10^{-5} (0.001)	7.44×10^{-5} (0.001)
Policy_a5	0.075 (0.254)	0.075 (0.252)	-0.0002 (0.0010)	-0.0001 (0.0010)
Policy_a6	0.175 (0.263)	0.174 (0.261)	0.0009 (0.0010)	0.0009 (0.0010)
Policy_a7	-0.007 (0.246)	-0.007 (0.244)	-0.0002 (0.0009)	-0.0001 (0.0009)
Policy_a8	-0.350 (0.317)	-0.350 (0.315)	-0.0005 (0.0009)	-0.0005 (0.0009)
Policy_a9	-0.387 (0.354)	-0.388 (0.352)	-0.0010 (0.0009)	-0.0009 (0.0009)
Policy_a10	-0.325 (0.248)	-0.324 (0.247)	-0.001 (0.0009)	-0.001 (0.0009)
Observations	2,873,567	2,873,567	3,495,104	3,495,104
Pseudo R^2	0.312	0.312	-0.021	-0.021
θ_i	✓	✓	✓	✓
λ_t	✓	✓	✓	✓
ProvCode×year	✓	✓	✓	✓
ProvCode×week	✓	✓	✓	✓
ProvCode×DOW	✓	✓	✓	✓

Table C2. Control Variables Selection

	TG_Covid		TG_Policy	
	(1)	(2)	(3)	(4)
	Logit	OLS	Logit	OLS
(Intercept)	-38.1***	-4.04***	5.70	1.69
	(12.7)	(0.965)	(7.80)	(1.49)
Pop	1.56**	0.196***	0.135	0.011
	(0.641)	(0.069)	(0.511)	(0.093)
PopGrowth	0.056	-0.0002	-0.196***	-0.036***
	(0.062)	(0.005)	(0.049)	(0.007)
GDPper	1.92**	0.229***	-0.548	-0.109
	(0.977)	(0.087)	(0.654)	(0.124)
GDPGrowth	-0.024	-0.004	0.015	0.005
	(0.135)	(0.014)	(0.105)	(0.020)
FracFisc	13.8**	2.10***	3.77	0.764
	(6.39)	(0.613)	(5.69)	(1.02)
FracInc	-1.33	-0.130	-1.51	-0.227
	(2.10)	(0.219)	(1.71)	(0.314)
Transp	0.992**	0.093**	0.331	0.060
	(0.399)	(0.040)	(0.331)	(0.058)
DistWuhan	-0.004**	-0.0003***	-0.002***	-0.0004***
	(0.002)	(7.28×10^{-5})	(0.0005)	(7.39×10^{-5})
Observations	238	238	238	238
R^2	0.395	0.309	0.175	0.164

Table C3. Regression with Control Variables

	ProbCharity					
	(1)	(2)	(3)	(4)	(5)	(6)
	Logit	Logit	Logit	Logit	Logit	Logit
$Covid_{j,t}$	-0.958***	-0.957***	-0.957***	-0.958***	-0.946***	-0.938***
	(0.156)	(0.156)	(0.156)	(0.156)	(0.156)	(0.157)
$Policy_{j,t}$	0.781***	0.783***	0.786***	0.777***	0.779***	0.790***
	(0.157)	(0.157)	(0.157)	(0.157)	(0.157)	(0.160)
Controls:Covid	✓	✓	✓	✓	✓	✓
Controls:Policy	✓	✓	✓	✓	✓	✓
Disaster		✓		✓	✓	✓
Disaster (Massive)			✓			
Matching Rescue				✓	✓	✓
Poor County					✓	✓
Num. Poor County						✓
Observations	2,276,564	2,276,591	2,276,651	2,276,569	2,276,588	2,276,558
Pseudo R^2	0.305	0.305	0.305	0.305	0.306	0.306
θ_i	✓	✓	✓	✓	✓	✓
λ_t	✓	✓	✓	✓	✓	✓
$\phi_{p,y}$	✓	✓	✓	✓	✓	✓
$\psi_{p,w}$	✓	✓	✓	✓	✓	✓
$\rho_{p,d}$	✓	✓	✓	✓	✓	✓

Table C4. National Poor Counties 2020

Province	Number	County
广西 (Guangxi)	8	隆林县 (Longlin)、融水县 (Rongshui)、罗城县 (Luocheng)、乐业县 (Leye)、那坡县 (Napo)、大化县 (Dahua)、三江县 (Sanjiang)、都安县 (Duan)
四川 (Sichuan)	7	美姑县 (Meigu)、布拖县 (Butuo)、昭觉县 (Zhaojue)、金阳县 (Jinyang)、喜德县 (Xide)、越西县 (Yuexi)、普格县 (Puge)
贵州 (Guizhou)	9	紫云县 (Ziyun)、望谟县 (Wangmo)、从江县 (Congjiang)、晴隆县 (Qinglong)、沿河县 (Yanhe)、榕江县 (Rongjiang)、赫章县 (Hezhang)、纳雍县 (Nayong)、威宁县 (Weining)
云南 (Yunnan)	9	会泽县 (Huize)、镇雄县 (Zhenxiong)、宁蒗县 (Ninglang)、澜沧县 (Lancang)、屏边县 (Pinbian)、广南县 (Guangnan)、泸水市 (Lushui)、福贡县 (Fugong)、兰坪县 (Lanpin)
甘肃 (Gansu)	8	宕昌县 (Tanchang)、西和县 (Xihe)、礼县 (Li)、东乡县 (Dongxiang)、临夏县 (Linxia)、镇原县 (Zhenyuan)、通渭县 (Tongwei)、岷县 (Min)
宁夏 (Ningxia)	1	西吉县 (Xiji)
新疆 (Xinjiang)	10	皮山县 (Pishan)、洛浦县 (Lopu)、策勒县 (Cele)、墨玉县 (Moyu)、于田县 (Yutian)、叶城县 (Yecheng)、伽师县 (Jiashi)、英吉沙县 (Yingjisha)、莎车县 (Shache)、阿克陶县 (Aketao)

Table C5. Matching Policy

Supporter (province)	Recipient (city)	Supporter (province)	Recipient (city)	Supporter (province)	Recipient (city)
Guangdong	Wuhan, Jingzhou	Zhejiang	Wuhan, Jingmen	Chongqing	Wuhan, Xiaogan
Jiangsu	Wuhan, Huangshi	Fujian	Wuhan, Yichang	Shannxi	Wuhan
Tianjin	Wuhan, Enshi	Shanxi	Wuhan, Xiantao, Tianmen, Qianjiang	Yunnan	Wuhan, Xianning
Xinjiang	Wuhan	Shandong	Wuhan, Huanggang	Hunan	Wuhan, Huanggang
Heilongjiang	Wuhan, Xiaogan	Jiangxi	Wuhan, Suizhou	Henan	Wuhan
Guizhou	Wuhan, Ezhou	Liaoning	Wuhan, Xiangyang	Jilin	Wuhan
Gansu	Wuhan	Ningxia	Wuhan, Xiangyang	Sichuan	Wuhan
Beijing	Wuhan	Anhui	Wuhan	Guangxi	Wuhan, Shiyan
Shanghai	Wuhan	Neimeng	Wuhan, Jingmen	Hebei	Wuhan, Shengnongjia
Hainan	Wuhan, Jingzhou	Qinghai	Wuhan		

Table C6. Robustness Check 1

	ProbCharity	NumActivity		ProbCharity
	(1)	(2)	(3)	(4)
	OLS	OLS	Poisson	Logit
$Covid_{j,t}$	-0.002**	-0.003***	-0.768***	-0.963***
	(0.0006)	(0.001)	(0.194)	(0.110)
$Policy_{j,t}$	0.005***	0.006***	0.644***	0.639***
	(0.0009)	(0.001)	(0.196)	(0.130)
Observations	3,495,104	3,495,104	3,094,248	1,598,161
Pseudo R^2	-0.021	-0.051	0.368	0.263
θ_i	✓	✓	✓	✓
λ_t	✓	✓	✓	✓
$\phi_{p,y}$	✓	✓	✓	✓
$\psi_{p,w}$	✓	✓	✓	✓
$\rho_{p,d}$	✓	✓	✓	✓
2019, 2020 Subsample				✓

Table C7. Robustness Check 2

			ProbCharity		
	(1)	(2)	(3)	(4)	(5)
	Logit	Logit	Logit	Logit	Logit
$Covid_{j,t}$	-0.413***	-0.498***	-0.519**	-1.00***	-1.00***
	(0.141)	(0.162)	(0.225)	(0.227)	(0.237)
$Policy\_p, t$	0.760***	0.705***	0.605**	0.734**	0.734**
	(0.148)	(0.173)	(0.243)	(0.292)	(0.296)
Cluster	Org.	Org.	Org.	City	City & Date
Observations	1,307,941	610,706	131,276	2,873,614	2,873,569
Pseudo R^2	0.292	0.324	0.287	0.312	0.312
θ_i	✓	✓	✓	✓	✓
λ_t	✓	✓	✓	✓	✓
CityByYear	✓				
CityByWeek	✓				
CityByDOW	✓				
CountyByYear		✓			
CountyByWeek		✓			
CountyByDOW		✓			
OrgByYear			✓		
OrgByWeek			✓		
OrgByDOW			✓		
ProvByYear				✓	✓
ProvByWeek				✓	✓
ProvByDOW				✓	✓

Table C8. Spillover Effect

	ProbCharity			
	(1)	(2)	(3)	(4)
	Logit	Logit	Logit	Logit
$Queen_{j,t}$	-0.224	-0.041		
	(0.165)	(0.162)		
$Rook_{j,t}$			-0.224	-0.041
			(0.165)	(0.162)
$Covid_{j,t}$		-0.998***		-0.998***
		(0.113)		(0.113)
$Policy_{j,t}$		0.732***		0.732***
		(0.134)		(0.134)
Observations	2,873,578	2,873,642	2,873,567	2,873,610
Pseudo R^2	0.310	0.312	0.310	0.312
θ_i	✓	✓	✓	✓
λ_t	✓	✓	✓	✓
$\phi_{p,y}$	✓	✓	✓	✓
$\psi_{p,w}$	✓	✓	✓	✓
$\rho_{p,d}$	✓	✓	✓	✓

D FIGURES

Figure D1. Market Structure

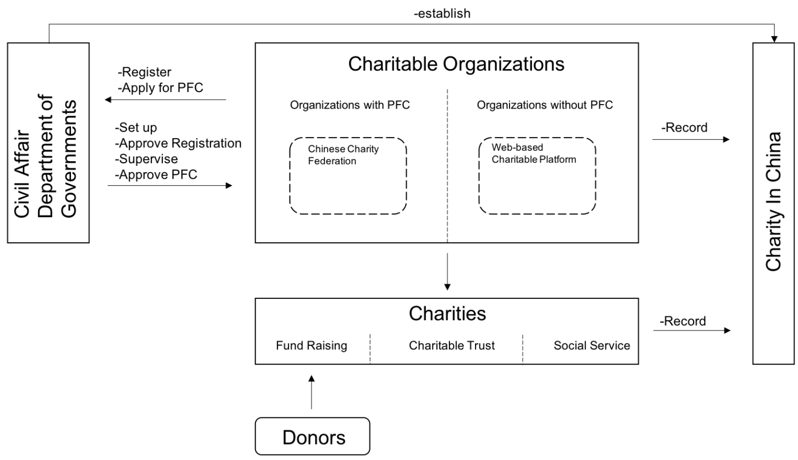

Figure D2. Placebo Test

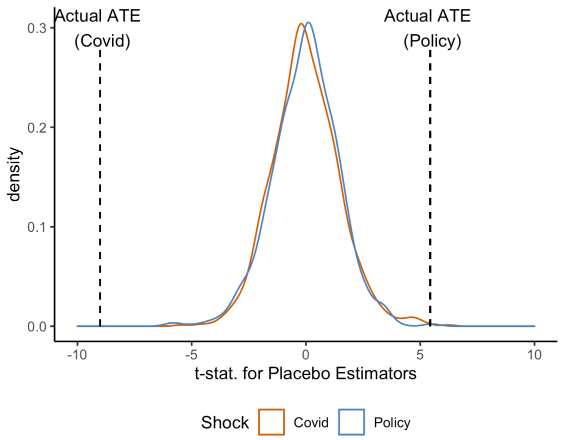

Figure D3. Leading and Lagging the Treatment Period

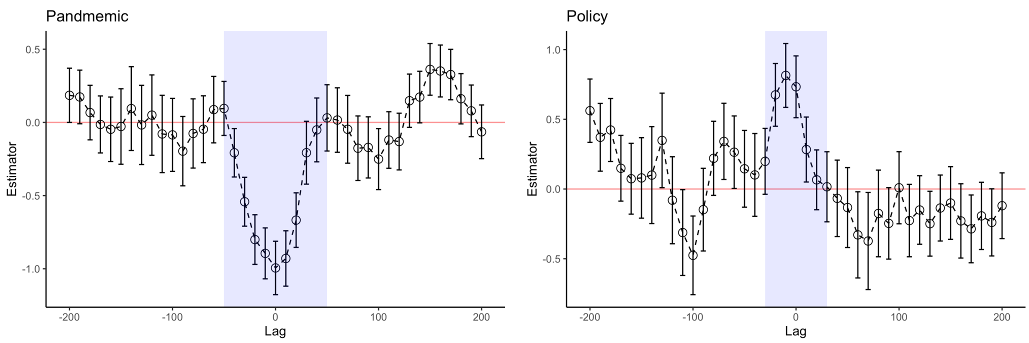

(a) (b)

Figure D4. Event Study: Spillover Effect

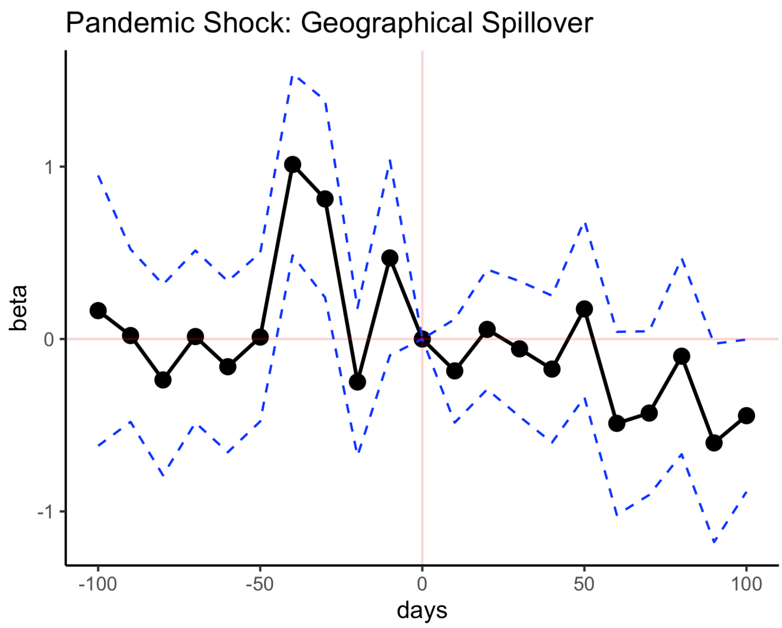

Figure D5. Spatial Distribution of the National Poor Counties

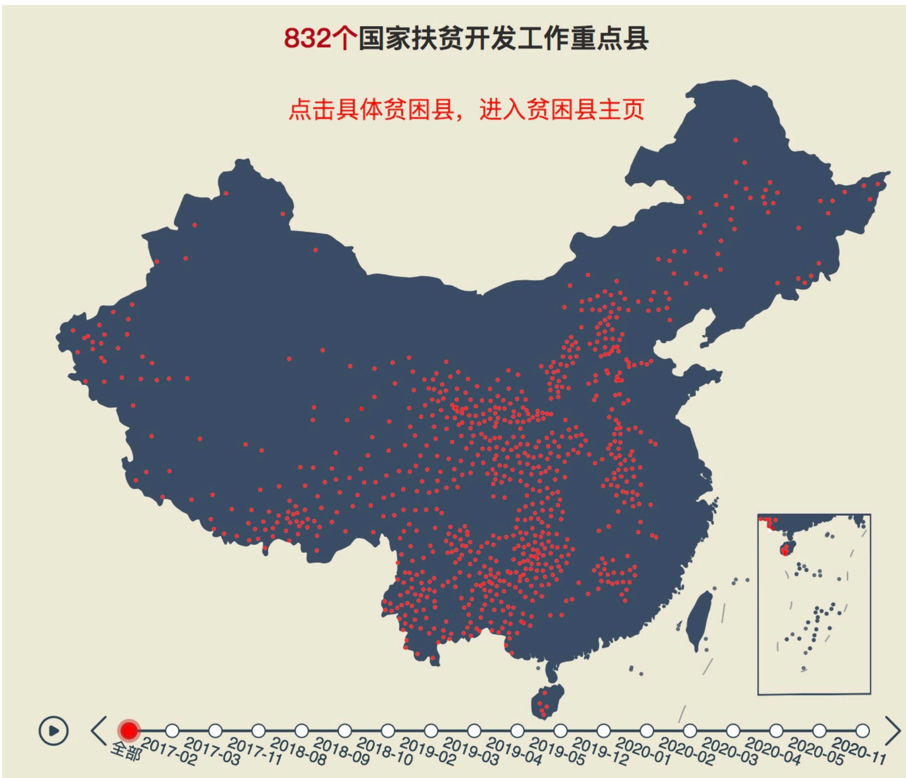

Figure D6. Event Study (LPM)

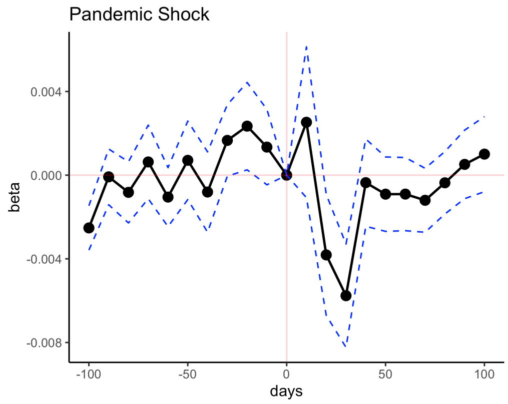

(a)

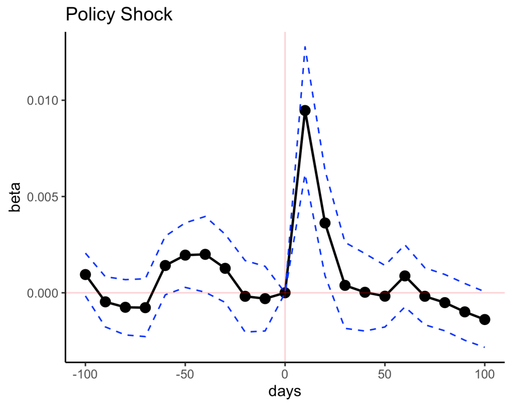

(b)

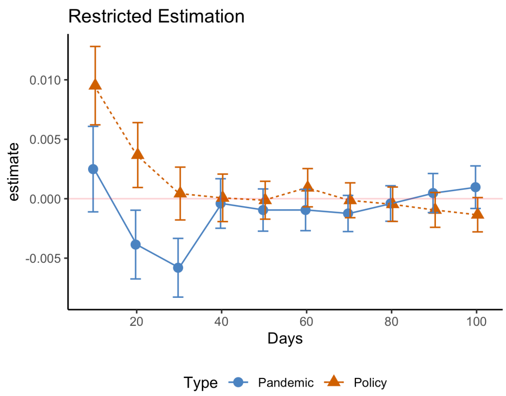

(c)

Figure D7. Baidu Mobility

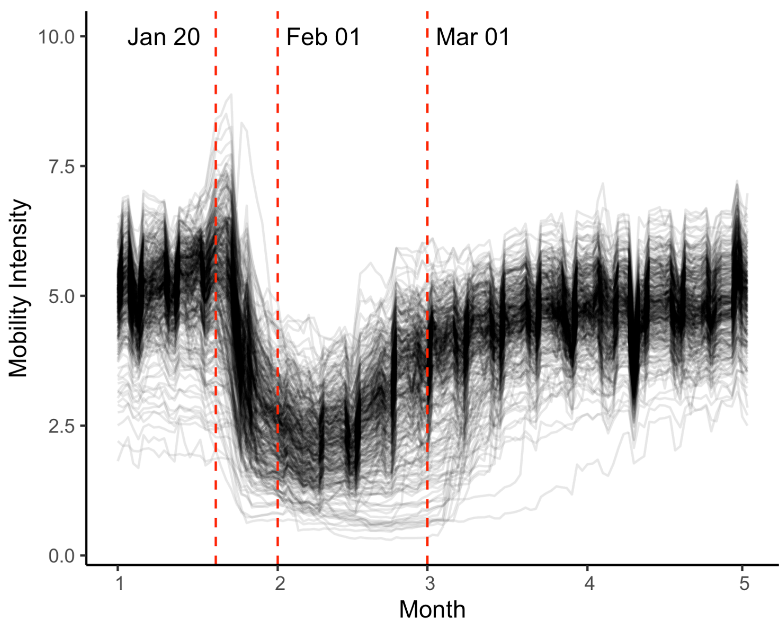

Figure D8. Examples of Collaborative Advocacy during Covid Pandemics

民政部关于动员慈善力量依法有序参与新型冠状病毒感染的肺炎疫情防控工作的公告

（民政部公告第476号）

党中央、国务院高度重视湖北省武汉市等多个地区发生的新型冠状病毒感染的肺炎疫情。习近平总书记作出重要指示，要求把人民群众生命安全和身体健康放在第一位，制定周密方案、组织各方力量开展防控，采取切实有效措施，坚决遏制疫情蔓延势头。中共中央政治局常务委员会召开会议，对疫情防控特别是患者治疗工作进行再研究、再部署、再动员。李克强总理作出重要批示，国务院召开常务会议对有关工作作出部署。为深入贯彻习近平总书记的重要指示和李克强总理的重要批示精神，认真落实党中央和国务院的部署，更广泛地动员社会慈善力量，依法有序支持疫情防控工作，现就有关事项公告如下：

一、倡导各级慈善组织发挥自身优势、动员社会力量、汇聚人民群众爱心，发扬一方有难八方支援的优良传统，采取切实有效措施，对湖北省武汉市等疫情严重地区提供支持，协助党和政府遏制疫情蔓延势头并做好后续相关工作，为全国各地疫情防控工作贡献力量。

二、开展相关慈善和志愿服务活动的慈善组织、志愿服务组织应当配合湖北省、武汉市等地新型冠状病毒感染的肺炎防控指挥部的安排。慈善组织为湖北省武汉市疫情防控工作募集的款物，由湖北省红十字会、湖北省慈善总会、湖北省青少年发展基金会、武汉市慈善总会、武汉市红十字会接收，除定向捐赠外，原则上服从湖北省、武汉市等地新型冠状病毒感染的肺炎防控指挥部的统一调配。外地慈善组织、志愿服务组织在疫情应对响应终止之前，不派工作人员、不发动组织志愿者进入湖北省。

三、慈善组织应当根据湖北省武汉市等疫情严重地区的需求确定募捐方案，首先帮助筹集用于疫情防控的物资，包括：医用防护服、N95口罩、医用（外科）口罩、正压隔离衣、防护面罩、护目镜、消毒液等。现阶段慈善组织暂不为疫情严重地区募集和转送与疫情防控无关的物资，下一步根据疫情严重地区的需求再适时调整募捐方案。

四、开展公开募捐的慈善组织应当按照慈善法和《慈善组织公开募捐管理办法》的规定，将募捐方案报送登记的民政部门备案。慈善组织要依法依规开展募捐，定期公布捐赠收入和支出明细，确保信息长期可查询，并接受捐赠人和社会的监督。各互联网公开募捐平台要为慈善组织开展互联网公开募捐做好服务和社会监督。不具有公开募捐资格的组织或者个人，可以依法与具有公开募捐资格的慈善组织合作开展公开募捐活动。

五、各级民政部门要引导慈善组织、志愿服务组织在党委和政府的统一指挥和统筹协调下，依法有序参与疫情防控；要做好捐赠款物数据的统计和汇总工作，并及时回应社会对捐赠工作的关切；要加强事中事后监管，指导有关组织按照募捐方案使用捐赠款物，保障社会爱心切实用于疫情防控工作。

六、其他社会组织参与疫情防控工作参照上述要求执行。

(a) MCF 476

湖北省民政厅关于社会组织有序参与新型冠状病毒感染肺炎疫情防控工作的通知

（鄂民政函〔2020〕51号）

全省各社会组织：

当前，防控新型冠状病毒感染肺炎疫情的形势仍十分严峻。为贯彻党中央、国务院和省委、省政府关于疫情防控的决策部署，全面落实联防联控措施，现就社会组织参与疫情防控工作的有关事项通知如下。

一、切实提高政治站位。党中央、国务院极为关切、高度重视新型冠状病毒感染肺炎疫情防控，习近平总书记多次过问，作出重要指示批示，主持召开中央政治局常委会议，提出重要要求。李克强总理亲临湖北一线，考察指导疫情防控。湖北省委、省政府靠前指挥，把做好疫情防控作为当前最紧急、最重要的工作。全省各社会组织要积极响应党的号召，把学习贯彻习近平总书记一系列重要指示精神作为当前重要政治任务，及时向本组织工作人员和会员单位、个人传达当地党委政府的防控措施、防控要求，普及防控知识。要坚决按照省委、省政府的决策部署，强化风险意识和底线思维，讲政治、顾大局，不信谣、不传谣、不造谣。各社会组织党组织和党员要发挥战斗堡垒作用和先锋模范作用，广泛动员会员单位个人，全面落实防控措施，为构筑群防群治的严密防线贡献力量。对于在疫情防控期间不遵守政治纪律和政治规矩，顶风违纪违法的社会组织，将依法严肃查处。　　二、切实做好自身防护。各社会组织要按照当地党委政府的统一部署，落实业务主管单位、行业管理部门和居地社区的具体要求，自觉遵守疫情防控的各项规定，自觉采取必要的疫情防控措施，切实加强自身安全防护。疫情防控期间，不组织大型会议、展览、交流等人员大范围聚集活动，已确定时间的，择期另行召开，积极探索通过短信、微信、在线平台等方式传达相关精神和有关决策部署。人群聚集的民办非企业单位要严格落实业务主管部门的各项具体要求，将防控工作责任落实落细。要加强内部消毒清洁、疫情监测和人员排查，出现疑似症状立即隔离、发现疫情主动报告。社会组织年检、年报、登记等工作，以通信咨询、在线办理为主，非必要、非紧急事项，不到登记管理机关现场办理。　　三、切实履行社会责任。在疫情防控斗争中，各社会组织要积极践行"非营利性"初心使命，结合自身优势奋力担当作为，依法有序参与疫情防控。行业协会商会要充分发挥行业引导、规范、自律作用，鼓励有条件的会员企业加急生产紧缺防控医药产品和设备，大力推动会员企业加强自律，坚决杜绝囤积居奇、哄抬物价行为。学术类、科技类社会组织和专业性社会组织，要主动发挥自身凝聚专家学者和专业人才的优势，通过多种形式加强疫情防治宣传，加强科学普及，引导社会公众相信科学，不信谣、不传谣，共同维护社会稳定。慈善组织和志愿服务组织要严格按照《民政部关于动员慈善力量依法有序参与新型冠状病毒感染的肺炎疫情防控工作的公告》要求，科学有序地参与疫情防控工作。社会工作服务机构、社区社会组织要积极协助做好疫情排查和宣传教育等工作。网络社会组织要做好网络舆情引导工作，引导网民正确认识疫情态势，加强疫情防控正面引导和宣传。其他社会组织要结合自身实际，有序参与和积极支持，为疫情防控取得胜利做出力所能及的贡献。　　**四**、切实规范捐赠工作。疫情防控期间，具备社会捐赠接收资格的社会组织要按照省疫情防控指挥部的要求，热情接待，周到服务，规范做好社会捐赠接收工作，自觉接受捐赠人和社会监督。支持具备募捐资格的慈善组织，发挥自身优势，在当地党委政府指导下，依法动员社会力量有序参与疫情防控慈善救助和帮扶活动，重点募集疫情防控急需的物资设备，暂不募集、转运与疫情防控无关的物资。不具备公开募捐资格的社会组织，可依法与具备募捐资格的慈善组织合作协助其开展相关募捐活动，确保捐赠活动有序开展。其它有捐赠意向的社会组织，应通过合法途径捐赠，不得向会员单位、个人摊派。凡以社会组织名义发布的与疫情防控有关的捐赠数据，必须真实、准确、有据，不得虚假宣传、夸大宣传。只有捐赠意向、未实施捐赠的，不得事先宣传。违者一经查实，列入社会组织异常活动目录。

(b) Example of Local Advocacy

Does Epidemiology Matter? Policy Functions in Economic Epidemiological Models of Covid *

Aditya Goenka[†] Lin Liu[‡] Haokun Pang [§]

December 7, 2024

Abstract

Economic epidemiology models have become a major application of dynamic general equilibrium theory to understand the interaction of infectious diseases and economic outcomes following the Covid pandemic. The papers have used differing assumptions of the epidemiology dynamics off-the-shelf from the epidemiology literature, where an unanswered question is what are the implications for optimal policies and the equilibrium outcomes of these assumptions. In a unified framework, we use both the Hamiltonian approach and a continuous time dynamic programming (HJB) approach to explore this issue. We numerically compute the policy and value functions under SIR (where recovery from an infection confers lasting immunity to subsequent infections) and SIRS (where it does not) dynamics. The value functions look qualitatively similar as does the policy function for consumption. However, the policy functions for the health expenditures differ. We present the phase portraits and the dynamics of the variables of interest. These differ greatly. We also conduct counterfactual analysis by assuming that the social planner misspecifies the epidemiology model by applying the health policy of SIR model to the pandemics with SIRS dynamics, and vice versa. We find the value loss of misspecifying the SIRS model is larger than that misspecifying the SIR model.

Keywords: Covid-19, optimal policies, SIRS, SIR, Long Covid, infectious diseases, NPI, growth model, value function, policy function, neural networks.

JEL Classification: *E13, E22, D15, D50, D63, I10, I15, I18, O41, C61.*

*We thank Raouf Boucekkine, Alex Citanna, Mich Tvede, and seminar participants in EWET Conference 2022, Naples; SAET Conference 2022, Paris; and ISI, Delhi for their helpful comments. The usual disclaimer applies

[†]Department of Economics, University of Birmingham, Email: a.goenka@bham.ac.uk

[‡]Management School, University of Liverpool, Email: lin.liu@liverpool.ac.uk

[§]Department of Economics, University of Birmingham, Email: h.pang.1@bham.ac.uk

I. INTRODUCTION

The Covid-19 pandemic led to a surge in economic epidemiological modelling. The economics literature not only looks at the interaction between the incidence of the disease with the economy but also generally studies optimal policies rather than compare simulations of different scenarios in the epidemiology literature (e.g. the influential papers by Flaxman et al. (2020) and Ferguson et al. (2020)). These models generally used Pontriagin's maximum principle to study the optimal control problem of how to control the morbidity and mortality from the pandemic while minimizing the economic loss. These models were generally parsimonious to avoid the curse of dimensionality and many did not model capital or used a partial equilibrium approach[1] where the economic variables such as consumption and interest rates are held fixed[2]. This paper uses a continuous time dynamic programming approach in a fully general equilibrium model (as in Goenka and Liu (2012, 2020); Goenka, Liu and Nguyen (2024)) so as to bring the modelling in parallel with standard macroeconomic modelling of economic fluctuations.

This paper focuses on how optimal health policy is influenced by epidemiological assumptions. We identify two key sources that lead to differences in health policy. The first source is the policy functions, which map observable state variables to optimal health policy. The second source is the state dynamics, which describe how the state variables evolve over time. Our analysis of policy functions and dynamics provide a clear framework for designing interventions as state variables change, aligning with the actions of governments during the COVID-19 pandemic. For instance, the "dashboard approach" adopted by the UK Health Security Agency (UKHSA)[3] involves releasing selected data metrics on a public dashboard and implementing intervention policies based on these metrics rather than pre-specified dates.

The use of dynamic programming enables the characterisation of the value and policy functions. In the maximum principle approach, while the optimal trajectory can be calculated, it does not provide guidance if either some characteristics of the disease or the economic state variables were to change. Moreover, the economic epidemiology models are usually non-linear, which further increase the difficulty in solving optimal paths using maximum principle approach. The literatures that integrating new-classical framework with epidemiology compartment models usually rely on steady-state analysis, which particularly don't provide any short-run and fast-response policy implication (e.g. Goenka, Liu and Nguyen (2021, 2024) etc.). However, the iteration-based dynamic programming technique (e.g. finite-

[1]E.g. Achdou et al. (2022), Alvarez, Argente and Lippi (2021).

[2]See i.e. Eichenbaum, Rebelo and Trabandt (2021).

[3]The success of this approach has led to its extension to other infectious diseases beyond COVID-19, as well as to chemical, environmental, and radiological health threats.

differencing (Achdou et al., 2022)) usually suffer from the Curse of Dimensionality that the coding complexity and run time are exponential to number of state variables. We overcome this curse by globally approximating the value function by deep learning neural networks (Fernández-Villaverde, Hurtado and Nuno, 2023; Fernandez-Villaverde et al., 2020). To increase the precision of the approximation, the steady state by the maximum principle method is used to guide the training of the network. We show the consistency between two approaches that the simulated path by neural network converges to the steady state solution by Hamiltonian.

The underlying economic model we use is the economic epidemiology model developed in Goenka, Liu and Nguyen (2021) where the state variables are the health states and capital. Covid-19 has two effects – mortality and morbidity. The earlier paper modelled both effects. By end of 2022, while morbidity remains significant, for most countries mortality from Covid-19 ceases to be of primary importance. The intervention we model are consumption reducing expenditures, which we label as health expenditure, that can decrease the likelihood of infections which includes social distancing.[4] While the earlier literature used SIR dynamics to model the disease dynamics, it has become clear that subsequent immunity to infections either from vaccines or prior infections is not long lasting so that SIRS dynamics are more appropriate.[5] In the paper, we analyse both SIR and SIRS dynamics as it also facilitates an understanding of how the details of epidemiology modelling will affect policies while taking into account the economic interactions.

A striking result is that the value functions and consumption policy functions for both the two epidemiology specifications look very similar, the policy function for health expenditures is very different in terms of their magnitudes. Moreover, when we look at the dynamics of the health components as well as consumption and health expenditures, they vary for the two different specifications. We further conduct counterfactual analysis by assuming that the social planner misspecifies the epidemiology model. Specifically, we assume that the health policy for SIR model is mistakenly applied when the disease actually follows the SIRS dynamics, and vice versa. As a result, we find the value loss from misspecifying the SIRS model is larger than that from misspecifying the SIR model, especially at the beginning of the pandemics.

As an extension we incorporate mortality from the disease. The total population would be affected by the path of excess infection-induced mortality. Thus, the dis-

[4]Goenka, Liu and Nguyen (2024) model optimal lockdowns but in this paper we do not model it as in the policy space the use of lockdowns looks unlikely going forward.

[5]See e.g. Cele et al. (2021); Hansen et al. (2021); Sabino et al. (2021); Cagigi et al. (2021) The SARS-Cov-2 virus is not a stable virus. The mutation is quick and hard to track. This further reduces the effectiveness of immunity that data shows the most reinfection happens among different variants of virus (ONS, 2023).

count rate is endogenous as a function of the cumulative excess mortality (Goenka, Liu and Nguyen, 2021, 2024). We do not avoid the endogenous discounting problem as Alvarez, Argente and Lippi (2021) who hold the population size constant and model the deceased in a new state where they do not consume or produce. Instead, as in (Goenka, Liu and Nguyen, 2021, 2024), we introduce an extra state variable for modelling the changing discount rate into value function.[6] The performance of our approximation is not much affected by the inclusion of the additional state variable as the deep learning technique enables us to handle high-dimensional dynamic programming problem.

From the control theoretic point of view, the sufficiency conditions of Arrow and Mangasarian fail in economic epidemiology models. For our model, the results in Goenka, Liu and Nguyen (2021) and Goenka, Liu and Nguyen (2024) cover the SIR and SIRS cases respectively. The dynamic programming approach side-steps this problem (see Calvia et al. (2024)) as concavity of the objective is retained but we do not need any such assumption on the evolution of the state variables.[7]

For modelling purposes we use continuous time rather than discrete time. From a practical level, it should not matter which assumption is used as it is just a matter of calibrating the model to the right frequency. However, the HJB approximation in the continuous time approach has better performance in both accuracy and efficiency Achdou et al. (2022). Furthermore, from a theoretical point of view, the disease dynamics in discrete time are unimodal so that if the contact rate is high enough, there can be cycles and chaos Goenka and Liu (2012). The pure epidemiology continuous time specification on the other hand does not admit endogenous fluctuations.[8] As estimates of the contact rate have varied dramatically over the pandemic[9], it would seem reasonable to use a continuous time specification as the time frequency should not become an independent source of complexity.

The plan of the paper is as follows. section II. outlines the economic epidemiology model. section III. numerically solves for the both the SIR and SIRS models the steady states, the value and policy functions, and the stable manifolds of the dynamical system. The difference between the dynamics of the two models is shown. section IV. applies the model to study the effect from vaccination. We also introduce Covid-induced mortality in this section.

[6]This follows Uzawa (2017).

[7]The sufficiency results cited above also rely on concavity of the objective function and sufficiency can be shown directly.

[8]See i.e. the discussion in Boucekkine et al. (2024).

[9]The variant BF.7 that is dominant in China in December 2022 has a reproduction rate 10.8-18.6. In 2020 it was estimated to be an average of 2.2 in Western Europe (Linka, Peirlinck and Kuhl, 2020).

II. The Economic Epidemiology Model

A. Model Setup

The model is based on the growth model with in Goenka and Liu (2012, 2020) and Goenka, Liu and Nguyen (2014, 2021, 2024). In this paper we use an underlying neoclassical growth model with epidemiological dynamics. We use model agents as large representative households to avoid keeping track of the history of health status.

Households. We assume the economy is populated by a continuum of non-atomic identical households who are the representative decision-making agents. The size of the population is $\mathcal{N}$. The total population grows over time at the rate of $b - d \geq 0$, where b is the birth rate and d is the natural death rate. Within each household, an individual is either healthy or infected or recovered from the diseases. We will introduce the epidemiology compartment in detail later.

We model the infectious disease as causing morbidity — reducing productivity of the infected. We make the simplifying assumption that when an infected individual is incapacitated by the disease that the productivity falls to zero.[10] We further assume the labour is supplied inelastically.[11] The infectious disease externality, where individuals ignore the effect of their own actions on the dynamics of the disease, can have significant effects. In this paper we are interested in what a policymaker should do based on the state of the pandemic and thus, focus on the optimal policy.[12]

The objective for the representative household is to maximize the discounted utility

$$\int_0^\infty e^{-[\rho-(b-d)]t}u(c_t)dt, \tag{1}$$

where ρ is the discount factor with $\rho - b + d > 0$; c_t is the consumption. The size of household is assumed to be one. The growth rate of total population is $b - d$[13].

Assumption 1. *The utility function $u : \mathbb{R}_+ \to \mathbb{R}$ is $\mathcal{C}^2$ with $u' > 0, u'' < 0$. The discount rate $\rho > b - d$.*

Epidemiology and labour supply. The epidemiology model we use are the SIRS and SIR models. We assume that diseases follow the SIRS dynamics. The

[10] How much productivity is affected varies across diseases and see Goenka, Liu and Nguyen (2021) for a discussion of this. If we assume partial decrease in productivity the qualitative results are not affected.

[11] Goenka and Liu (2012) endogenized the labour-leisure choice with SIS disease dynamics and showed that the dynamics are invariant under standard assumptions.

[12] Goenka and Liu (2020) have a comprehensive discussion of the effects of the disease externality in a similar model but with SIS dynamics.

[13] In section IV., we introduce mortality. The population growth rate and the discount rate would be endogenous as functions of state variable.

SIR dynamics will be a special case for SIRS with different parameterization. An individual can be in one of three health states: $\mathcal{S}$ – healthy and susceptible to the disease; $\mathcal{I}$ – infected and capable of transmitting infections, that is, infectious; $\mathcal{R}$ – recovered from the disease and having immunity from the disease. If there are vaccinations, then an individual has immunity to the disease without going through an infection. In this paper, we do not model vaccinations. However, as we will mention later, if we change initial conditions of the state variables in the model by increasing the fraction of $\mathcal{R}$ then one could interpret this as individuals having immunity from the disease either conferred from recovery from infections or from vaccinations.

In the epidemiology model, susceptible group get infected by contacting the infectious disease. The contact rate, which is key to determine the prevalence of infectious disease, is Poisson. We assume it is affected by health expenditure, that is, each household can control infection by investing in health expenditure $h = H/\mathcal{N}$. This can be thought of preventive measures taken to prevent the transmission of the disease. This is the specification used in Goenka and Liu (2012); Goenka, Liu and Nguyen (2014). The second paper also modeled expenditures that increase recovery rates from the disease but we abstract from this in this paper as there are no known therapies for recovery from Covid-19.[14] Eichenbaum, Rebelo and Trabandt (2021) interpret this loss of output, h, in our context, as the cost of a lockdown which also reduces the transmission rate α and thus, is also consistent with interpreting it as the cost of a lockdown which reduces transmission of the disease by forgoing output.[15]

Assumption 2. *The contact rate is a function of health expenditure h, i.e. $\alpha(h)$. We assume $\alpha' < 0; \alpha'' > 0$ and $\lim_{h\to 0} \alpha(h) = \bar{\alpha}$.*

For the recovery process, we assume the infected group recovers at an exogenous rate of γ. We analyse both SIRS and SIR model, where the key difference lies in the immunity for the recovered group. For the SIRS model, the recovered group would lose their immunity at some rate. We denote ψ as the rate of re-entering the susceptible group. In the SIR model, the immunity is life-long, implying $\psi = 0$. With the assumptions above, the flow of population in each compartment can be shown in Figure 1.

By normalizing the population in each compartment that

[14] Antivirals and anti-inflammatory drugs are now known to reduce mortality but these are inexpensive and widely available prior to the outbreak. While ventilators are used in severe cases, there is an emerging view that their use can complicate recovery and in fact cause ventilator induced lung injury (Marini and Gattinoni, 2020).

[15] In Goenka, Liu and Nguyen (2024), we have a different way of modeling a lockdown or quarantine where a fraction of the non-infective population has to work from home with a reduced productivity.

Figure 1. Flow of Epidemiological Compartments

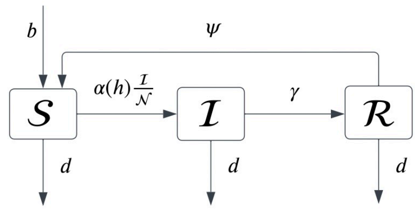

$$s = \frac{\mathcal{S}}{\mathcal{N}}; \quad i = \frac{\mathcal{I}}{\mathcal{N}}; \quad r = \frac{\mathcal{R}}{\mathcal{N}}. \tag{2}$$

we can have set of differential equations to represent the motion of the compartments as follow

$$\begin{aligned} \dot{s} &= b - bs - \alpha(h)si + \psi r, \\ \dot{i} &= \alpha(h)si - \gamma i - bi, \\ \dot{r} &= \gamma i - \psi r - br. \end{aligned} \tag{3}$$

Production. The production side of the model is a standard neoclassical growth model where households can invest in capital which is productive next period and depreciates at rate δ[16]. Households own representative firms that use capital and labour as inputs.

Assumption 3. *The production function $f(k,l)$, $f : \mathbb{R}_+^2 \to \mathbb{R}_+$ is $\mathcal{C}^2$ with*

1. $f_k > 0, f_l > 0$,
2. *f is concave and homogeneous of degree 1,*
3. $f(0,\cdot) = f(\cdot,0) = 0$,
4. $\lim_{k\to 0} f_k(k,\cdot) = \lim_{l\to 0} f_l(\cdot,l) = \infty$, $\lim_{k\to\infty} f_k(k,\cdot) = 0$,
5. *The physical capital depreciates at the rate $\delta \in [0,1]$.*

The law of evolution of capital stock is $\dot{K} = f(K, \mathcal{N} - \mathcal{I}) - C - H - \delta K$. We define for each household, physical capital per capita $k = K/\mathcal{N}$ and consumption per capita $c = C/\mathcal{N}$. The law of motion for physical capital per capita can be rewritten as:

$$\dot{k} = f(k, 1-i) - c - h - \delta k - (b-d)k. \tag{4}$$

[16] Goenka and Liu (2020) have an endogenous growth model where there is human capital accumulation and households choose time to work and time for human capital accumulation. It uses SIS dynamics without disease related mortality.

B. Optimization Problem for Social Planner

The social planner maximizes the discounted utility Equation 1 subjected to the motion of capital Equation 4 and the motions of epidemiological compartments Equation 3.[17].

$$
\begin{aligned}
\max_{c,h} \quad & \int_0^\infty e^{-[\rho-(b-d)]t} u(c) dt \\
s.t. \quad & \dot{k} = f(k, 1-i) - \delta k - c - h - (b-d)k, \\
& \dot{s} = b - bs - \alpha(h) si + \psi(1-i-s), \\
& \dot{i} = \alpha(h) si - bi - \gamma i.
\end{aligned} \tag{5}
$$

The control variables are consumption and health expenditure (c, h), and the state variables are (k, i, s). There are alternative ways of solving the optimal control problem. If we use the Hamiltonian approach as has been done in most of the literature, the optimal policy in the steady state can be easily computed. However, the optimal policy along a convergence path is difficult to characterize. The issue is that optimal policy in steady state throughout the convergence path causes value loss and the dynamics of the state variables are unknown. In addition, typically for epidemiological model, second order condition do not hold. This was recognized in the first papers (see e.g. Goldman and Lightwood (2002)) but ignored by the literature other than by Goenka, Liu and Nguyen (2014, 2021, 2024). The alternative is to use a continuous time dynamic programming approach that largely circumvents these problems (see e.g. (Achdou et al., 2022; Calvia et al., 2024)). However, to characterize the optimal policy and equilibrium paths, there is the curse of dimensionality.[18] This can be addressed by using neural networks (Fernandez-Villaverde et al., 2020; Fernández-Villaverde, Hurtado and Nuno, 2023). To use this the challenge is which domain to train the neural network in. The most direct way is to globally approximate the value function of the dynamic programming problem, as the universal approximation theorem (Barron, 1993) enable the neural network to approximate any Borel measurable function mapping finite-dimensional spaces to any desired degree of accuracy. The convergence of the approximation is uncorrelated with the number of dimension (Barron, 1993).

In our paper, we apply both approaches. In practice, We firstly pin down the

[17]As the fraction of population in each compartment lies in the simplex The last equation in Equation 3 is redundant by letting $r = 1 - i - s$.

[18]The coding and computing complexity is exponential to number of state variables. To illustrate this, we take the popular iterated-based algorithm Finite Differencing Method (FDM) (Achdou et al., 2022) as an example. Each state variable has 2 numerical differencing directions (forward, backward). There would be $2^3 = 8$ directions in combined for our (k, i, s) state space ($2^4 = 16$ when we introduce mortality later). Furthermore, suppose each state variable is discretized by (usually) 1000 grids. The FDM needs to invert a $1000^3 \times 1000^3$ matrix.

steady state by Hamiltonian Equation 6. $\lambda_1, \lambda_2, \lambda_3$ are the costate variables for the states respectively. μ_1, μ_2, μ_3 are the Lagrangian multipliers for $r > 0, h > 0$. We show the solution strategy for the Hamiltonian in Appendix B.

$$\begin{aligned} \mathcal{H} = \max_{c,h} \quad & e^{-[\rho-(b-d)]t}u(c) + \lambda_1[f(k, 1-i) - \delta k - c - h - (b-d)k] \\ & + \lambda_2[b - bs - \alpha(h)si + \psi(1-s-i)] \\ & + \lambda_3[\alpha(h)si - bi - \gamma i] + \mu_1 s + \mu_2 i + \mu_3 h. \end{aligned} \tag{6}$$

For the policy function and the dynamics, we use the dynamic programming approach, which is verified and guild by our analytical solution from Hamiltonian. We target at solving the current value Hamiltonian-Jacobian-Bellman Equation (Equation 7), where $v(k, s, i)$ is the value function. The derivation of HJB is shown in Appendix C.

$$\begin{aligned} (\rho - b + d)v(k, s, i) = \max_{c,h} \quad & u(c) + \frac{\partial v}{\partial k}\dot{k} + \frac{\partial v}{\partial i}\dot{i} + \frac{\partial v}{\partial s}\dot{s} \\ = \max_{c,h} \quad & u(c) + \frac{\partial v}{\partial k}[f(k, 1-i) - \delta k - c - h - (b-d)k] \\ & + \frac{\partial v}{\partial i}[\alpha(h)si - bi - \gamma i] \\ & + \frac{\partial v}{\partial s}[b - bs - \alpha(h)si + \psi(1-s-i)]. \end{aligned} \tag{7}$$

The F.O.C. for the HJB reads

$$\begin{cases} c: \quad u'(c) - v_k(k, s, i) = 0 \\ h: \quad -v_k(k, s, i) + \alpha'(h)si[v_i(k, s, i) - v_s(k, s, i)] = 0, \end{cases} \tag{8}$$

which implies that the optimal policy could be expressed as functions of state variables and the marginal value as follow

$$\begin{cases} c^* = u'^{-1}(v_k) \\ h^* = \alpha'^{-1}\left(\frac{v_k}{si(v_i - v_s)}\right). \end{cases} \tag{9}$$

The expression of the optimal health expenditure h^* is quite intuitive. The inverse function of marginal contact α'^{-1} is feasible only with negative input as the contact function α is assumed to be decreasing. While (v_k, s, i) being positive, the optimal health expenditure requests $v_i < v_s$. This implies that it is optimal to spend positive amount of precautionary expenditure only when the marginal value by one more infected people being smaller than the marginal value by one more susceptible people. When the gap in the marginal values $|v_i - v_s|$ gets wilder, it becomes more beneficial to control the pandemic. The social planner would hence optimally spend more on health.

In our paper, the HJB is approximated by the deep learning neural network normally around the steady state obtained independently by Hamiltonian approach. We demonstrate our neural network algorithm in Appendix D. We found the combination of two approaches boots the efficiency and precision that the paths computed by the neural network indeed converge to the steady state that can be determined theoretically via the Hamiltonian approach.

C. Parameterization

The model is calibrated in the quarterly frequency. The birth rate $b = 0.005$ implies 2% of annual birth rate; death rate $d = 0.0031$ implies an 80 years of life expectancy. For the utility function, we assume CRS preference with $\sigma = 2$, subjective discount rate $\rho = 0.0138$.

$$u(c) = \frac{c^{1-\sigma}}{1-\sigma}. \tag{10}$$

The production function takes the standard C-D form that $f(k, 1-i) = Ak^{\beta}(1-i)^{1-\beta}$ with $\beta = 0.36$; Depreciation rate $\delta = 0.0125$; Technology $A = 3$.

Our parameterization for the epidemiology part of the model follows the discussion by Goenka, Liu and Nguyen (2021, 2024). We assume $\gamma = 9$, which generates 10 days of recovery time from infection.[19] We also calibrate $\psi = 1$ for the SIRS model where the immunity could only last for a quarter; $\psi = 0$ for the SIR model where permanent immunity is assumed. Finally, the contact rate function in our paper takes the form of Equation 11. We parameterize this function to be in line with assumption 2 and large enough to generate endemic steady state. However, we notice that it is hard to find empirical evidence to calibrate the contact function. In our baseline model, we let $\epsilon_0 = 11.03, \epsilon_1 = -0.3, \epsilon_2 = 0.01$, implying that the basic reproduction number without any health expenditure would be 5[20], and the contact rate elasticity of health expenditure converges to -0.3 as h increases.[21]

$$\alpha(h) = \epsilon_0(h + \epsilon_2)^{\epsilon_1}. \tag{11}$$

[19]See i.e. UK Health Security Agency (2023) shows that most studies report a virus clearance time around 7 to 15 days.

[20]The basic reproduction number in the pure epidemiological model is calculated by the ratio of contact rate with recovery rate, i.e. $R_0 = \frac{\alpha}{b+\gamma}$. In the data, R_0 for the Delta variant is estimated to be around 3.3 to 6.4 (See i.e. the summary by Sepandi, Alimohamadi and Esmaeilzadeh (2022)); for the Omicron variant is estimated to be around 5.5 to 24 (See i.e. summary by Liu and Rocklöv (2022)).

[21]The contact rate elasticity of health expenditure in our contact function would be $\frac{d\alpha}{dh} \times \frac{h}{\alpha} = \frac{\epsilon_1}{1+\frac{\epsilon_2}{h}}$.

Under the parameterization above, the Hamiltonian (Equation 6) presents an endemic steady state with $k^{SIRS} = 316, i^{SIRS} = 0.0478, s^{SIRS} = 0.52, h^{SIRS} = 0.23, c^{SIRS} = 18.3$, and $k^{SIR} = 331, i^{SIR} = 0.0004, s^{SIR} = 0.2, h^{SIR} = 0, c^{SIR} = 19.46$. In Appendix B, we vary elasticity parameter ϵ_1 and the reinfection rate ψ in complement to our baseline calibration.

III. BASELINE RESULT

Optimal Health Policy. We now begin presenting the main results of our paper. We firstly show the health policy functions $h(k, s, i)$.[22] We notice that there is a natural difficulty in visualizing a function with 3 continuous input. Therefore, we marginalize one dimension by holding $k = k^{ss}$ in the main text.

Figure 2 shows the corresponding results. Panel (a) represents the SIRS model where recovered people have temporary immunity. Panel (b) represents the SIR model where immunity is permanent. One can easily observe that the policy functions between different models looks qualitatively similar. The health expenditure is increasing with both susceptible rate (s) and infection rate (i) for both models. However, compared with the SIRS model, the magnitude for SIR model is much smaller, with a large area of 0. This is because for the SIR model, infection brings life-long immunity which migrates part of the loss. Value of controlling the pandemic is not as substantive as that in the SIRS model.

Dynamics. Although the health policy functions for two models look qualitatively similar, they would generate structural differences for the dynamics of state variables. To see this, we assign the initial state with $(k_0, i_0, s_0) = (280, 1\%, 99\%)$ and simulate two models using the corresponding policy functions. Figure 3 shows the generated dynamics of epidemiological states.[23] For the SIRS model in the left, s doesn't reduce too much as the recovered people would lose their immunity and back to the susceptible group. The infection rate i is persistent that people keep getting infected due to a large group of susceptible.

Conversely, for the SIR model in the right Panel, the infection rate peaks at around one month after the outbreak, which comes much earlier than that in the SIRS model. The peak infection rate hits 48% which is also much higher than that of 10% in the SIRS model. However, during the pandemic, the size of susceptible shrinks down very quickly while the recovered group expands. This is because people obtain permanent immunity as they get over the disease. Consequently, the infection rate in the SIR model eventually reduces to very small in the steady state as there are little susceptibles left.

[22]Consumption and value function are shown in the appendix Figure A1 and Figure A2. They are decreasing with both s and i. In magnitude, SIR model shows larger consumption and value.

[23]In the appendix Figure A3, we plot the simulated path for capital and labour participation.

Figure 2. Policy Functions H

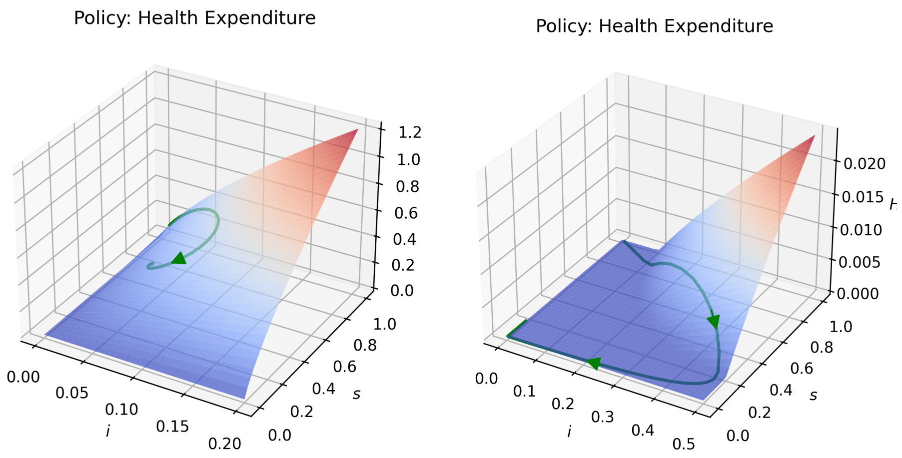

(a) SIRS **(b)** SIR

Notes: (i) Panel (a) and (b) show the optimal health policy function $h^*(k, i, s)$ for SIRS and SIR model. We marginalize the capital at its steady state k^{SS}. (ii) The green solid line with arrows are the simulated convergence paths initialized with $(k_0, i_0, s_0) = (280, 1\%, 99\%)$

Despite the different magnitudes in the health policy functions, the different motions of state (s, i) also affect the optimal paths for health expenditure h. As shown in the green lines in Figure 2, the ways that h^* moves on the equilibrium surface are not similar to each other. For the SIRS model, the motion of health expenditure h^* moves to the central of the surface, with $h^* > 0$ all the time. For the SIR model, however, the motion moves towards the corner with low infection and susceptible rates, where $h^* = 0$.

To further visualize the dynamics of the model, we now plot the phase diagrams[24] for SIRS and SIR models in Figure 4. The red solid curves separate the regions with different directions of motion. The black dash curves are the paths of our simulated example in Figure 3. The blue area represents the sample density for our neural network approximation. Moreover, as we mentioned before, we solve the steady states of the models analytically by Hamiltonian as validations for our neural network approach. We mark the Hamiltonian solution by the yellow crosses in the Figure. It further validates our neural network approach that the analytical solutions for steady states are sufficiently close to the simulated solutions where two red curves join together.

Notice that the dynamics of (s, i) in a pure epidemiological SIRS model, i.e. Hethcote (2000), is a spiral sink as shown in the Appendix Figure A4. The phase diagrams in our model would show a similar pattern — (s, i) evolves following a

[24]As complements for the phase diagram, we plot the surface for $(s, i, \dot{s}), (s, i, \dot{i})$ in appendix Figure A5 and Figure A6

Figure 3. Composition Change for Compartments

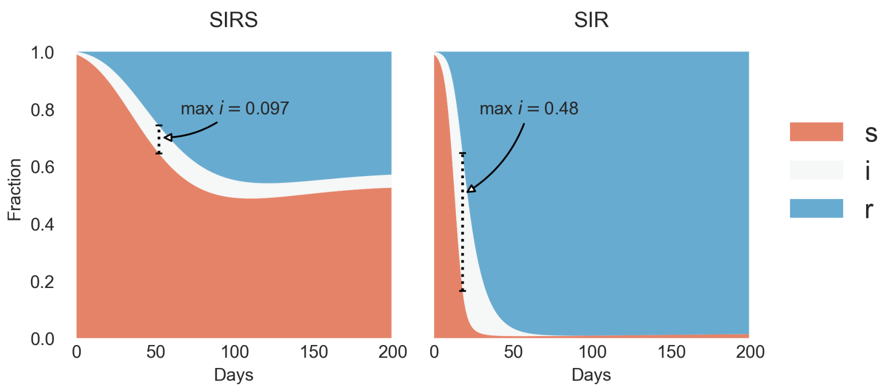

Notes: (i) This is the stack plot for epidemiological compartments in SIRS and SIR model. The red, white and blue area denote the fractions of susceptible, infective and recovered groups respectively. The horizontal axis is the days of simulation. (ii) The little dash bars show the maximum infection rate throughout the simulated periods.

stable focus dynamics. When it comes to the comparison between different model specifications, we find that the space with increasing motion of susceptible (area with $\dot{s} > 0$) is largely squeezed for the SIR model. Correspondingly, the susceptible size in the SIR model decreases for the most of the time. The second key difference is that the threshold line $\dot{i} = 0$ in the SIRS model is steeper due to a more active health policy. Consequently, there shows a smaller area for infection expansion with $\dot{i} > 0$. Thus, the infection rate in the SIRS model goes through the increasing stage easier and generates a lower peak of infection as we mentioned before.

Misspecified Model. We now discuss the consequence of misspecifying the epidemiological models. We simulate the dynamics given the same initial states but with the misspecified health policy. For example, when the disease follows the SIRS dynamics, we assume that the social planner mistakenly applies the optimal health policy for the SIR model. Practically, we exogenously impose the SIR health policy to the simulation of the SIRS model. Same logic is applied for the case of disease with SIR dynamics. This is to see the counter-factual effect of adopting the optimal policy for the wrong dynamics. This gives an estimate for how much the epidemiological component matters in an economic epidemiology model.

The corresponding paths for the state variables (s, i) with the misspecified model are plot in green dash line in Figure 4. It could be viewed that if the social planner mistakenly imposes the SIR health policy, while SIRS is the actual epidemiology model, the consequential infection rate increases further away from its optimum for both steady state and transitional path. Conversely, if the SIR model is misspecified as the SIRS model, the social planner spends more health expenditure than the optimal level. The increase of infection rate therefore gets milder. However, as we

Figure 4. Phase Diagram

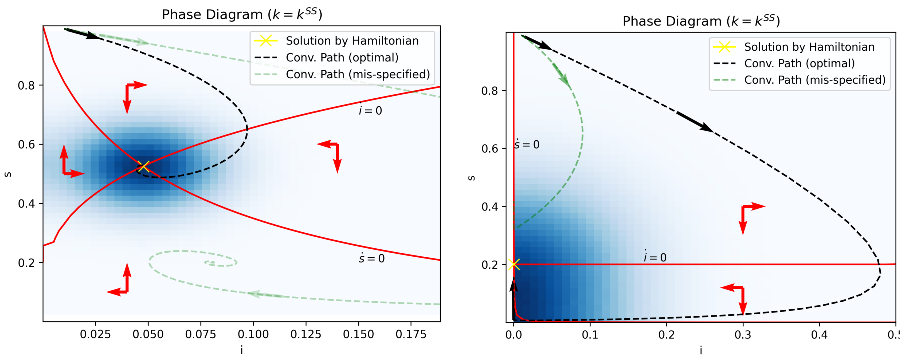

(a) SIRS **(b)** SIR

Notes: (i) This Figure plots the phase diagrams at (s, i) panel for SIRS and SIR model. The other state variable k is marginalized to its steady state. (ii) The red curves represent combinations with s or i being steady. The intersections of two lines are the simulated steady states where both variables remain unchanged. (iii) The yellow crosses are the analytical solutions of steady states obtained by Hamiltonian (Equation 6). (iv) The black dash lines with arrows are the simulated paths for demonstration. (v) The blue area is the density for the combinations used to train the neural network.

show in the appendix Figure A3, the extra spending in health slows down the capital accumulation. The capital goes eventually below optimum, although the infection rate is effectively controlled.

What is the net loss for misspecifying the epidemiology model? We calculate the value loss, which is defined as the gap between the optimal and counterfactual value functions. Figure 5 shows the corresponding results. We find the loss for misspecifying model is always positive. We would like to mark that the value losses for different models originate from different sources. For the SIRS model, the loss comes from the extra infection that incapacitates more labour. For the SIR model, the loss comes from the extra financial cost of health expenditure.

It can be further noticed that the loss for misspecifying SIRS model is higher than that for misspecifying SIR model, especially at the beginning of the pandemic. Such observation may have deep policy implications for the social planner. When the characteristics of the disease is unknown that misspecification could happen, the maximin strategy[25] for the social planner would be treating the disease using the SIRS model. In a plain word, it would be better-off for the policymaker to control the spread of the disease when it is unclear whether re-infection could take place.

To further discuss this argument, we present a pay-off matrix as Table I. The columns in the matrix denote the actual epidemiology model, while the rows denote the health policy applied. For example, the first element indicates the pay-off when the social planner correctly identify the SIR disease and use the optimal health policy

[25]A strategy that maximizes the minimum payoff.

Figure 5. Value Loss of being Laissez-Faire

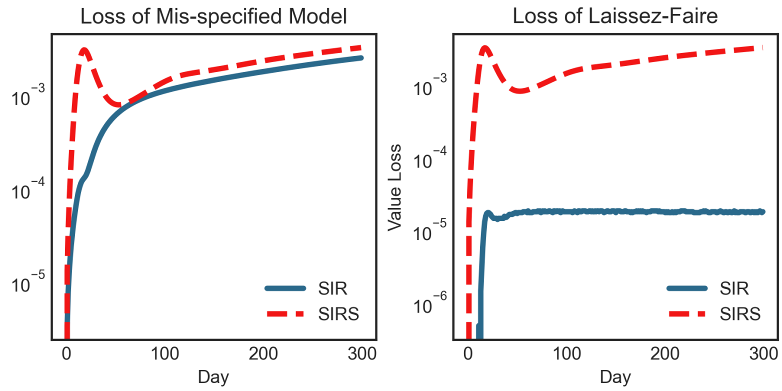

Notes: (i) This Figure plots the value loss under different scenarios. The red and blue curves denote SIRS and SIR models respectively. (ii) The left panel shows the case of model mis-specification that social planner use the health policy from the other model. (iii) The right panel shows the case of Laissez-Faire that social planner does not impose any intervention.

Table I. Pay-off Matrix

	Models	
	SIR	*SIRS*
Controls		
SIR	-0	-0.43
SIRS	-0.055	-0.36
Laissez-Faire	-0.003	-0.44

Notes: For visualizing a tidier table, the elements are the standardized payoff $+100$

derived from the SIR model. Just for illustration, we use the value at the steady state as the pay-off and standardize the first element to be -100. From the matrix, one can easily show that when the type of model is known, the correctly-specified policy yield higher pay-off. However, when the type is unknown, the minimax strategy in case of the worst situation, i.e. situation when re-infection could take place, would be treating the unknown disease using the SIRS model. Moreover, if we let p to be the probability that the disease follow the SIRS dynamics, we can easily solve out a cut-off value $p^* = 0.43$, above which SIRS strategy is optimal.

IV. Vaccination and Mortality

Vaccination. We model vaccination in a simple way similar to Federico, Ferrari and Torrente (2022). We notice that vaccinated group essentially shares similar characteristics with recovered group. They both carry temporary immunity to disease. The key difference is the way of obtaining immunity. People in recovered group naturally gain immunity by overcoming infection, while vaccination brings susceptible people directly to the immune group without going through infection. Thus, a higher vaccination rate implies more recovered and less susceptible before the pandemic hit the economy. With this property, we could model the effect of vaccination efficiently by altering the size of pre-existing susceptible group. We vary the simplex of initial shares of epidemiological compartments (s_0, i_0) and simulate the corresponding paths.[26] We fix the initial infection rate $i_0 = 1\%$ as our previous studies. The initial susceptible s_0 is varied from 3% to 100%. Smaller s_0 implies more pre-existing immunity by higher vaccination rate.

In Figure 6, we plot the simulated paths $\{(s_t, i_t)\}_{t=(0,\infty)}$ with blue dash lines. We mark the share of the vaccinated population at the edges of the paths. It could be seen that all paths converge to the same steady state. However, with a lower rate of vaccination, the economy shows steeper increase and higher peak value of infection rate. In line with the previous section, using the same initial values, we also simulate paths under the scenarios that the model is misspecified, where we assume that the SIR health policy is used. We plot the corresponding results using the red dash line. Compared with the optimal paths, the misspecified paths converge to a different steady state with higher infection but lower susceptible rate. The economy would thus go through worse pandemic. Panel (b) of Figure 6 shows the counterpart using SIR model. We could have similar findings that higher vaccination rate generates lower peak of infection during the outbreak.

Introducing Mortality. In the canonical epidemiological economic models presented above, mortality is absent. The reasons why we abstract mortality in the main part of the paper are two folded. Firstly, the later evidence of Covid-19 pandemic when Omicron variant dominates shows that the mortality rate is small.[27] The second reason is technical. When introducing disease related mortality into the model, the total population in the economy changes as a function of endogenous state (s, i).[28] This makes the discounting endogenous (Goenka, Liu and Nguyen, 2024). In dynamic programming, the additional state variable due to mortality also makes it even harder for visualizing the policy function and phase diagram as the state space is four-dimensional.

[26]Another possible approach is to introduce a new compartment for vaccinated group like e.g. Sun and Yang (2010); Safan, Kretzschmar and Hadeler (2013); Garriga, Manuelli and Sanghi (2022) (another health status in our model). The vaccinated group is mostly similar to the recovered group as they both carries temporary immunity. The only difference is on their reinfection probability. Clinical evidence shows immunity from previous infection lasts longer than from primary series or first booster of vaccination. But the gap is not pronounced (Bobrovitz et al., 2023)

[27]UK data shows around 100 or less of daily numbers of deaths of people whose death certificate mentioned COVID-19 as one of the causes.

[28]As a preview of the result, in Appendix Figure A9, we plot the change of compartment composition as in Figure 3. It could be seen that the total population is decreasing with time due to the extra mortality by disease.

Figure 6. Vaccination

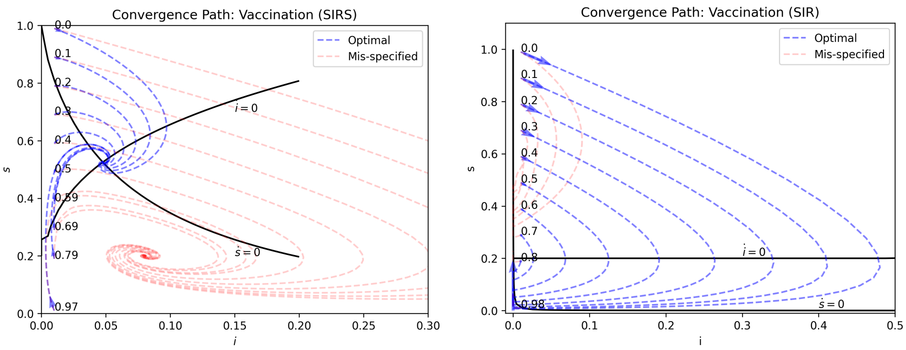

(a) SIRS **(b)** SIR

Notes: (i) This Figure shows the simulated paths with multiple initial values. The numbers at the left edge are the fractions of pre-existing recovery group. We use it as a proxy for vaccinated group. (ii) The blue and red lines are the convergence paths under optimal and Laissez-Faire scenario respectively.

Here, to further or analysis, we augment our model by introducing mortality in the following way.[29] Mortality of the infected from the disease is at the rate of ϕ. This implies that the change of total population satisfies expression $\frac{\dot{N}}{N} = b - d - \phi i$. The social discount rate is hence endogenous as a function of cumulative mortality rate.[30] Specifically, the social planner discount his utility by $e^{-\theta_t}$, where

$$\begin{aligned} \theta_t &= \int_0^t (\rho - b + d + \phi i_\tau) d\tau, \\ \dot{\theta}_t &= \rho - b + d + \phi i_\tau. \end{aligned} \tag{12}$$

We additionally adopt the assumption of non-pecuniary punishment of disease-induced mortality. That is, we directly deduct the loss of mortality from the utility function.[31] Let the relative loss to social welfare from mortality be $\chi(\phi i)$ and it satisfies $\chi'(\cdot) > 0, \chi''(\cdot) \geq 0$. The utility function for the social planner becomes $u(c) - \chi(\phi i)$. In parameterization, we set $\phi = 0.5\%$ in our paper, in lined with Sorensen et al. (2022)'s estimation for 39 countries that the Infection Fatality Ratio (IFR) to be around 0.233% - 0.84% at 2020, and around 0.314% - 0.551% at 2021. For the functional form of $\chi(z)$, we follow Goenka, Liu and Nguyen (2024) to assume a linear non-pecuniary punishment that $\chi(z) = \xi z$. The value of χ is linked with the Value of Statistical Life (VSL).[32] We vary parameter ξ in 1.028, 3.77 and 6.42,

[29] We show the flow chart for the extended model in appendix Figure A7
[30] See e.g. Goenka, Liu and Nguyen (2024).
[31] See e.g. the discussion in Acemoglu et al. (2021); Boucekkine et al. (2024); Goenka, Liu and Nguyen (2024) etc..
[32] VSL is the value of increasing the survival probabilities marginally (Acemoglu et al., 2021). We follow Andersson and Treich (2011) to obtain the VSL at steady state by $\Delta y / \Delta \phi i$ while there is concave utility in the objective function.

corresponding to the steady-state VSL of 1, 40 and 80 times of production per capita. This is in lined with Alvarez, Argente and Lippi (2021) where the benchmark VSL is 40 times of GDP per capita.

We follow the same strategy as section II. for analysing the model. To solve the steady state as the first step, we specify the Hamiltonian as Equation 13. Then, we study the dynamics of the model by solving HJB Equation 14. We show the process of solving Hamiltonian and specifying HJB in Appendix B and Appendix C.

$$\begin{aligned}\mathcal{H} = \max_{c,h} \quad & e^{-\theta}[u(c) - \chi(\phi i)] \\ & + \lambda_1 \{f(k, 1-i) - \delta k - c - h - (b - d - \phi i)k\} \\ & + \lambda_2 \{b - bs - \alpha(h)si + \psi(1 - s - i) + \phi si\} \\ & + \lambda_3 \left\{\alpha(h)si - bi - \gamma i - \phi i + \phi i^2\right\} \\ & + \lambda_4 \{r - b + d + \phi i\} + \mu_1 s + \mu_2 i + \mu_3 h.\end{aligned} \tag{13}$$

$$\dot{\theta} V(k, i, s, \theta) = \sup_{c,h} \left\{ u(c) - \chi(\phi i) + \frac{\partial V}{\partial k}\dot{k} + \frac{\partial V}{\partial i}\dot{i} + \frac{\partial V}{\partial s}\dot{s} + \frac{\partial V}{\partial \theta}\dot{\theta} \right\}. \tag{14}$$

Figure 7 shows the convergence path with different calibrations of parameter ξ in the non-pecuniary punishment function. For comparison, we also plot the convergence paths of the baseline SIRS model in the gray dash lines. We find the basic structure of the dynamics looks similar for models with or without mortality. The health policy is pro-cyclical to the social infection rate. The convergence paths of capital and consumption are negatively affected by pandemic during the first 100 days. The labour is also dampened during the pandemic and recover back to its steady state, which is smaller than the initial value. Differently, we find that the steady labour is smaller than our baseline model.

The paths also show some counter-intuitive results. We find that for the calibration with lower mortality punishment, i.e. VSL equals output (blue lines) and VSL equals 40 times of output (red lines), the optimal health expenditure is smaller than the standard SIRS model without mortality. The corresponding infection rate is thus higher.

We provide a possible explanation on why mortality oppositely reduces optimal health expenditure in the following way. The excess death by the pandemic decreases the total population, which implies that each person could share more capital. The social benefit of holding more capital could overweight the loss by higher infection. This could be roughly shown by the simulation with $VSL = 40y$ (red lines) in Figure 7. The infection rate under this calibration is slightly higher than that in the baseline. However, higher infection doesn't imply lower capital as we anticipate. We find the reduction in capital is not as much as that in the baseline during the

Figure 7. Convergence Path for SIRS model with Mortality

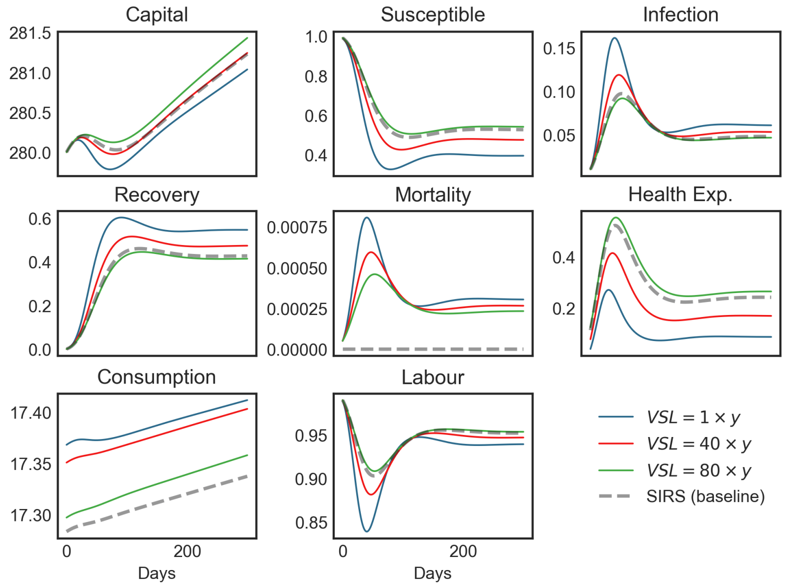

Notes: (i) This Figure shows the convergence paths under different levels of direct punishment on mortality. (ii) The gray dash lines are the referenced paths in our baseline SIRS model without mortality and Long Covid.

first few months. Moreover, when we further increase the direct punishment, i.e. $VSL = 80y$ (green lines), the optimal health expenditure becomes strictly higher than the baseline. There is another epidemiological reason why mortality has this counter-intuitive effect. Higher mortality reduces the number of infective individuals reducing the transmission of the disease. That is, mortality has a self-limiting effect on the transmission of the disease. Without further useful insights, we plot the transitional paths of the SIR model with mortality in Appendix Figure A8.

V. CONCLUSION

Our paper computes value and policy functions in the canonical epidemiological economic models by using the deep-learning dynamic programming approach. We visualize and compare the policy functions for health expenditure and the dynamics for two basic epidemiological models (SIR and SIRS models). We conclude with the following remarks: (1) The optimal health policy under SIR and SIRS looks qualitatively similar that it increases with both susceptible and infection rates. The magnitude and dynamics for health policy are different for two models. The optimal health expenditure is larger and persistent under SIRS model. However, for SIR model, health expenditure is smaller during pandemic and is 0 at the steady state. (2) The epidemiological states follows the stable focus dynamics. For SIR, the outbreak of infection is more severe but the stable rate is low. For SIRS, reinfection induces higher infection rate at the steady state. However, the outbreak is milder because of the intervention of health expenditure. (3) If the model is misspecified that the social planner uses the health policy function in the other model, value loss would be induced. The loss of misspecifying SIRS model is larger than that of misspecifying SIR model. Thus, the social planner could be better-off by treating the disease by SIRS model when disease characteristics are unknown. (4) For vaccination, we show that a higher weight of vaccinated people could efficiently milden the peak infection rate. (5) When we introduce mortality and Long Covid into the model, the optimal path for health expenditure does not necessarily increase as people could share more capital per capita when there is less population. It depends on the contest between the value of statistical life and the gain by holding more capital per capita.

References

Acemoglu, Daron, Victor Chernozhukov, Iván Werning, and Michael D Whinston. 2021. "Optimal targeted lockdowns in a multigroup SIR model." American Economic Review: Insights, 3(4): 487–502.

Achdou, Yves, Jiequn Han, Jean-Michel Lasry, Pierre-Louis Lions, and Benjamin Moll. 2022. "Income and wealth distribution in macroeconomics: A continuous-time approach." The review of economic studies, 89(1): 45–86.

Alvarez, Fernando, David Argente, and Francesco Lippi. 2021. "A simple planning problem for COVID-19 lock-down, testing, and tracing." American Economic Review: Insights, 3(3): 367–382.

Andersson, Henrik, and Nicolas Treich. 2011. "The value of a statistical life." In A handbook of transport economics. Edward Elgar Publishing.

Barron, Andrew R. 1993. "Universal approximation bounds for superpositions of a sigmoidal function." IEEE Transactions on Information theory, 39(3): 930–945.

Bobrovitz, Niklas, Harriet Ware, Xiaomeng Ma, Zihan Li, Reza Hosseini, Christian Cao, Anabel Selemon, Mairead Whelan, Zahra Premji, Hanane Issa, et al. 2023. "Protective effectiveness of previous SARS-CoV-2 infection and hybrid immunity against the omicron variant and severe disease: a systematic review and meta-regression." The Lancet Infectious Diseases.

Boucekkine, Raouf, Shankha Chakraborty, Aditya Goenka, and Lin Liu. 2024. "Economic epidemiological modelling: A progress report." Journal of Mathematical Economics, 103011.

Cagigi, Alberto, Meng Yu, Björn Österberg, Julia Svensson, Sara Falck-Jones, Sindhu Vangeti, Eric Åhlberg, Lida Azizmohammadi, Anna Warnqvist, Ryan Falck-Jones, et al. 2021. "Airway antibodies emerge according to COVID-19 severity and wane rapidly but reappear after SARS-CoV-2 vaccination." JCI insight, 6(22).

Calvia, Alessandro, Fausto Gozzi, Francesco Lippi, and Giovanni Zanco. 2024. "A simple planning problem for COVID-19 lockdown: a dynamic programming approach." Economic Theory, 77(1): 169–196.

Cele, Sandile, Inbal Gazy, Laurelle Jackson, Shi-Hsia Hwa, Houriiyah Tegally, Gila Lustig, Jennifer Giandhari, Sureshnee Pillay, Eduan Wilkinson, Yeshnee Naidoo, et al. 2021. "Escape of SARS-CoV-2 501Y. V2 from neutralization by convalescent plasma." Nature, 593(7857): 142–146.

Eichenbaum, Martin S, Sergio Rebelo, and Mathias Trabandt. 2021. "The macroeconomics of epidemics." The Review of Financial Studies, 34(11): 5149–5187.

Federico, Salvatore, Giorgio Ferrari, and Maria-Laura Torrente. 2022. "Optimal vaccination in a SIRS epidemic model." Economic Theory, 1–26.

Ferguson, Neil, Daniel Laydon, Gemma Nedjati Gilani, Natsuko Imai, Kylie Ainslie, Marc Baguelin, Sangeeta Bhatia, Adhiratha Boonyasiri, ZULMA Cucunuba Perez, Gina Cuomo-Dannenburg, et al. 2020. "Report 9: Impact of non-pharmaceutical interventions (NPIs) to reduce COVID19 mortality and healthcare demand."

Fernandez-Villaverde, Jesus, Galo Nuno, George Sorg-Langhans, and Maximilian Vogler. 2020. "Solving high-dimensional dynamic programming problems using deep learning." Unpublished working paper.

Fernández-Villaverde, Jesús, Samuel Hurtado, and Galo Nuno. 2023. "Financial frictions and the wealth distribution." Econometrica, 91(3): 869–901.

Flaxman, Seth, Swapnil Mishra, Axel Gandy, H Juliette T Unwin, Thomas A Mellan, Helen Coupland, Charles Whittaker, Harrison Zhu, Tresnia Berah, Jeffrey W Eaton, et al. 2020. "Estimating the effects of non-pharmaceutical interventions on COVID-19 in Europe." Nature, 584(7820): 257–261.

Garriga, Carlos, Rody Manuelli, and Siddhartha Sanghi. 2022. "Optimal management of an epidemic: Lockdown, vaccine and value of life." Journal of Economic Dynamics and Control, 140: 104351.

Goenka, A, and L Liu. 2020. "Human capital, infectious diseases and economic growth." Economic Theory, 70(1).

Goenka, Aditya, and Lin Liu. 2012. "Infectious diseases and endogenous fluctuations." Economic Theory, 50: 125–149.

Goenka, Aditya, Lin Liu, and Manh-Hung Nguyen. 2014. "Infectious diseases and economic growth." Journal of Mathematical Economics, 50: 34–53.

Goenka, Aditya, Lin Liu, and Manh-Hung Nguyen. 2021. "SIR economic epidemiological models with disease induced mortality." Journal of Mathematical Economics, 93: 102476.

Goenka, Aditya, Lin Liu, and Manh-Hung Nguyen. 2024. "Modelling optimal lockdowns with waning immunity." Economic theory, 77(1): 197–234.

Goldman, Steven, and James Lightwood. 2002. "Cost optimization in the SIS model of infectious disease with treatment." Topics in Economic Analysis & Policy, 2(1): 1007.

Hansen, Christian Holm, Daniela Michlmayr, Sophie Madeleine Gubbels, Kåre Mølbak, and Steen Ethelberg. 2021. "Assessment of protection against reinfection with SARS-CoV-2 among 4 million PCR-tested individuals in Denmark in 2020: a population-level observational study." The lancet, 397(10280): 1204–1212.

Hethcote, Herbert W. 2000. "The mathematics of infectious diseases." SIAM review, 42(4): 599–653.

Linka, Kevin, Mathias Peirlinck, and Ellen Kuhl. 2020. "The reproduction number of COVID-19 and its correlation with public health interventions." Computational mechanics, 66: 1035–1050.

Liu, Ying, and Joacim Rocklöv. 2022. "The effective reproductive number of the Omicron variant of SARS-CoV-2 is several times relative to Delta." Journal of travel medicine, 29(3): taac037.

Marini, John J, and Luciano Gattinoni. 2020. "Management of COVID-19 respiratory distress." Jama, 323(22): 2329–2330.

ONS. 2023. "More information on data sources related to coronavirus (COVID-19)."

Sabino, Ester C, Lewis F Buss, Maria PS Carvalho, Carlos A Prete, Myuki AE Crispim, Nelson A Fraiji, Rafael HM Pereira, Kris V

Parag, Pedro da Silva Peixoto, Moritz UG Kraemer, et al. 2021. "Resurgence of COVID-19 in Manaus, Brazil, despite high seroprevalence." The Lancet, 397(10273): 452–455.

Safan, Muntaser, Mirjam Kretzschmar, and Karl P Hadeler. 2013. "Vaccination based control of infections in SIRS models with reinfection: special reference to pertussis." Journal of mathematical biology, 67: 1083–1110.

Sepandi, Mojtaba, Yousef Alimohamadi, and Firooz Esmaeilzadeh. 2022. "Estimate of the basic reproduction number for delta variant of sars-cov-2: a systematic review and meta-analysis." Journal of Biostatistics and Epidemiology.

Sorensen, RJD, RM Barber, DM Pigott, Austin Carter, CN Spencer, SM Ostroff, RC Reiner, Cristiana Abbafati, Christopher Adolph, Adrien Allorant, et al. 2022. "Variation in the COVID-19 infection-fatality ratio by age, time, and geography during the pre-vaccine era: A systematic analysis." The Lancet, 399(10334): 1469–1488.

Sun, Chengjun, and Wei Yang. 2010. "Global results for an SIRS model with vaccination and isolation." Nonlinear Analysis: Real World Applications, 11(5): 4223–4237.

UK Health Security Agency. 2023. "COVID-19 Omicron variant infectious period and transmission from people with asymptomatic compared with symptomatic infection: a rapid review."

Uzawa, Hirofumi. 2017. "Time preference, the consumption function, and optimum asset holdings." In Value, capital and Growth. 485–504. Routledge.

Appendices

A Figures

Figure A1. Consumption Policy Functions

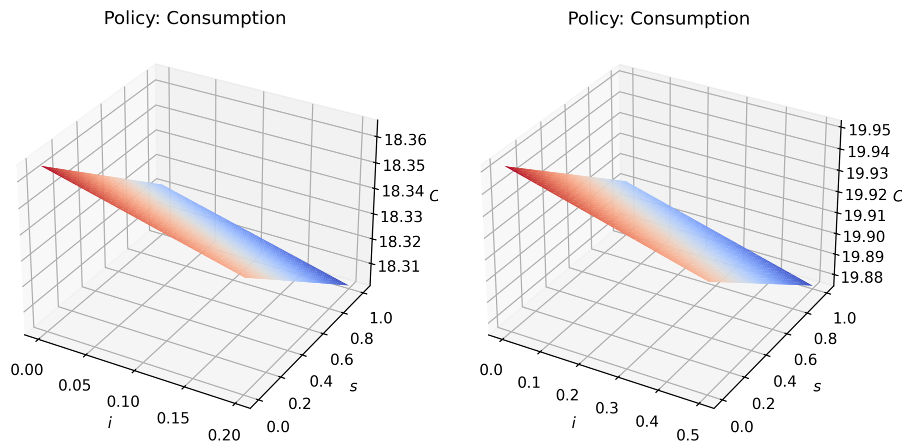

(a) SIRS **(b)** SIR

Figure A2. Value Functions

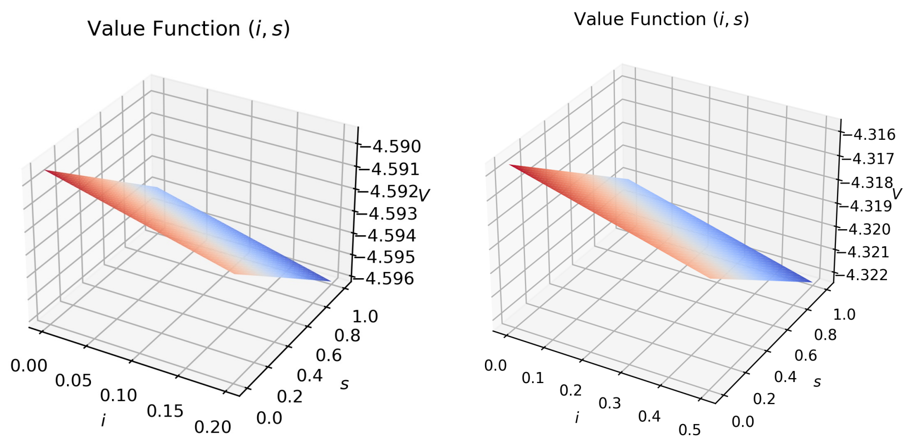

(a) SIRS **(b)** SIR

Figure A3. Path of Capital and Labour Participation

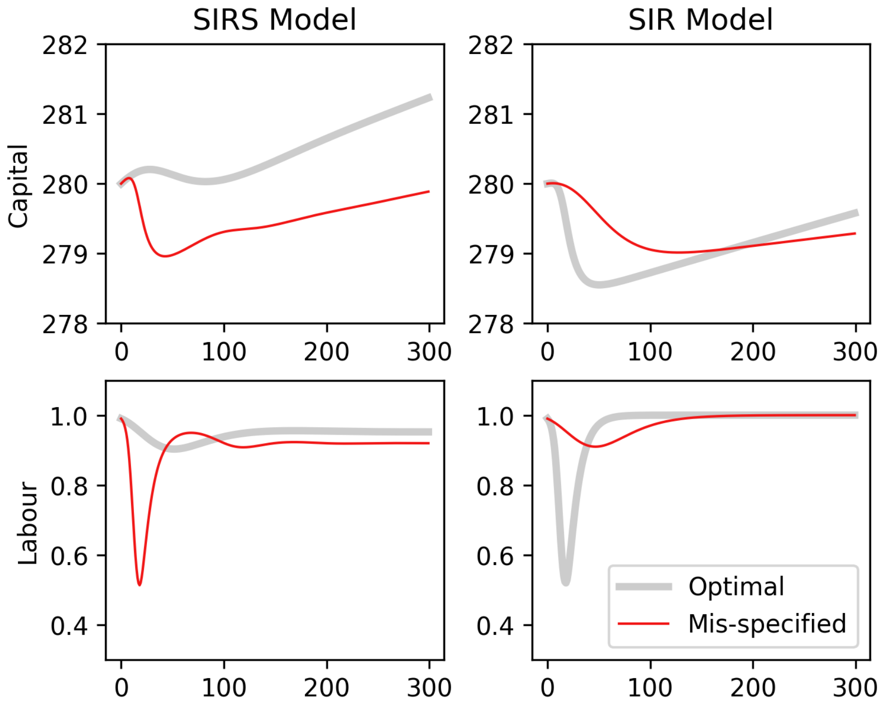

Figure A4. Pure SIRS

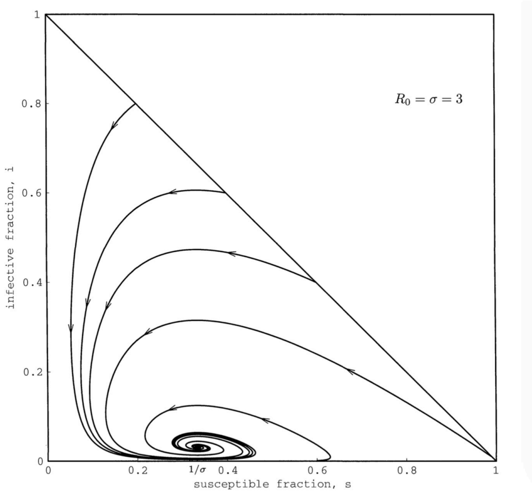

Figure A5. $\dot{i}$ for SIRS and SIR Models

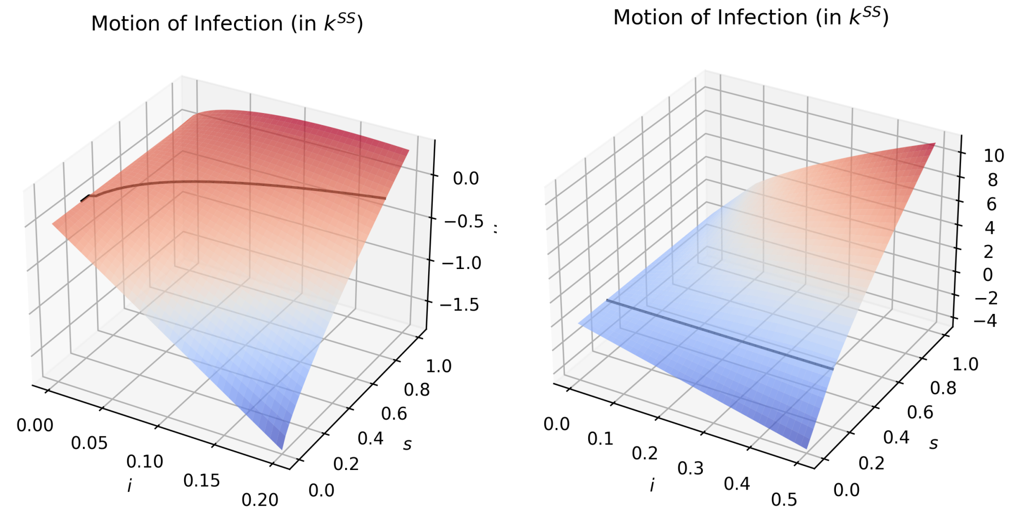

(a) SIRS **(b)** SIR

Figure A6. $\dot{s}$ for SIRS and SIR Models

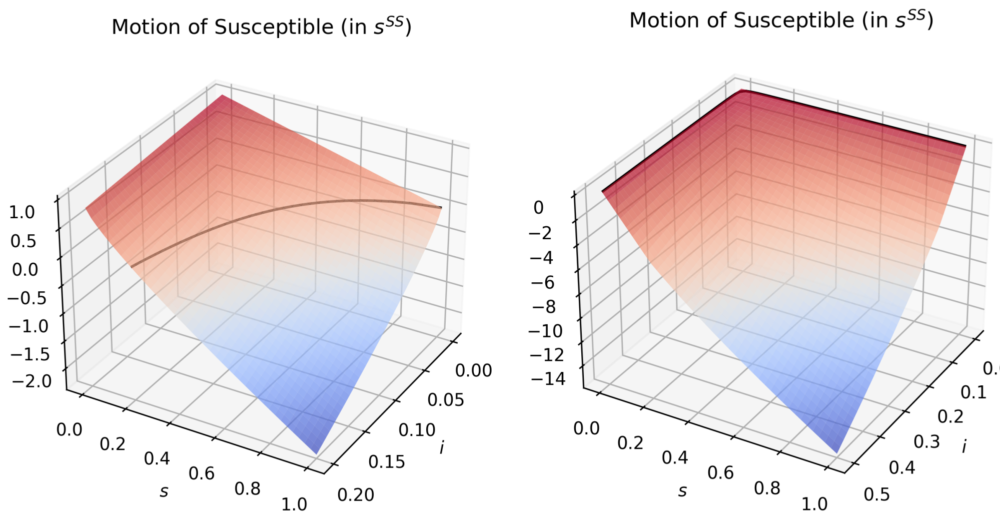

(a) SIRS **(b)** SIR

Figure A8. Convergence Path for SIR model with Mortality

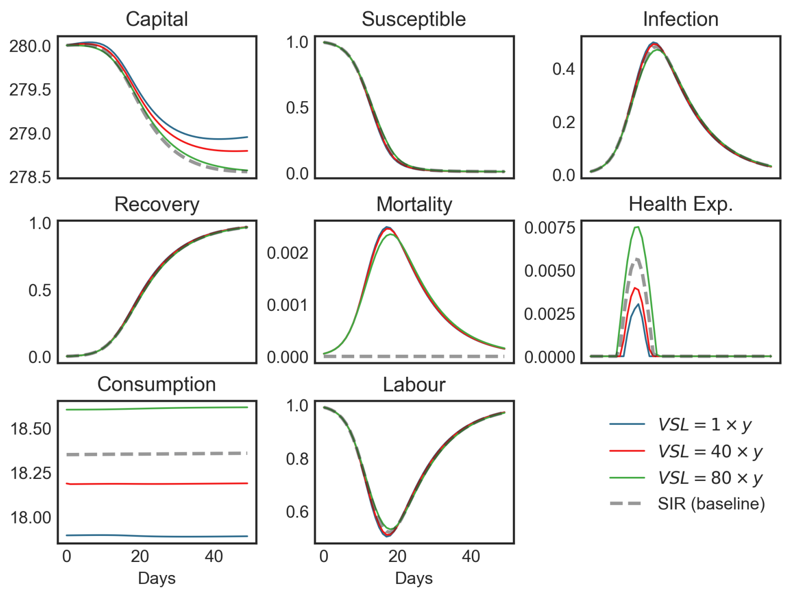

Figure A7. Flow of Epidemiological Compartments

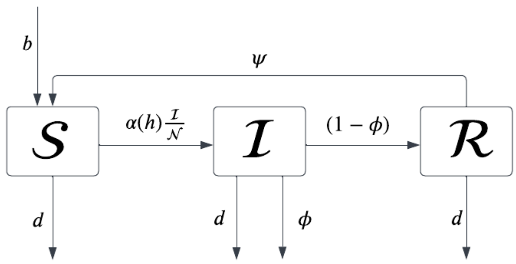

Figure A9. Composition Change for Compartments (Models with Mortality)

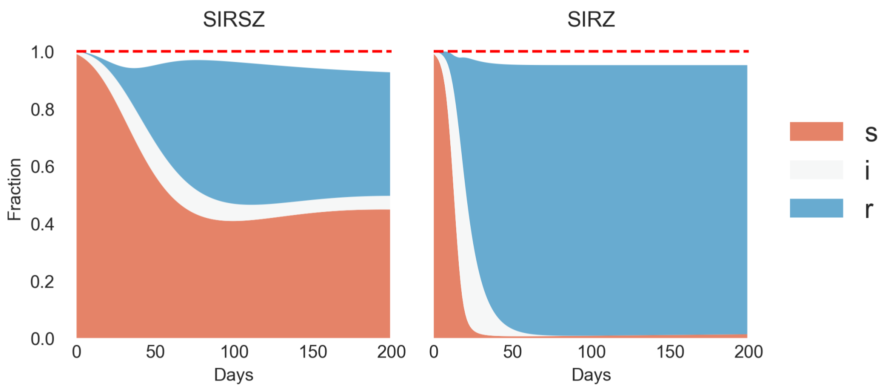

B Hamiltonian

A. *Baseline SIRS/SIR Model*

$$
\begin{aligned}
\max_{c,h} \quad & \int_0^\infty e^{-\rho t} u(c) N_0 dt \\
s.t. \quad & \dot{k} = F(k, 1-i) - \delta k - c - h - (b-d)k, \\
& \dot{s} = b - bs - \alpha(h)si + \psi(1-s-i), \\
& \dot{i} = \alpha(h)si - bi - \gamma i, \\
& s \geq 0, \\
& i \geq 0, \\
& h \geq 0,
\end{aligned}
\tag{A1}
$$

where $\rho = r - (b-d)$. For simplicity, let the initial population $N_0 = 1$, the present value Hamiltonian is

$$
\begin{aligned}
\mathcal{H} = \max_{c,h} \quad & e^{-\rho t} u(c) + \lambda_1 [F(k, 1-i) - \delta k - c - h - (b-d)k] \\
& + \lambda_2 [b - bs - \alpha(h)si + \psi(1-s-i)] \\
& + \lambda_3 [\alpha(h)si - bi - \gamma i] + \mu_1 s + \mu_2 i + \mu_3 h.
\end{aligned}
\tag{A2}
$$

Disease Free Steady State

By Goenka, Liu and Nguyen (2021), there exist disease-free steady state. The disease-free steady state is stable when the contact number

$$\frac{\alpha(0)}{b+\gamma} \leq 1. \tag{A3}$$

The disease-free steady state is determined by

$$
\begin{aligned}
& f_1(k, 1) = r + \delta, \\
& c = f(k, 1) - \delta k - (b-d)k.
\end{aligned}
\tag{A4}
$$

Endemic Steady State

If $\frac{\alpha(0)}{b+\gamma} > 1$, the disease-free steady state is unstable, while the endemic steady state is stable.

The optimal health expenditure h^* is determined by the $G(h)$ function.

Given the endemic steady state, we have $\mu_1 = \mu_2 = 0$. The F.O.C. are

$$
\begin{aligned}
c: &\quad e^{-\rho t}u'(c) - \lambda_1 = 0, && \text{(A5)}\\
h: &\quad -\lambda_1 - \lambda_2 \alpha'(h) si + \lambda_3 \alpha'(h) si + \mu_3 = 0, && \text{(A6)}\\
k: &\quad -\dot{\lambda}_1 = \lambda_1[F_1 - \delta - (b-d)], && \text{(A7)}\\
s: &\quad -\dot{\lambda}_2 = \lambda_2[-b - \alpha(h)i - \psi] + \lambda_3 \alpha(h) i, && \text{(A8)}\\
i: &\quad -\dot{\lambda}_3 = -\lambda_1 F_2 + \lambda_2[-\alpha(h)s - \psi] + \lambda_3[\alpha(h)s - b - \gamma]. && \text{(A9)}
\end{aligned}
$$

By the Equation A5 and Equation A6, we have

$$\mu_3 = \lambda_1 - (\lambda_3 - \lambda_2)\alpha'(h)si. \tag{A10}$$

- $\mu_3 > 0 \Rightarrow MC > MR \Rightarrow h = 0$,
- $\mu_3 = 0 \Rightarrow MC > MR \Rightarrow h > 0$,
- We just need to pin down λ_3, λ_2 and c.

In steady state, we have $\frac{\dot{\lambda}_1}{\lambda_1} = \frac{\dot{\lambda}_2}{\lambda_2} = \frac{\dot{\lambda}_3}{\lambda_3} = -\rho$. From F.O.C.s we have

$$
\begin{aligned}
&-\frac{\dot{\lambda}_2}{\lambda_2} = -b - \alpha(h)i - \psi + \frac{\lambda_3}{\lambda_2}\alpha(h)i = \rho\\
\Rightarrow &\quad \lambda_3 \alpha(h) i = [\rho + b + \alpha(h)i + \psi]\lambda_2.
\end{aligned} \tag{A11}
$$

From Equation A9 we have

$$
\begin{aligned}
&-\frac{\dot{\lambda}_3}{\lambda_3} = -\frac{\lambda_1}{\lambda_3}F_2 + \frac{\lambda_2}{\lambda_3}[-\alpha(h)s - \psi] + [\alpha(h)s - b - \gamma] = \rho\\
\Rightarrow &\quad -\lambda_1 F_2 + [\alpha(h)s - b - \gamma - \rho]\lambda_3 = \lambda_2[\alpha(h)s + \psi]\\
\Rightarrow &\quad -e^{-\rho t}u'(c)F_2 + [\alpha(h)s - b - \gamma - \rho]\lambda_3 = \lambda_2[\alpha(h)s + \psi].
\end{aligned} \tag{A12}
$$

Hence, by

$$
\begin{cases}
\lambda_3 \alpha(h) i = [\rho + b + \alpha(h)i + \psi]\lambda_2\\
-e^{-\rho t}u'(c)F_2 + [\alpha(h)s - b - \gamma - \rho]\lambda_3 = \lambda_2[\alpha(h)s + \psi].
\end{cases} \tag{A13}
$$

We can solve out

$$
\begin{cases}
\lambda_2 = \frac{e^{-\rho t}u'(c)F_2}{M}\\
\lambda_3 = \left[\frac{\rho + b + \alpha(h)i + \psi}{\alpha(h)i}\right]\lambda_2,
\end{cases} \tag{A14}
$$

where

$$M = \frac{[\alpha(h)s - b - \gamma - \rho][\rho + b + \alpha(h)i + \psi]}{\alpha(h)i} - \alpha(h)s - \psi. \tag{A15}$$

Define $\tilde{\lambda}_1 = \frac{1}{e^{-\rho t}}\lambda_1$, $\tilde{\lambda}_2 = \frac{1}{e^{-\rho t}}\lambda_2$, $\tilde{\lambda}_3 = \frac{1}{e^{-\rho t}}\lambda_3$. So we have

$$\begin{cases} \tilde{\lambda}_2 = \frac{u'(c)F_2}{M} \\ \tilde{\lambda}_3 = \left[\frac{\rho+b+\alpha(h)i+\psi}{\alpha(h)i}\right]\tilde{\lambda}_2. \end{cases} \tag{A16}$$

Then, we can have

$$\begin{aligned} \frac{\mu_3}{e^{-\rho t}} &= \tilde{\lambda}_1 - (\tilde{\lambda}_3 - \tilde{\lambda}_2)\alpha'(h)si \\ &= u'(c) - \left[\frac{\rho + b + \alpha(h)i + \psi}{\alpha(h)i} - 1\right]\frac{u'(c)F_2}{M}\alpha'(h)si \\ &= u'(c) - \left[\frac{\rho + b + \psi}{\alpha(h)i}\right]\frac{u'(c)F_2\alpha'(h)si}{M} \\ &= u'(c)\left[1 - \frac{(\rho + b + \psi)F_2\alpha'(h)s}{\alpha(h)M}\right]. \end{aligned} \tag{A17}$$

Define the G function as

$$G(h) = 1 - \frac{(\rho + b + \psi)F_2\alpha'(h)s}{\alpha(h)M}. \tag{A18}$$

The solution for the optimization problem is determined by the following equations

$$s = \frac{b+\gamma}{\alpha(h)}, \tag{A19}$$

$$i = \frac{b - bs + \psi(1-s)}{\alpha(h)s + \psi}, \tag{A20}$$

$$f(k, 1-i) - \delta k - c - h - (b-d)k = 0, \tag{A21}$$

$$f_1(k, 1-i) = r + \delta, \tag{A22}$$

$$\mu_3 h = 0. \tag{A23}$$

Solution Strategy:

- From the first 2 expression, we can have i, s as function of h. i.e. $\hat{\imath}(h), \hat{s}(h)$.
- From the forth equation $f(k, 1-\hat{\imath}(h))$, we can solve out k as a function of h. i.e. $\hat{k}(h)$.
- Calculate $G(0)$.
  - If $G(0) > 0$, Corner Solution, the we have $h^* = 0$.

– If $G(0) < 0$, Interior Solution, the solution of h^* is given by $G(h) = 0$.

Figure A10. G Function

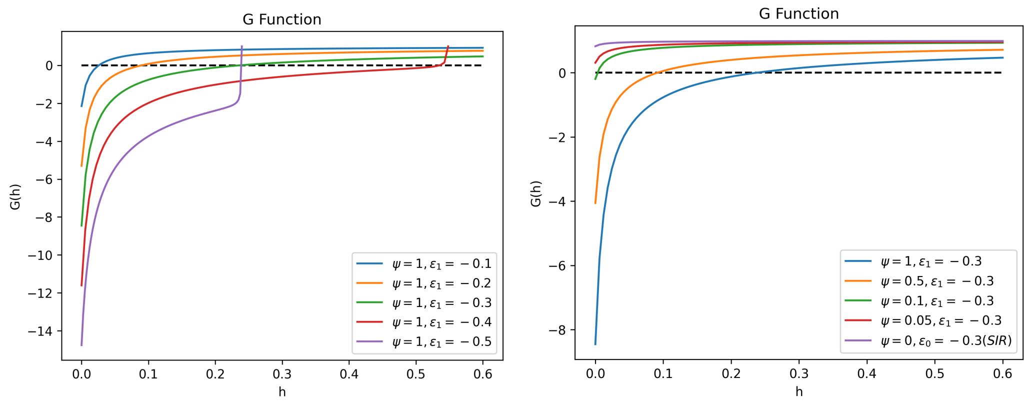

(a) Varying ϵ_1 **(b)** Varying ψ

B. SIRS Model with Mortality and Long Covid

We focus on the endemic steady state. For generalization, we draw further assumption that the recovered people are also faced with η fraction of productivity loss. This assumption could be used to model Long Covid. The Hamiltonian for the optimization problem is

$$\begin{aligned} \mathcal{H} = \max_{c,h} \quad & e^{-\Theta}[u(c) - \chi(\phi i)] \\ & + \lambda_1 \{f(k, 1 - i - \eta(1 - s - i)) - \delta k - c - h - (b - d - \phi i)k\} \\ & + \lambda_2 \{b - bs - \alpha(h)si + \psi(1 - s - i) + \phi si\} \\ & + \lambda_3 \left\{\alpha(h)si - bi - \gamma i - \phi i + \phi i^2\right\} \\ & + \lambda_4 \{r - b + d + \phi i\} + \mu_1 s + \mu_2 i + \mu_3 h. \end{aligned} \tag{A24}$$

The F.O.C.s are

$$c: \quad e^{-\Theta}u'(c) - \lambda_1 = 0, \tag{A25}$$
$$h: \quad -\lambda_1 - \lambda_2\alpha'(h)si + \lambda_3\alpha'(h)si + \mu_3 = 0, \tag{A26}$$
$$k: \quad -\dot{\lambda}_1 = \lambda_1(f_1 - \delta - b + d + \phi i), \tag{A27}$$
$$s: \quad -\dot{\lambda}_2 = \lambda_1 f_2\eta + \lambda_2[-b - \alpha(h)i - \psi + \phi i] + \lambda_3\alpha(h)i + \mu_1, \tag{A28}$$
$$i: \quad -\dot{\lambda}_3 = -e^{-\Theta}\chi'(\phi i)\phi + \lambda_1[f_2(\eta - 1) + \phi k] + \lambda_2[-\alpha(h)s - \psi + \phi s] \tag{A29}$$
$$+\lambda_3[\alpha(h)s - b - \gamma - \phi + 2\phi i] + \lambda_4\phi + \mu_2, \tag{A30}$$
$$\Theta: \quad -\dot{\lambda}_4 = -e^{-\Theta}[u(c) - \chi(\phi i)]. \tag{A31}$$

From the Equation A27, we have

$$\begin{aligned} -\frac{\dot{\lambda}_1}{\lambda_1} &= f_1 - \delta - b + d + \phi i \\ &= f_1 - \delta - b + d + \phi i. \end{aligned} \tag{A32}$$

From F.O.C.c we have

$$\begin{aligned} \frac{\dot{\lambda}_1}{\lambda_1} &= -\dot{\Theta} + \frac{u''(c)}{u'(c)}\dot{c} \\ &= -(r - b + d + \phi i) + \frac{u''(c)}{u'(c)}\dot{c} \end{aligned} \tag{A33}$$

Using $\dot{c} = 0$ in steady state, we have

$$\frac{\dot{\lambda}_1}{\lambda_1} = -(r - b + d + \phi i). \tag{A34}$$

Therefore, we have $f_1 = r + \delta$.
Then, using condition that growth rate for co-states are the same

$$\frac{\dot{\lambda}_1}{\lambda_1} = \frac{\dot{\lambda}_2}{\lambda_2} = \frac{\dot{\lambda}_3}{\lambda_3} = \frac{\dot{\lambda}_4}{\lambda_4} = -(r - b + d + \phi i) \equiv g. \tag{A35}$$

Equation A28 yields

$$\begin{aligned} -g\lambda_2 &= \lambda_1 f_2\eta + \lambda_2[-b - \alpha(h)i - \psi + \phi i] + \lambda_3\alpha(h)i \\ [-g + b + \alpha(h)i + \psi - \phi i]\lambda_2 - \lambda_3\alpha(h)i &= \lambda_1 f_2\eta \\ [r + d + \psi + \alpha(h)i]\lambda_2 - \lambda_3\alpha(h)i &= \lambda_1 f_2\eta \\ [r + d + \psi + \alpha(h)i]\tilde{\lambda}_2 - \alpha(h)i\tilde{\lambda}_3 &= f_2\eta\tilde{\lambda}_1. \end{aligned} \tag{A36}$$

where we let $\tilde{\lambda}_j = \frac{\lambda_j}{e^{-\Theta}}$

Similarly, Equation A30 yields

$$\begin{aligned}[-g-\alpha(h)s+b+\gamma+\phi-2\phi i]\lambda_3 &= -e^{-\Theta}\chi'(\phi i)\phi+\lambda_1[f_2(\eta-1)+\phi k]+\lambda_2[-\alpha(h)s-\psi+\phi s]+\lambda_4\phi \\ [r+d-\phi i-\alpha(h)s+\gamma+\phi]\lambda_3 &= -e^{-\Theta}\chi'(\phi i)\phi+e^{-\Theta}u'(c)[f_2(\eta-1)+\phi k]+\lambda_2[-\alpha(h)s-\psi+\phi s] \\ &\quad + \frac{e^{-\Theta}[u(c)-\chi(\phi i)]}{-(r-b+d+\phi i)}\phi.\end{aligned} \tag{A37}$$

That is

$$[\alpha(h)s+\psi-\phi s]\tilde{\lambda}_2+[r+d-\phi i-\alpha(h)s+\gamma+\phi]\tilde{\lambda}_3 = -\chi'(\phi i)\phi+u'(c)[f_2(\eta-1)+\phi k]-\frac{u(c)-\chi(\phi i)}{r-b+d+\phi i}\phi. \tag{A38}$$

Then, we can solve out $\tilde{\lambda}_2, \tilde{\lambda}_3$ unitedly by

$$\begin{cases}[r+d+\psi+\alpha(h)i]\tilde{\lambda}_2-\alpha(h)i\tilde{\lambda}_3 = f_2\eta u'(c) \\ [\alpha(h)s+\psi-\phi s]\tilde{\lambda}_2+[r+d-\phi i-\alpha(h)s+\gamma+\phi]\tilde{\lambda}_3 = -\chi'(\phi i)\phi+u'(c)[f_2(\eta-1)+\phi k]-\frac{u(c)-\chi(\phi i)}{r-b+d+\phi i}\phi.\end{cases} \tag{A39}$$

Notate the coefficients for $\tilde{\lambda}_2$ and $\tilde{\lambda}_3$ we have

$$\begin{cases} w_{11}\tilde{\lambda}_2+w_{12}\tilde{\lambda}_3 = I_1 \\ w_{21}\tilde{\lambda}_2+w_{22}\tilde{\lambda}_3 = I_2.\end{cases} \tag{A40}$$

From Equation A26 we have

$$\begin{aligned}\mu_3 &= \lambda_1+\lambda_2\alpha'(h)si-\lambda_3\alpha'(h)si \\ &= e^{-\Theta}u'(c)+(\lambda_2-\lambda_3)\alpha'(h)si \\ &= e^{-\Theta}[u'(c)+(\tilde{\lambda}_2-\tilde{\lambda}_3)\alpha'(h)si].\end{aligned} \tag{A41}$$

Define the G function such that

$$\mathcal{G} = u'(c)+(\tilde{\lambda}_2-\tilde{\lambda}_3)\alpha'(h)si. \tag{A42}$$

Solution Strategy

Using the steady state condition $\dot{i}=0, \dot{s}=0$, we have

$$\begin{cases}\alpha(h)s-b-\gamma-\phi+\phi i = 0 \\ b-bs-\alpha(h)si+\psi(1-s-i)+\phi si = 0.\end{cases} \tag{A43}$$

we can solve out i and s as functions of h, denoted by $i^*(h), s^*(h)$

Using the F.O.C. $f_1(k, 1-i-\eta(1-s-i)) = r+\delta$, we can solve out k as function of h, denoted by $k^*(h)$.

Using $\dot{k} = 0$ we can solve out $c^*(h)$. Finally, we can express and plot $\mathcal{G}(h)$. We can solve out h^* by $\mathcal{G}(h^*) = 0$.

C HJB

A. General Approach of HJB

- state $X_t \in \mathbb{R}^d$
- control $a_t \in \mathcal{A}$
- value function $V(t, X_t)$
- return function $\mathcal{R}(t, X_t, a_t)$

$$V(t, X_t) = \sup_{a_t} \mathbb{E} \int_t^{\infty} \mathcal{R}(\tau, X_\tau, a_\tau) d\tau. \tag{A44}$$

By Bellman optimization principle, given a small interval dt

$$\begin{aligned} V(t, X_t) &= \sup_{a_t} \{\mathcal{R}(t, X_t, a_t)dt + \mathbb{E}[V(t+dt, X_{t+dt})]\} \\ 0 &= \sup_{a_t} \{\mathcal{R}(t, X_t, a_t)dt + \mathbb{E}[V(t+dt, X_{t+dt}) - V(t, X_t)]\} \\ 0 &= \sup_{a_t} \{\mathcal{R}(t, X_t, a_t)dt + \mathbb{E}[dV(t, X_t)]\} \\ 0 &= \sup_{a_t} \left\{\mathcal{R}(t, X_t, a_t)dt + \mathbb{E}\left[\frac{\partial V}{\partial t}dt + \langle \nabla_X V, dX_t \rangle\right]\right\}. \end{aligned} \tag{A45}$$

Cancel out dt, we can specify the HJB as

$$\sup_{a_t} \left\{\mathcal{R}(t, X_t, a_t) + \mathbb{E}\left[\frac{\partial V}{\partial t} + \langle \nabla_X V, \dot{X}_t \rangle\right]\right\} = 0. \tag{A46}$$

B. Application to the Baseline SIRS/SIR Model

The present value HJB is

$$0 = \sup_{c,h} \left\{e^{-\rho t} u(c) + \frac{\partial V}{\partial t} + \frac{\partial V}{\partial k}\dot{k} + \frac{\partial V}{\partial i}\dot{i} + \frac{\partial V}{\partial s}\dot{s}\right\}. \tag{A47}$$

We can change the present value HJB to current value

$$0 = \sup_{c,h} \left\{e^{-\rho t} \left(u(c) + e^{\rho t}\frac{\partial V}{\partial t} + e^{\rho t}\frac{\partial V}{\partial k}\dot{k} + e^{\rho t}\frac{\partial V}{\partial i}\dot{i} + e^{\rho t}\frac{\partial V}{\partial s}\dot{s}\right)\right\}. \tag{A48}$$

Now we define the current value HJB $W = e^{\rho t} V(k, i, s, t)$. We have $\frac{\partial W}{\partial k} = e^{\rho t}\frac{\partial V}{\partial k}$; $\frac{\partial V}{\partial i} = e^{\rho t}\frac{\partial V}{\partial i}$; $\frac{\partial V}{\partial s} = e^{\rho t}\frac{\partial V}{\partial s}$. For $\frac{\partial W}{\partial t}$

$$\begin{aligned}\frac{\partial W}{\partial t} =& e^{\rho t}V + e^{\rho t}\frac{\partial V}{\partial t} \\ =& \rho W + e^{\rho t}\frac{\partial V}{\partial t}.\end{aligned} \tag{A49}$$

Thus, we could rewrite

$$0 = \sup_{c,h}\left\{e^{-\rho t}\left(u(c) + \frac{\partial W}{\partial t} + \frac{\partial W}{\partial k}\dot{k} + \frac{\partial W}{\partial i}\dot{i} + \frac{\partial W}{\partial s}\dot{s} - \rho W\right)\right\}. \tag{A50}$$

The equation

$$0 = \sup_{c,h}\left\{u(c) + \frac{\partial W}{\partial t} + \frac{\partial W}{\partial k}\dot{k} + \frac{\partial W}{\partial i}\dot{i} + \frac{\partial W}{\partial s}\dot{s} - \rho W\right\}, \tag{A51}$$

is the Current Value HJB. PV-HJB and CV-HJB present the same solutions for the control variables as their F.O.C./S.O.C. are identical. Furthermore, We notice that for the CV-HJB

$$W = e^{\rho t}V = \sup_{a_t}\mathbb{E}\int_t^\infty e^{-\rho(\tau - t)}u(c_\tau)d\tau. \tag{A52}$$

The time dimension is normalized by t. Thus, the current value W is uncorrelated to time t that $\frac{\partial W}{\partial t} = 0$. Therefore, we could derive the HJB for our baseline model

$$\rho W(k,i,s) = \sup_{c,h}\left\{u(c) + \frac{\partial W}{\partial k}\dot{k} + \frac{\partial W}{\partial i}\dot{i} + \frac{\partial W}{\partial s}\dot{s}\right\}. \tag{A53}$$

The F.O.C. reads

$$\begin{aligned}&u'(c) - \partial_k W = 0 \\ &- \partial_k W + (\partial_i W - \partial_s W)\,\alpha'(h)si = 0.\end{aligned} \tag{A54}$$

We can now see how related between Hamiltonian and HJB. Recall that the $\mathcal{G}(h)$ function in Hamiltonian is

$$\mathcal{G}(h) = u'(c) + (\tilde{\lambda}_s - \tilde{\lambda}_i)\alpha'(h)si, \tag{A55}$$

where $\tilde{\lambda}_s, \tilde{\lambda}_i$ are the co-state for s, i

Manipulate the F.O.C. for HJB we have

$$u'(c) + (\frac{\partial W}{\partial s} - \frac{\partial W}{\partial i})\alpha'(h)si. \tag{A56}$$

C. Application to the Baseline SIRS with Mortality

There would be endogenous discount issue in this case.
Recall that the PV-HJB for value $V = \sup_{c,h} \int_0^\infty e^{-\rho\tau} u(c_\tau) d\tau$ reads

$$0 = \sup_{c,h} \left\{ e^{-\rho t} u(c) + \frac{\partial V}{\partial t} + \frac{\partial V}{\partial k}\dot{k} + \frac{\partial V}{\partial i}\dot{i} + \frac{\partial V}{\partial s}\dot{s} \right\}. \tag{A57}$$

Analogue this expression, for endogenous discount

$$V = \sup_{c,h} \int_t^\infty e^{-\theta_\tau} [u(c_\tau) - \chi(\phi i)] d\tau. \tag{A58}$$

The PV-HJB is

$$0 = \sup_{c,h} \left\{ e^{-\theta} [u(c) - \chi(\phi i)] + \frac{\partial V}{\partial \theta}\dot{\theta} + \frac{\partial V}{\partial k}\dot{k} + \frac{\partial V}{\partial i}\dot{i} + \frac{\partial V}{\partial s}\dot{s} \right\}. \tag{A59}$$

Go through the similar process as the baseline case

$$0 = \sup_{c,h} \left\{ e^{-\theta} \left[[u(c) - \chi(\phi i)] + e^{\theta}\frac{\partial V}{\partial \theta}\dot{\theta} + e^{\theta}\frac{\partial V}{\partial k}\dot{k} + e^{\theta}\frac{\partial V}{\partial i}\dot{i} + e^{\theta}\frac{\partial V}{\partial s}\dot{s} \right] \right\}. \tag{A60}$$

Define $W = e^{\theta} V$, we have

$$\begin{aligned} 0 &= \sup_{c,h} \left\{ e^{-\theta} \left[u(c) - \chi(\phi i) + (\frac{\partial W}{\partial \theta} - W)\dot{\theta} + \frac{\partial W}{\partial k}\dot{k} + \frac{\partial W}{\partial i}\dot{i} + \frac{\partial W}{\partial s}\dot{s} \right] \right\}, \\ 0 &= \sup_{c,h} \left\{ e^{-\theta} \left[u(c) - \chi(\phi i) + \frac{\partial W}{\partial \theta}\dot{\theta} + \frac{\partial W}{\partial k}\dot{k} + \frac{\partial W}{\partial i}\dot{i} + \frac{\partial W}{\partial s}\dot{s} - \dot{\theta} W \right] \right\}. \end{aligned} \tag{A61}$$

Because $\theta = \int_0^t (r - b + d + \phi i_\tau) d\tau$ is not a direct function of the controls c, h, solving

$$0 = \sup_{c,h} \left\{ u(c) - \chi(\phi i) + \frac{\partial W}{\partial \theta}\dot{\theta} + \frac{\partial W}{\partial k}\dot{k} + \frac{\partial W}{\partial i}\dot{i} + \frac{\partial W}{\partial s}\dot{s} - \dot{\theta} W \right\}, \tag{A62}$$

presents the same solution for controls.

D Deep Learning Algorithm

Deep Learning Neural Network (DLNN) approximate the value function. Recall that value function satisfies the HJB

$$u(c^*) + \partial_k V \dot{k} + \partial_i V \dot{i} + \partial_s V \dot{s} - (\rho - b + d)V = 0 \tag{A63}$$

Let $V^{NN}(k, s, i; \Theta)$ as an approximation for $V(k, s, i)$, where Θ is the hyper-parameter for the network. We define the HJB loss

$$Loss_{hjb} = u(c^*) + \partial_k V^{NN} \dot{k} + \partial_i V^{NN} \dot{i} + \partial_s V^{NN} \dot{s} - (\rho - b + d)V^{NN} \tag{A64}$$

Secondly, from FOC (Appendix C Equation A54), and SOC (**??**), we require $\partial_k V > 0$ and $\partial_i V - \partial_s V \leq 0$, we further define the FOC loss and SOC loss as follow

$$\begin{aligned} Loss_{foc} &= \max\{-\partial_k V^{NN}, 0\} \\ Loss_{soc} &= \max\{\partial_i V^{NN} - \partial_s V^{NN}, 0\} \end{aligned} \tag{A65}$$

The Mean Square Loss function is hence

$$MSE(\Theta) = Loss_{hjb}^2 + Loss_{foc}^2 + Loss_{soc}^2 \tag{A66}$$

The deep learning neural network V^{NN} is constructed using the following procedure

- Construct M linear combinition of (k, s, i) i.e. $z_m^{(0)} = \theta_0^{(0)} + \theta_{km}^{(0)} k + \theta_{sm}^{(0)} s + \theta_{im}^{(0)} i; \quad m = 1, 2, 3, ...M$
- Let $\phi^{(1)}(\cdot)$ be any activation function (ReLu, Tanh etc.)
- Construct linear combinition again $z_m^{(1)} = \theta_0^{(1)} + \sum_m \theta_m^{(1)} \phi^{(1)}(z_m^{(0)})$ (First Hidden Layer)
- Construct linear combinition again $z_m^{(2)} = \theta_0^{(2)} + \sum_m \theta_m^{(2)} \phi^{(2)}(z_m^{(1)})$ (Second Hidden Layer)
- etc.
- Deep learning approximation of L layers ($L - 1$ hidden layers) would be

$$v^{NN} = \theta_0^{(L)} + \sum_m \theta_m^{(L)} \phi^{(L)}(z_m^{(L-1)}) \tag{A67}$$

- Figure A11 shows the general structure for neural network

Figure A11. Deep Learning Neural Network

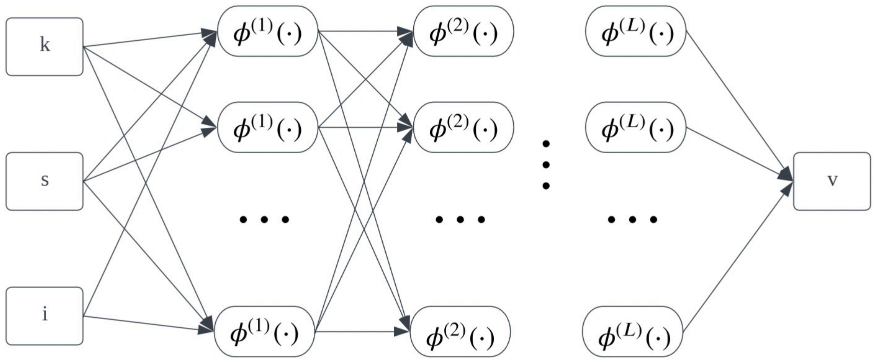

By the **Universal approximation theorem** (Hornik, Stinchcombe, and White, 1989), a neural network with at least one hidden layer can approximate any Borel measurable function mapping finite-dimensional spaces to any desired degree of accuracy. We just need to find proper architecture for the neural network and train the hyper-parameter $\Theta = \{\theta_0^{(0)} ... \theta_M^{(J)}\}$ to minimize MSE in Equation A66.

The architecture we select is $M = 10$ neurals, and $L = 7$ hidden layers. We use `ReLu` as the activation function for the first 6 hidden layers and `Tanh` for the last hidden layer. To train the neural network, we apply the Stochastic Gradient Descending (SGD) algorithm with mini-batch of 64[33]. `Adam` (Kingma et al., 2014) with the learning rate of 1e-3 is the optimizer for the training. We also apply 0.001 weight decay to prevent the over-fit problem.

Figure A12 plots the training loss and the verification loss along the convergence path. It shows that both type of losses are sufficiently small. Hence, our neural networks well approximate the HJB equations.

[33]To boost the training efficiency, we draw the mini-batch noramally around the steady state, which is obtained by Hamiltonian in Appendix B

Figure A12. MSE Losses

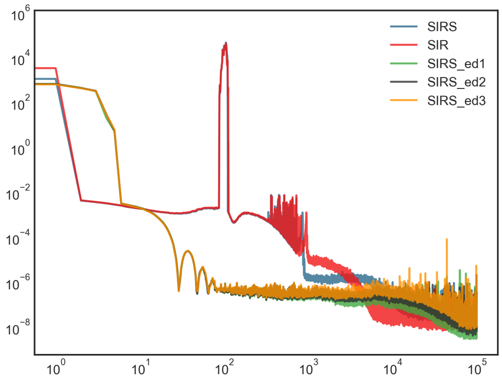

(a) Training Loss

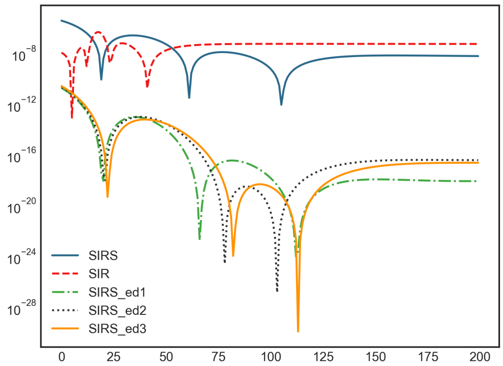

(b) Verification Loss

Health and Economic Inequality During Pandemics*

Aditya Goenka† Lin Liu‡ Haokun Pang §

December 7, 2024

Abstract

This paper studies the evolution of health and economic inequality during pandemics. It focuses on optimal preventive and treatment actions by agents who differ in their productivity, wealth and health status. Unlike the canonical Aiyagari-Bewley-Huggett framework where the income risk is exogenous, in our framework it is affected by individual choices and the endogenously determined economic and epidemiological variables. We have a heterogeneous agent continuous time (HACT) model where even if there are no exogenous productivity shocks the infection process introduces individual level heterogeneity and macroeconomic level fluctuations due to the interaction of the infection process, the control decisions, and effects on economic variables such as labour productivity and capital. Consistent with the evidence from the Covid-19, income, wealth, and health (proxied by infection rates) inequality increase during pandemics. The increase in income inequality is temporary but that of wealth is persistent. The increase in inequalities is driven by the increasing elasticities of health expenditures with wealth. We characterise the policy functions, the stationary equilibrium distributions and simulate the transitional dynamics to stationary equilibrium. We also evaluate the effect of government's income support scheme.

Keywords: Covid-19, SIRS model, Wealth and Health Heterogeneity, Aiyagari Model, HACT, Optimal Health Expenditure
JEL Classification: *E13, E22, D15, D50, D63, I10, I15, I18, O41, C61.*

---

*We thank seminar participants in the 2024 AMES Econometric Society; 2024 MMF Conference, Surrey; 2023 Conference on Advances in the economics and operational control of Covid, Rennes; CEMAP Conference 2023, Durham; SAET 2023, Paris; Rice and RSB Conference on Frontiers in Modelling in Epidemiological Economics 2023, Paris; 2023 EWMES Econometric Society, Manchester; 2024 AMSCW Econometric Society, Delhi; University of Birmingham, Delhi School of Economics, Presidency University, University of Sheffield, and Zhongnan University of Economics and Law, especially Raouf Boucekkine, Shankha Chabraborty, and Franck Portier for their helpful comments. The usual disclaimer applies. Aditya Goenka acknowledges research support from the British Academy.

†Department of Economics, University of Birmingham, Email: a.goenka@bham.ac.uk
‡Management School, University of Liverpool, Email: lin.liu@liverpool.ac.uk
§Department of Economics, University of Birmingham, Email: h.pang.1@bham.ac.uk

I. INTRODUCTION

The Covid-19 pandemic has had asymmetric effects in terms of health outcomes (infections and mortality)[1] as well as having increased income inequality with many countries (summarized in Stantcheva (2022)). The mechanisms driving these changes are not fully understood. Are the asymmetric outcomes driven only by the underlying heterogeneities such as age, household characteristics, occupations and ability to Work-From-Home, or are they also driven by endogenous optimal responses of individuals in response to the infections in society? Abstracting from all heterogeneities other than wealth inequality, the paper studies the role of optimal health and economic decisions in determining the joint evolution of inequality in health and economic outcomes. A parsimonious heterogeneous agent continuous time framework (HACT) is used to model the joint determination of health inequalities measured in terms of infections and economic inequality in terms of income and wealth inequality.

The paper incorporates a disease dynamics into a heterogeneous agent model, à la Aiyagari (1994). In Aiyagari (1994), income shocks are exogenously given. In our paper, income are directly affected by the health status of the individuals. Individuals, who are healthy either susceptible or recovered from the diseases, receive full income, while individuals who are infected receive no income. Moreover, the transmission probabilities between health states are endogenous, determined by health expenditures.

There are two types of health expenditures, incurred in response to a pandemic: (1) Preventive health expend expenditures that reduce consumption, for example, reducing mobility and isolating at home, cost incurred by wearing a mask and other preventive actions that reduce utility of consumption, etc. These reduce the chance of catching infectious diseases and thus, affects the transmission probability from being healthy and susceptible to being infected. (2) Treatment or recuperative expenditures incurred when being infected and requiring treatment. This is any expenditure increases recuperation rate and which reduces consumption. The change in health state acts like a productivity shock and as the health expenditures affect evolution of the health status it makes the individuals states endogenous. This is different from the classical Aiyagari model where the individual productivity shocks are exogenous. As individual productivity is determined by the health status, which

[1] See Blundell et al. (2020), ONS (2020), and PHE (2020) that document differences in health outcomes in UK across several dimensions — income deciles, OSA areas measured in terms of deprivation, rural-urban and regional differentials, age and gender differentials, attitudes towards risk, etc. Also see Belot et al. (2020), Borgonovi, Andrieu and Subramanian (2020), Brown and Ravallion (2020), Coven and Gupta (2020), Fan, Orhun and Turjeman (2020), Galasso et al. (2020), Lewandowski, Lipowska and Magda (2021), Mongey, Pilossoph and Weinberg (2021), Papageorge et al. (2021), Weill et al. (2020).

is controlled by health expenditures, the individual productivity shock becomes endogenous in our framework. In the Krusell-Smith extension of the classical model (Krusell and Smith, 1998; Fernández-Villaverde, Hurtado and Nuno, 2023), there can be an aggregate shock which is also exogenous. In our framework, as the individual decisions affect the evolution of infections which in turn affects wages and interest rates, the aggregate shock also becomes endogenous. Thus, our framework is an extension of the HACT model as in Achdou et al. (2022).

The epidemiological component of the model is a *SIRS* model which matches the dynamics of Covid-19. As we use a heterogeneous agent framework, the individuals take the decisions of other as given when choosing their optimal actions. As they are infinitesimal, they ignore the effect of their actions on the aggregate variables. Thus, we have the classical *disease externality* which has been modelled in different ways (see Gersovitz and Hammer (2004), and Goenka and Liu (2020)). In this mean field, we want to know how rational optimizing decisions by agents who differ in wealth and health status affect the equilibrium evolution of the disease and the economy. Thus, we shut down all other forms of heterogeneity such as education, ability to work from home, gender, age, location, access to health services, ethnicity, etc. which are important elements in matching the data.[2] This enables us to characterize the policy functions of the different agents and see to how these differ depending on wealth. If being ill is not just a productivity shock, but also brings a welfare loss, then the policy functions for preventive and treatment expenditures are increasing in wealth. In equilibrium only the susceptible individuals spend resources on prevention and only the infective on treatment. We also show that the elasticity of both types health expenditures are increasing in wealth. The endogenous optimal response to the pandemic, thus ends up increasing health inequalities as in equilibrium, the wealthier are less likely to get infected and recover faster. The two types of economic inequalities are affected by different mechanisms. Income inequality is largely affected by productivity (the health shock) and wages. The income inequality as documented in Stantcheva (2022) increases but its effects are not long lasting if there is an unanticipated shock to infection dynamics (which acts like a MIT shock). Wealth inequality is driven flow of income, returns on assets, and accumulation of assets. As capital adjusts slower than infections in the model (there are no adjustment costs) and health status of the wealthier is better, the wealth inequality also increases. This is much longer lasting in the event of an unanticipated change to disease dynamics.

The economic epidemiology literature has largely studied models where individ-

[2]See Adams-Prassl et al. (2020), Alipour, Falck and Schüller (2023), Bartik et al. (2020), Dingel and Neiman (2020), Gottlieb et al. (2021), Hensvik, Le Barbanchon and Rathelot (2020), and Lekfuangfu et al. (2020).

ual are homogeneous (Alvarez, Argente and Lippi, 2021; Atkeson, 2021) for early partial equilibrium models, Goenka, Liu and Nguyen (2021, 2022) for general equilibrium models with capital. Acemoglu et al. (2021) have age heterogeneity in a partial equilibrium framework. Kaplan, Moll and Violante (2020) have a HACT model with *SIRS* dynamics and wealth heterogeneity where the disease dynamics are exogenous. Angelopoulos et al. (2021) model wealth heterogeneity in a non-compartmental model so the disease dynamics are not explicitly modelled. Glover et al. (2023) model age hetergoeneity in an 3-period overlapping generations framework with SIR dynamics. In our framework, the model is a HACT model with capital and the *SIRS* dynamics are affected by optimal endogenous decisions. The model becomes a mean-field game. The usual approach in the earlier literature was to study an optimal control problem using Hamiltonians. There is a difficulty as one is not able to derive policy functions but only trajectories, and the sufficiency conditions can fail due to the non-convexity of the disease dynamics (see Goenka, Liu and Nguyen (2014, 2021, 2022)). As we use a dynamic programming approach, the second problem is avoided (see Calvia et al. (2023)). However, policy functions become difficult to compute. We adopt a finite-differencing method (Achdou et al. (2022)) to solve the computational issues.

In the model there are a continuum of individuals who can be in one of three health states, S healthy and Susceptible to the disease, I infected with the disease and Infective, or R, Recovered from the disease and immune from infection. This immunity is not long-lasting and individuals can become Susceptible as the virus mutates. They also have different wealth levels due to past saving decisions, so that that individual state is two-dimensional. They make optimal decisions on preventive and treatment actions, and how much to consume and save. Consistent with the later part of the pandemic we concentrate on morbidity from the disease which reduces labour productivity. The infection process acts like a productivity shock but this is endogenous and the health decisions act like a private partial self-insurance mechanism. The individual takes aggregate disease dynamics as given when making the health decisions and ignores the effect of own preventive and treatment actions on the evolution of the disease so that there is a disease externality. We characterize the optimal decisions and show how these depend on the individual states. In the baseline case where morbidity decreases utility, only the Susceptible make preventive expenditures and only the Infective on treatment. As mentioned above both the preventive and treatment expenditures are increasing in wealth and their elasticity is increasing as well. If morbidity acts only as a productivity shock then the optimal health expenditures are zero.[3] In a stationary equilibrium the wealthier individuals

[3]This is consistent with the results on the welfare loss from mortality in Goenka, Liu and Nguyen (2022).

have lower infection rates consistent with the higher health expenditures. One of the questions is if the wealthier have better lower infection rates to what extent do their decision increase inequalities. We look at different specifications and show that both preventive social distancing and treatment increase capital and income, reduce the disease incidence, but also increase the wealth inequality.

We also study the transitional dynamics to stationary equilibrium given a specific initial distribution of health status. The initial rate of recovered group is used to interpret the vaccination rate, as both vaccinated and recovered people carry immunity to infection. The simulated dynamics match the aggregate infection motion of Omicron B.A.1 outbreak in UK. As expected, infections increases that reduces labour supply and this drop in labour supply will increase wages. This increases the income inequality as the effect off falling ill is accentuated when wages are increasing. There is also a drop in investment leading to a decrease in interest rates. Other than the decrease in capital, the other changes are temporary. There is an increase in wealth inequality which is driven by the slow recovery of capital. The wealthier increase their health expenditures, which has leads to better health outcomes which also increase the differences is wages earned on average (note that in the model, the wage is the same for everyone who have the same productivity). The decrease in aggregate earned income and increased health expenditures, decreases aggregate consumption.[4]

We apply our model to evaluate the effect of government income support plan. We assume there is a government compensates the infected group by lump-sum transfer during the first 3 months after pandemic outbreak. Government budget constraint is imposed exogenously that the finance of budget is abstracted from the model. We find the income support generates trade-off between health and inequality at the aggregate level. The support scheme firstly reduces both income and wealth inequality and the effect is smaller when government has tighter constraint. Consistent with the empirical evidence, when the support is large enough, the rising wealth inequality could be turned around. However, the support scheme also mitigates the value loss of being infected and thus discourages health expenditure. Therefore, the aggregate infection rate is higher and the equilibrium labour and production are lower with income support.

The plan of the paper is as follows: section II. present new empirical facts on wealth distribution during Covid-19 pandemic, section III. presents the model, sec-

[4] Chetty et al. (2023) show that there are differences in consumption and savings across income groups. The income groups in their will be highly correlated with the wealth groups in our model. Their evidence indicates the high income groups sharply reduced their consumption and increased savings. While this also happens in our model, we will be able to match their results better if we distinguished between consumption of goods and services. The decrease in consumption documented in the paper by higher income groups was largely driven by decrease in consumption of services.

tion IV. addresses the computation and calibration, section V. characterises the stationary distribution and policy functions, section VI. studies transitional dynamics under various MIT shocks, and section VII. concludes.

II. Empirical Evidence

In this part of the paper, we present some empirical evidence. We firstly focus on the change of wealth inequality from 2012 to 2022 using the data in Global Wealth Report (GWR) by Credit Suisse.[5] The reports are released annually, providing information on wealth inequality of 165 countries from 2010. Figure 1 plots the wealth Gini index of each country at 2016, 2019, 2020, 2022 against the index at the base year.[6] The size of the scatter reflects the wealth per capita for each country. In Panel A, we find the wealth inequality worsened during the period of 2012-2016, with most countries lying above the 45 degree line. For the subsequent phase from 2016 to 2019, as shown in Panel B, a large number of countries, especially for those poor economies, shift below the 45 degree line. This implies a trend of improving wealth equality. When it goes to the post-Covid era in Panel C and D, we observe different trajectories that economies with higher wealth per capita, indicated by larger scatter, locate below the 45 degree line. The poorer economies with smaller scatters, in contrast, lie above the line. This evidence shows that the wealth equality is further progressive after 2019 for some richer economies like UK and Netherlands, but is worsened for economies with less wealth. The divergence in wealth Gini is even more significant when it comes to a relatively longer run towards 2022 in Panel D.

We suspect the different motion of wealth inequality between richer and poorer countries is due to the government income support scheme in Covid-19 relief. The Covid-19 Government Response Tracker (Hale et al., 2022) shows that there are 168 out of 185 countries ever covered part of the income loss during the pandemic. The short-run policy response could turn the direction of income/wealth equality (Stantcheva, 2022). Hence, we merge the GWR data with the tracker data. The dash-dot line in Panel C and D of Figure 1 are the fitted value of linear model,

[5] See https://www.credit-suisse.com/about-us/en/reports-research/global-wealth-report.html

[6] In the time series plot at Appendix Figure A1, we could identify that the global wealth Gini index increased from 2012 to 2016 and then decreased. We hence split the sample period into 3 phases: before 2016; 2016-2019 and the post Covid era from 2020

Figure 1. Change of Gini Index

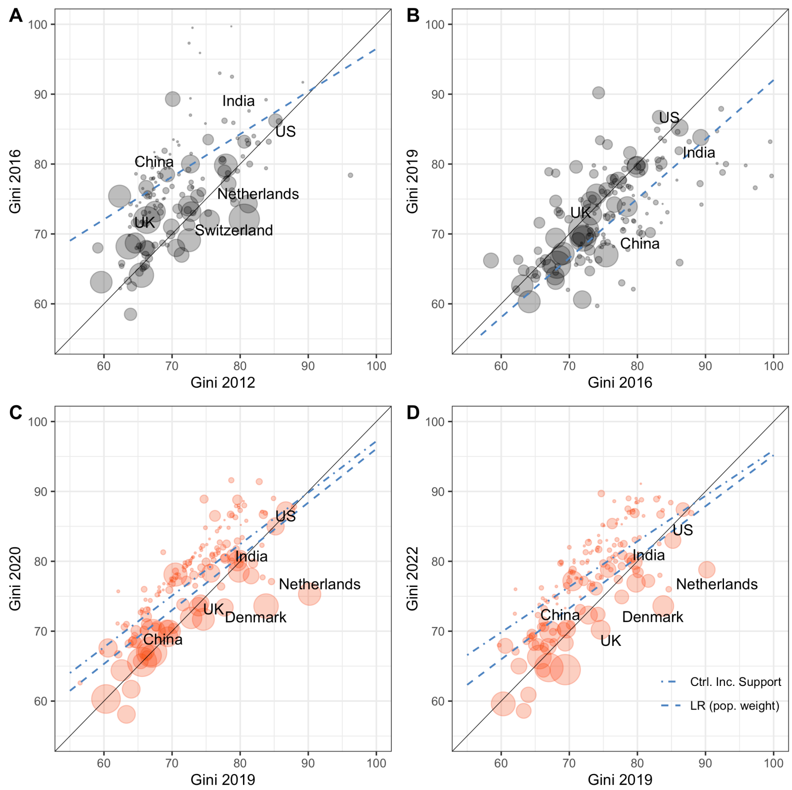

Notes: (a) This figure shows the change of Gini index from 2012 to 2019. The horizontal axis is the Gini index at the base year (2012,2016,2019). The horizontal axis is the Gini index evaluation year (2016, 2019, 2020, 2022). (b) The size of the scatters measures the medium of wealth per capita. (c) The dash line is the regression fitted value; the dash dot line is the fitted value removing the effect from government support scheme. All regressions are weighted by number of adults.

controlling the level of income support.[7] Compared with the effect without income support (dash line), we find that the fitted lines lie well above. It indicates that the wealth equality would be further worsened without government support scheme.

Our model will link the change of wealth inequality to individual optimal choice of health expenditure. However, it could be hard to provide supportive empirical evidence using the country data of the GWR. We thus turn to the subregional data of UK lower tier local authorities. We use the mobility index from Google Community Mobility Report (GCMR) data[8] as a proxy to general preventive health expenditure.

[7] We regress $Gini_i = \beta_0 + \beta_1 BaseGini_i + \beta_2 GovSupp_i + \varepsilon_i$, where $GovSupp_i$ is the average government income support index for country i from Feb 2020 to Dec 2023. The the dash-dot line removes the effect of support index that it plots the fitted value $\hat{Gini}_i = \hat{\beta}_0 + \hat{\beta}_1 BaseGini_i$. The dash line is the fitted value for the regression without controlling government support. Both regressions are weighted by number of adults in each country. The estimation results are shown in Appendix Table B1

[8] https://www.google.com/covid19/mobility/. The GCMR data provides the change of mobility index compared to Jan 2020. The data is of daily frequency, we collapse the data to monthly frequency by simple average.

Figure 2. Income and Mobility on Oct 2022

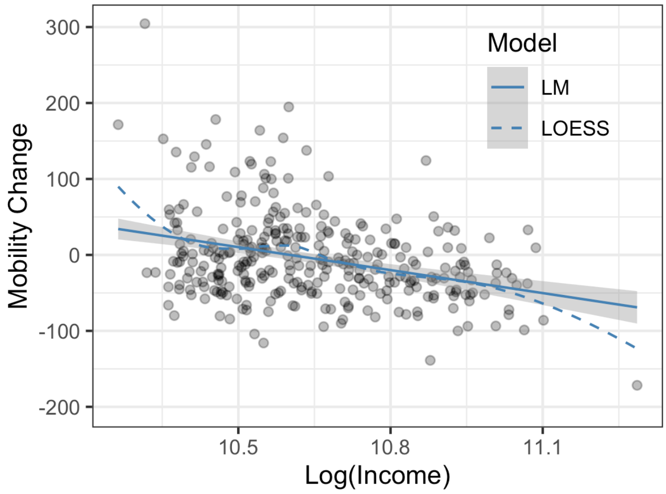

Notes: (a) The horizontal axis is the log income for UK lower tier local authorities. The vertical axis is the change of mobility index related to Jan 2020. (b) The solid and dash lines are the fitted value of linear and Loess model.

Smaller value of the index implies higher preventive response to the disease. Then, we merge the mobility data with 2018 UK household annual income.[9]

We firstly consider cross-sectional evidence on Oct. of 2022 when all the social restrictions were removed to get rid of the impact of lockdown. Figure 2 plots the mobility change against the average log household income for UK local authorities. The solid line with gray shadow indicates the linear fit with 0.99 confidential interval to the data. We can observe a significant negative correlation between the change of community mobility with household income.[10] Furthermore, we notice that the fitted value is positive for the poor area while negative for the rich area. This implies individuals living in richer area have reduced mobility more, consistent with higher preventive actions after the pandemic while those in the poorer area do not. We also find that the linear model fits the correlation well, with small difference to the non-parametric LOESS fit (dash line) for most range of log income.

We further estimate the evolution of the marginal effect of income over time using Equation 1. In the specification, exploit the area-by-time variation. $M_{i,t}$ denotes the mobility index for local authority i at time t. The authority fixed effect is θ_i[11]

[9]We average the MSOA level data to local authority level for merging.

[10]Weill et al. (2020) also find the same pattern in USA where the response to mandates for social distancing is much higher in richer counties than poorer counties. In our model there are no mandates and all response is endogenous. The results we present are also consistent with Yan et al. (2021) who find disentangle effects of mandates and endogenous response and find that the former increase the latter.

[11]This term absorbs all endogeneity generated by cross-sectional variety, e.g. sector composition that leads to different work-from-home rate.

Figure 3. Income and Mobility

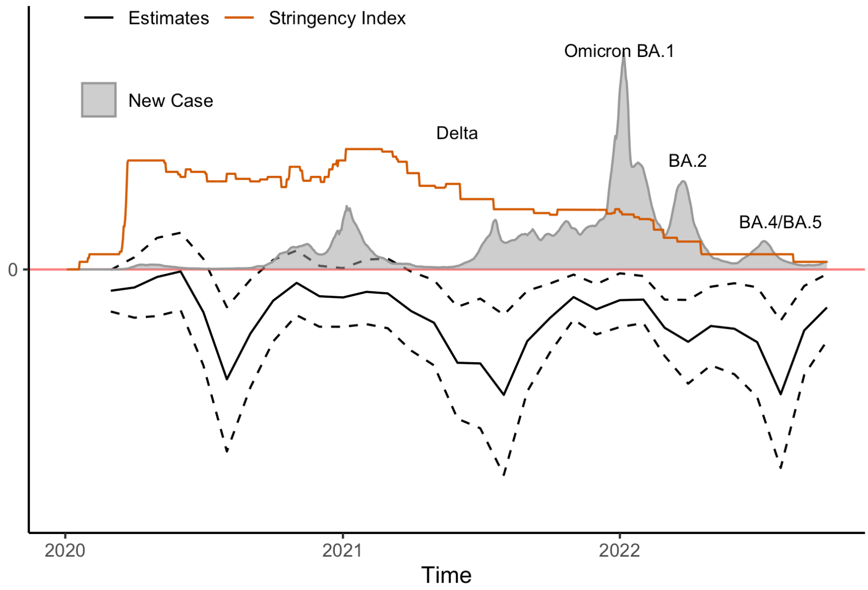

Notes: (a) The horizontal axis is the observation time. The black solid and dash lines are the estimates with 99% confidential interval for $\beta^{(\tau)}$ in regression Equation 1. (b) The gray area denotes the rate of new case of Covid infection in UK. (c) The orange line is the government stringency index. All components in this Figure are properly scaled.

and the time fixed effect η_t. Our main regressors are the interactive term between log income $\log(I_i)$ and time indicator $T_t^{(\tau)}$ which equals 1 if time $t = \tau$, 0 for the rest. We set $t =$ Feb2020 as the based time and exclude it from the summation part. By these settings, $\beta^{(\tau)}$ estimates the marginal effect on mobility $M_{i,t}$ from income, related to the base time. In the estimation, we also weight the samples by the population and cluster the standard error at the level of local authority.

$$M_{i,t} = \theta_i + \eta_t + \sum_{\tau \neq \text{Feb2020}} \beta^{(\tau)} \log(I_i) \times T_t^{(\tau)} + \varepsilon_{i,t}. \tag{1}$$

The black solid line in Figure 3 plots the corresponding estimates for $\beta^{(\tau)}$, with the 0.99 confidential interval on the dash line. We also plot the national infection rate in the gray shadowed area and the stringency index in the orange line.[12] The estimators are significantly negative for periods after the March of 2021, when the stringency index began to decline from its peak level. This implies individuals in the richer area reduced mobility more than those in the poorer area. We also detect a negative correlation between marginal effect $\beta^{(\tau)}$ with the infection rate for the periods after mid 2021. Therefore, the rich areas have higher prevention response to the disease when the infection rate is high.

[12]The stringency is provided by the Government Response Tracker. It measures the level of social restriction. All the components in Figure 3 are properly scaled for purpose of visualization.

In the next section we will build a heterogeneous agent model to model the empirical observations. The model links the growing wealth inequality with individuals' optimal health policy. Our predictions are consistent with the empirical findings that the wealthier individuals take higher preventive actions (and treatment response) to the disease and thus subjected to smaller risk of income loss by infection during the pandemic. The heterogeneous response to aggregate infection generates income and subsequent wealth gap between the rich and poor.

III. THE MODEL

The model is a marriage of the *SIRS* epidemiological model and Aiyagari-Bewley-Huggett model as in Kaplan, Moll and Violante (2020). In the Aiyagari-Bewley-Huggett model, individuals face uninsured idiosyncratic labour market risk, which is exogenous. In our model, individuals face a health risk, where the probability of transiting between health status is endogenous and affected by two types of health expenditure - preventive and treatment health expenditure. This is partial self-insurance against the health shock. Thus, the model is different from Kaplan, Moll and Violante (2020) which does not model the response of individuals to the pandemic and thus, the partial self-insurance against the health shock.

A. The Model Setup

Individuals. We assume that the transmission of infectious diseases follow the SIRS epidemiology model. There is a continuum of individuals who have different health status $h \in [\mathcal{S}, \mathcal{I}, \mathcal{R}]$, denoting susceptible, infected and recovered, respectively. Individuals could be healthy and susceptible to infectious diseases, that is, $\mathcal{S}$. They can get infected at the rate of λ, with their health status becoming $\mathcal{I}$. The infected individual could recover from diseases at the rate of γ and gain immunity. The corresponding health status is $\mathcal{R}$. But, the recovered individuals could lose immunity with rate ψ and back to the health status $\mathcal{S}$. Figure 4 shows the flow chart for the health status.

Figure 4. Flow of Epidemiological Compartments

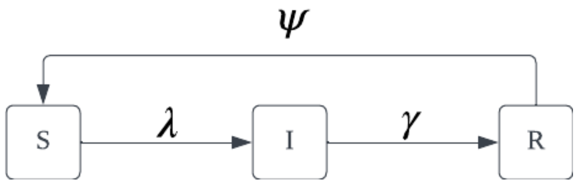

Notes: This Figure shows the motion of health status. The numbers on the arrows are the transition probabilities.

In the model, individuals infected with infectious diseases are unable to work in the full capacity. Individual productivity z depends on his health status and we assume $z : h \rightarrow [0, 1]$ with $0 \leq z(\mathcal{I}) < z(\mathcal{S}) = z(\mathcal{R}) = 1$.[13] Therefore, the idiosyncratic health shocks for individuals are essentially productivity shocks, which affect their income level. This model setup in fact is the same as the Aiyagari-Bewley-Huggett model where individuals face idiosyncratic income shocks. However, different from the Aiyagari-Bewley-Huggett model, where the income process is given exogenously, here the transition probability between health status is modelled endogenously. There are two types of health expenditure. Investment in preventive health expenditures $m_{\mathcal{P}}$ can reduce probability of getting infected λ, and investment in treatment health expenditures $m_{\mathcal{T}}$ can shorten the during of being infected and increase probability of getting recovered γ. With slight abuse, we will introduce health expenditures in detail later.

In the model, individuals also differ in their wealth level a. Denote w as wage and r as interest rate. They receive labour income $wz(h)$ and capital income ra, and accumulate wealth according to:

$$\dot{a} = wz(h) + ra - c - m_{\mathcal{P}} - m_{\mathcal{T}}, \tag{2}$$

where c is the consumption, $m_{\mathcal{P}}$ and $m_{\mathcal{T}}$ are the health expenditure. Individuals also face a borrowing constraint $a > \underline{a}$, where $-\infty < \underline{a} \leq 0$. The idiosyncratic component $z(h)$ generates heterogeneity in optimal policies and eventually in individual states. We denote the joint distribution on individual wealth and health as $g(a, h)$ with the probability measure μ.

Individuals derive utility from streams of current and future consumption c and health status h, discounted at rate $\rho \geq 0$. The consumption utility function is CES that $u(c) = \frac{c^{1-\sigma}}{1-\sigma}$. Individuals also suffer disutility χ if infected. It captures the direct health lost of being infected beside productivity lost.[14] Hence, individuals maximize his utility by choosing streams of consumption c and health expenditures - $m_{\mathcal{P}}$ and $m_{\mathcal{T}}$:

$$\max_{\{c, m_{\mathcal{P}}, m_{\mathcal{T}}\}} \quad \mathbb{E}_0 \int_0^{\infty} e^{-\rho t} [u(c) - \chi \mathbb{1}_{(h=\mathcal{I})}] dt. \tag{3}$$

Infection and Recovery. We endogenize the flow of epidemiological compartments using health expenditure in a similar way as Goenka, Liu and Nguyen (2014). Specifically, for infection process, we assume individuals contact with other

[13]Patient clinical reported outcome finds infection brings productivity loss to workers (Di Fusco et al., 2022). We also model Long Covid by letting $z(\mathcal{R}) < 1$ later.

[14]See e.g. Acemoglu et al. (2021); Alvarez, Argente and Lippi (2021), the non-pecuniary welfare loss is usually associated with mortality rate. In our paper, because mortality is not modelled to be in lined with the later evidence of Omicron variant, we assume morbidity could also induce non-pecuniary loss as people fall ill.

at a rate α, which is a decreasing function of preventive expenditure, i.e. $\alpha(m_{\mathcal{P}})$ in Assumption 1-(1). The preventive expenditure could be interpreted as any economic cost that reduces the chance of infection e.g. wearing mask, conducting regular lateral flow test, social distancing etc.. Now, to give a bird's eye view to the contact mechanism, lets' simply assume two individuals i, j with different preventive expenditures, say, $m^i_{\mathcal{P}}$ and $m^j_{\mathcal{P}}$. They would contact with each other with at a rate of the product $\alpha(m^i_{\mathcal{P}})\alpha(m^j_{\mathcal{P}})$.

The infection takes place once susceptible individual contacts with any infective individuals in the economy. Therefore, in the case of two individuals, susceptible i is infected with probability $\alpha(m^i_{\mathcal{P}})\alpha(m^j_{\mathcal{P}})$ if j carries the disease, with probability 0 if j doesn't. That is, the infection probability for i would be $\alpha(m^i_{\mathcal{P}})\alpha(m^j_{\mathcal{P}})\mathbb{1}_{(h^j=\mathcal{I})}$. We denote the latter two terms $\alpha(m_{\mathcal{P}})\mathbb{1}_{(h=\mathcal{I})}$ as the infectious contact rate. Thus, if individuals interact with all members in the economy, we can express the infected probability for a susceptible individual with $m_{\mathcal{P}}$ unit of preventive expenditure as

$$\lambda = \alpha(m_{\mathcal{P}})\zeta. \tag{4}$$

The first component $\alpha(m_{\mathcal{P}})$ is a susceptible individual's own contact rate. The second part ζ is the average infectious contact rate in the economy.[15] We further assume the population is large enough that individual's choice on own preventive expenditure has negligible effect on the social average variable. That is, ζ is perceived and taken as given in the individual maximization problem.

For recovery process, we assume recovery rate for the infective group is increasing with treatment expenditure, i.e. $\gamma(m_{\mathcal{T}})$ in 1-(2).

Assumption 1. *(1) The contact rate for individual is a decreasing function of preventive expenditure that*

$$\alpha(m_{\mathcal{P}}) : \mathbb{R}_+ \to \mathbb{R}_+ \quad \textit{with} \quad \alpha' < 0; \alpha'' > 0, \alpha(0) = \bar{\alpha}; \alpha(\infty) = \underline{\alpha}. \tag{5}$$

(2) The recovery rate is an increasing function of treatment expenditure that

$$\gamma(m_{\mathcal{T}}) : \mathbb{R}_+ \to \mathbb{R}_+ \quad \textit{with} \quad \gamma' > 0; \gamma'' < 0; \gamma(0) = \underline{\gamma}; \gamma(\infty) = \bar{\gamma}. \tag{6}$$

With these assumptions, we can represent the motion of health status in Figure 4 by a hypothetical transitional matrix as Equation 7. We mark that the transition

[15] This assumption is inspired by heterogeneous age group model in Hethcote (2000). The expression is a matching process between the susceptible and infected group. To help understand the interpretation of this expression, we assume discrete uniform distribution of N population. If individual i meets everyone in the economy, the probability of contacting with an infected people would be $1/N \sum_j \alpha(m^i_{\mathcal{P}})\alpha(m^j_{\mathcal{P}})\mathbb{1}_{(h^j=\mathcal{I})} = \alpha(m^i_{\mathcal{P}})[1/N \sum_j \alpha(m^j_{\mathcal{P}})\mathbb{1}_{(h^j=\mathcal{I})}]$. The second term would be the average infective contact rate. The continuous distribution case is an analogy integrating by density distribution function.

matrix is just for illustration. In our continuous-time setup, the transition will be a Poisson process, with the intensity in the matrix.

$$\pi(h'|h) = \begin{bmatrix} 1-\alpha(m_{\mathcal{P}})\zeta & \alpha(m_{\mathcal{P}})\zeta & 0 \\ 0 & 1-\gamma(m_{\mathcal{T}}) & \gamma(m_{\mathcal{T}}) \\ \psi & 0 & 1-\psi \end{bmatrix}_{3\times 3}. \tag{7}$$

Firms. The production landscape is a standard perfect competitive market. The representative firm has Cobb-Douglas production functions, giving $Y = AK^{\beta}L^{1-\beta}$, where Y is output, K is aggregate capital depreciated at rate δ, L is labour, A is technology and β is capital income share with $0 < \beta < 1$. The price of output is normalized to 1, and the profit maximization problem is given as:

$$\sup_{\{K,L\}} \Pi = AK^{\beta}L^{1-\beta} - rK - wL - \delta K. \tag{8}$$

The equilibrium interest rate and wage are given by the F.O.C. as Equation 9.

$$\begin{aligned} w &= A(1-\beta)\left(\frac{K}{L}\right)^{\beta}, \\ r &= A\beta\left(\frac{K}{L}\right)^{\beta-1} - \delta. \end{aligned} \tag{9}$$

B. Equilibrium

There are two types of equilibrium conditions we need to consider. One type of equilibrium conditions is the standard market clearing conditions. The demand for capital from firms equals to the supply of asset from individuals. Similarly, in labour market, the demand for labour from firms equals to the supply of labour from individuals. That is, aggregate capital and aggregate labour satisfy

$$\begin{aligned} K &= \int a g(a,h) d\mu, \\ L &= \int z(h) g(a,h) d\mu. \end{aligned} \tag{10}$$

The other type of equilibrium conditions is the epidemiological equilibrium condition. As noted in Equation 4, the infection probability depends on both individual's own contact function and his perception about the average infectious contact rate ζ. In equilibrium, the individuals' perception about the average infectious contact rate is in fact the true value.

$$\zeta = \int \alpha(m_{\mathcal{P}}) \mathbb{1}_{(h=\mathcal{I})} g(a,h) d\mu. \tag{11}$$

The formulation of our heterogeneous agent model is recognized to be a Mean-Field-Game (MFG) in Mathematics. Mean-field theory studies the strategic decision making by small interacting agents in very large populations. The paradigm of MFG is initiated by Lasry and Lions (2007); Huang, Malhamé and Caines (2006). When the number of players goes to infinity, the interaction between individuals is mean-field-type that he or she observes only averages of functions of the private states of the other players. Individuals' effect on distribution or aggregate variables is trivial. In the Nash equilibrium of the game, given a distribution, individual would not deviate from their optimal policy. Meanwhile, the distribution is the probability behaviour under individuals' optimal behaviour.

In our model, the joint distribution of individual states $g(a, h)$ formulates the aggregate variables and price. Individuals take the price as given when optimizing their life-time utility. In equilibrium, the price is exactly the aggregate outcome from individuals' optimal policy. In summary, we are looking for the equilibrium defined as follows.

Definition 1. *(Nash Equilibrium in MFG) Choice variables* $\{c^*, m^*_{\mathcal{P}}, m^*_{\mathcal{T}}\}$ *and distribution* $g^*(a, h)$ *satisfying*

(1) $\{c^*, m^*_{\mathcal{P}}, m^*_{\mathcal{T}}\}$ *solves the optimization problem Equation 3 subjected to the motion of wealth and health (Equation 2 and Equation 7), given the price* (w^*, r^*) *and social infective contact rate* ζ^**.*

(2) Distribution $g^*(a, h)$ *is the outcome of optimal policy* $\{c^*, m^*_{\mathcal{P}}, m^*_{\mathcal{T}}\}$*.*

(3) Distribution $g^*(a, h)$ *generates aggregate variables* $\{w^*, r^*, \zeta^*\}$ *using Equation 9, Equation 10 and Equation 11.*

IV. Computation and Calibration

A. HJB-KFP PDEs

We follow the Partial Differential Equation (PDE) viewpoint[16] in searching the equilibrium (see e.g. Achdou et al. (2013, 2020); Lauriere (2021); Achdou et al. (2022) etc.). The dynamic programming representation of the problem consists of two PDEs: (1) Hamiltonian-Jacobian-Bellman Equation (HJB); (2) Kolmogorov Forward Equation (or Fokker-Planck Equation, KFP).

Denote the value of maximization problem Equation 3 as $v(a, h)$. The value function satisfies the HJB as

[16] Another approach is the Stochastic Differential Equation (SDE) view point (see e.g. Carmona, Delarue et al. (2018); Cardaliaguet et al. (2019) etc.)

$$
\begin{aligned}
\rho v(a,h) = \sup_{\{c, m_{\mathcal{P}}, m_{\mathcal{T}}\}} & u(c) - \chi \mathbb{1}_{(h=\mathcal{I})} + \partial_a v(a,h)[wz(h) + ra - c - m_{\mathcal{P}} - m_{\mathcal{T}}] \\
& + \Lambda^{h'}(m_{\mathcal{P}}, m_{\mathcal{T}}, h)[v(a,h') - v(a,h)] \\
& + \nu_{\mathcal{P}} m_{\mathcal{P}} + \nu_{\mathcal{T}} m_{\mathcal{T}} + \partial_t v(a,h).
\end{aligned}
$$

In this expression, the discounted value equals the objective function plus the marginal value change brought by the motion of wealth and health. $\Lambda^{h'}(m_{\mathcal{P}}, m_{\mathcal{T}}, h)$ is the Poisson rate of switching from status h to h' (entries in the transitional matrix Equation 7) under the continuous time setup. This term departs from Aiyagari (1994) and Achdou et al. (2022) that the motion of the discrete state h is endogenized by health expenditure. $\nu_{\mathcal{P}}$ and $\nu_{\mathcal{T}}$ are the slack variables for the constraints $m_{\mathcal{P}}, m_{\mathcal{T}} \geq 0$. The FOCs for the maximization problem are listed as follows.

$$
\begin{aligned}
& c: \quad u'(c) - \partial_a v = 0, \\
& m_{\mathcal{P}}: \quad -\partial_a v + \frac{\partial \Lambda^{h'}(m_{\mathcal{P}}, m_{\mathcal{T}}, h)}{\partial m_{\mathcal{P}}}[v(a,h') - v(a,h)] + \nu_{\mathcal{P}} = 0, \\
& m_{\mathcal{T}}: \quad -\partial_a v + \frac{\partial \Lambda^{h'}(m_{\mathcal{P}}, m_{\mathcal{T}}, h)}{\partial m_{\mathcal{T}}}[v(a,h') - v(a,h)] + \nu_{\mathcal{T}} = 0, \\
& \nu_{\mathcal{P}} m_{\mathcal{P}} = \nu_{\mathcal{T}} m_{\mathcal{T}} = 0.
\end{aligned} \tag{12}
$$

The first FOC derives the optimal consumption policy that

$$c^* = u'^{-1}(\partial_a v). \tag{13}$$

For the second FOC, notice from Equation 7 that the infective probability is a function of preventive expenditure only for the susceptible group $\mathcal{S}$. For the rest of the health groups, preventive expenditure will not have impact on their transition probability. That is, for group $h = \{\mathcal{I}, \mathcal{R}\}$, we have $\partial_{m_{\mathcal{P}}} \Lambda^{h'}(m_{\mathcal{P}}, m_{\mathcal{T}}, h) = 0$. This implies a non-zero slack variable that $\nu_{\mathcal{P}} = \partial_a v > 0$. Therefore, the optimal preventive health policy for the infective and recovered groups is spending nothing.

$$m^*_{\mathcal{P}}(a, \mathcal{I}) = m^*_{\mathcal{P}}(a, \mathcal{R}) = 0. \tag{14}$$

For the susceptible group, we have $\Lambda^{\mathcal{I}}(m_{\mathcal{P}}, m_{\mathcal{T}}, \mathcal{S}) = \alpha(m_{\mathcal{P}})\zeta$. Thus, the optimal preventive expenditure satisfies the F.O.C. $-\partial_a v + \alpha'(m_{\mathcal{P}})\zeta[v(a,h') - v(a,h)] = 0$. Similar procedure could be gone through for the treatment expenditure $m_{\mathcal{T}}$. To round up, the optimal health policy can be derived as Equation 15

$$
\begin{aligned}
m_{\mathcal{P}}^{*} &= \begin{cases} 0; \quad h = \{\mathcal{I}, \mathcal{R}\} \\ \alpha'^{-1}\left(\dfrac{\partial_a v(a,\mathcal{S})}{\zeta[v(a,\mathcal{I}) - v(a,\mathcal{S})]}\right); \quad h = \mathcal{S}. \end{cases} \\
m_{\mathcal{T}}^{*} &= \begin{cases} 0; \quad h = \{\mathcal{S}, \mathcal{R}\} \\ \gamma'^{-1}\left(\dfrac{\partial_a v(a,\mathcal{I})}{v(a,\mathcal{R}) - v(a,\mathcal{I})}\right); \quad h = \mathcal{I}. \end{cases}
\end{aligned} \tag{15}
$$

The first expression implies that infected people would spend nothing on preventive expenditure to reduce their infectious contact rate, although it could lower the risk of transmitting disease to others. Such an externality is the nature of decentralized economy, where we abstract from altruism that individuals derive utility only from their own consumption and health status. Hence, individuals in group $\mathcal{I}$ would substitute all their preventive expenditure for treatment to shorten the infected period. Similarly, recovered people would not spend on prevention either, as they know they carry immunity.

For the susceptible group, the preventive expenditure is an increasing function of the value loss of being infected $v(a,\mathcal{I}) - v(a,\mathcal{S})$. Susceptible individuals would spend more on prevention if infection brings larger value loss for them. Therefore, one could expect that the equilibrium preventive expenditure would be larger with greater disease-induced productivity loss or direct punishment χ. The treatment expenditure is an increasing function of the value gain of recovery $v(a,\mathcal{R}) - v(a,\mathcal{I})$. Thus, people spend less on treatment if the symptoms get milder or there are no long-run health effect from infection.

The second part for the PDE system for the MFG is the Kolmogolov Forward Equation (KFP).

$$
\begin{aligned}
\frac{\partial g(a,h)}{\partial t} = &-\frac{\partial}{\partial a}[s(a,h,m_{\mathcal{P}},m_{\mathcal{T}})g(a,h)] \\
&- \Lambda^{h'}(m_{\mathcal{P}},m_{\mathcal{T}},h)g(a,h) + \Lambda^{h}(m_{\mathcal{P}},m_{\mathcal{T}},h'')g(a,h'').
\end{aligned} \tag{16}
$$

where $s(a,h,m_{\mathcal{P}},m_{\mathcal{T}})$ is the savings defined as $\dot{a}$ in Equation 2. The KFP evaluates the motion of the joint distribution of wealth and health. The change of the joint distribution over time $\partial_t g(a,h)$ could be broken into to the marginal change of a and h. Specifically, the first component is the flow of population at margin a. The last two components can be interpreted as the population flow-out of health state h to the next state, and flow-in from the previous state.

Under the Finite-Differencing-Scheme (Achdou et al., 2013), we can rewrite the HJB-KF system using matrix notation as Equation 17 and Equation 18, where $\mathbf{V}$ and $\mathbf{g}$ is the matrix for value and distribution. $\mathcal{A}$ is a sparse matrix for HJB equation with its adjoint $\mathcal{A}^*$ when the optimal conditions Equation 13, Equation 15 holds.

We show the construction for these matrices in Appendix D.

$$\text{(HJB)} \quad \rho \mathbf{V} = u(\mathbf{V}) + \mathcal{A}\mathbf{V} + \partial_t \mathbf{V}, \tag{17}$$

$$\text{(KFP)} \quad \partial_t \mathbf{g} = \mathcal{A}^* \mathbf{g}. \tag{18}$$

We can further represent the equilibrium conditions Equation 9 to Equation 11 by function $\mathcal{F}(\mathbf{g}_t) = \mathbf{0}$. Therefore, to find the Nash Equilibrium defined in Definition 1 is to solve the dynamic programming problem defined as follow.

Definition 2. *(Dynamic Programming for Nash Equilibrium in MFG) Find sequence of distribution $\{\mathbf{g}^*\}_t$ and value function $\{\mathbf{V}^*\}_t$ such that*

(1) $\{\mathbf{V}^*\}_t$ solves the HJB Equation 17.

(2) Motion of distribution $\{\mathbf{g}^*\}_t$ satisfies KFP Equation 18.

(3) $\{\mathbf{g}^*\}_t$ clears the market that $\mathcal{F}(\mathbf{g}^*) = \mathbf{0}$.

B. Parameterization

We calibrate the model in seasonal frequency. The parameterization for economy side of the model is standard. We let $\sigma = 2$ in the CES utility function and subjective discount rate $\rho = 0.0138$. The production function is Cobb-Douglas production with productivity $A = 1$, capital income share $\beta = 0.36$ and depreciation rate $\delta = 0.05$. For the direct disutility of being infected, we calibrate $\chi = 0.3$ in the baseline and vary this parameter in the comparative study.[17] We choose this value is to match the empirical observation that wealthier are more preventive to the disease with higher health expenditure. As we will show later, the health expenditure elasticity of income lies between 5% to 40% under this calibration. However, if we assume no non-pecuniary punishment with $\chi = 0$, health expenditure is inelastic to income.

The main goal for our parameterization is to calibrate the epidemiological part of the model to match the latter evidence of Covid-19. We firstly handle the key functional form of contract rate and recovery rate. We follow Goenka, Liu and Nguyen (2021) that the contact function and recovery function are assumed to be

$$\begin{aligned} \alpha(m_{\mathcal{P}}) &= \epsilon_0 (m_{\mathcal{P}} + \epsilon_2)^{\epsilon_1}, \\ \gamma(m_{\mathcal{T}}) &= \bar{\gamma} - \eta_0 (m_{\mathcal{T}} + \eta_2)^{\eta_1}. \end{aligned} \tag{19}$$

[17] In models with disease-induced mortality, e.g. Acemoglu et al. (2021); Alvarez, Argente and Lippi (2021), the weight χ is associated with the Value of Statistical Life (VoSL). The magnitude of χ is calibrated to 30-70 times output. Our paper is abstracted from mortality. We therefore calibrate this parameter such that the health expenditure elasticity of income be in a reasonable range.

In this expression of $\alpha(m_{\mathcal{P}})$, ϵ_1 is the maximum contact rate elasticity of preventive expenditure. We assume unit elasticity that $\epsilon_1 = -1$. We let $\epsilon_0 = 0.18, \epsilon_2 = 0.005$ so that $\alpha(0) = 36$. This implies individuals would meet 14 people on average per day if the prevention expenditure is 0 for everyone.[18] We notice that it is hard to find empirical evidence to calibrate the contact function. However, as will summarize later, the outcome of the parameters we choose match the basic reproduction number R_0 of the Omicron variant.

For the recovery function $\gamma(m_{\mathcal{T}})$, early evidence on alpha and pre-alpha variants shows the symptoms clearance duration is around 6 to 20 days [19](Beigel et al., 2020; Lechien et al., 2020). For the Delta variant, Hakki et al. (2022) finds 93% of samples shed viral RNA for over 7 days after symptom onset. And it takes around 14.6 days to clear the viral. Latter evidence on Omicron variants shows a shorter infective duration. The literature review by UK Health Security Agency (2023) shows that most studies report a clearance time around 7 to 15 days. Hence, we assume $\eta_1 = -1, \eta_2 = 0.005$ in analogy to the contact function. We calibrate $\bar{\gamma} = 12.85, \eta_0 = 0.034$ such that the recovery duration is bounded between 7 and 15 days.

For the rate of losing immunity ψ, Cagigi et al. (2021) shows the IgG levels had significant waning from 3 to 8 months[20] in patients who recovered from moderate and severe disease. Similar evidence of waning immunity could be found on antibody by vaccination. Gilboa et al. (2022) finds the IgG level decays at 2.26% (1.32%) per day for second dose (third dose) of BNT162b2 vaccine. The microneutralization assays begin to decay within 3 months after the third dose of vaccine. However, the data shows the most reinfection happens among different variants of virus (ONS, 2023a). The antibody could be even less effective against different variants. Therefore, considering that disease mutation is abstracted in our model, we assume a slightly higher rate of reinfection. We calibrate $\psi = 3/5$ such that the immunity only lasts for 5 months.

To further link our calibration with the empirical data of Covid-19, Table I summarizes the epidemiological characteristics of the model in stationary equilibrium and the empirical data. We roughly calculate the basic reproduction number R_0. Appendix C shows how R_0 is obtained in our heterogeneous agent model. We find

[18]The Poisson intensity of contacting others, regardless of the health status, would be $\alpha\bar{\alpha}$, where $\bar{\alpha}$ is the average contact rate in the economy. If all individuals spend 0 preventive expenditure, the contact rate is homogeneous that $\alpha(0)\alpha(\bar{0}) = \alpha(0)^2 = 1296$. This implies 1296 contacts on average per period. As our model is of seasonal frequency, the calibration implies 14.4 contacts per day.

[19]The double blind trial of Remdesivir (Beigel et al., 2020) finds the median time to recovery for patients not receiving oxygen, receiving low-flow oxygen, high-flow oxygen are around 6, 9 and 20. Patients with severe symptoms receiving ECMO or mechanical ventilation recover in around 1 month.

[20]Although systemic IgG levels were durable for up to 8 months, airway IgG and IgA declined significantly within 3 months.

our model produces $R_0^{(ss)} = 9.23$ at the baseline stationary equilibrium. We find this value matches the empirical studies on Omicron variant. Liu and Rocklöv (2022) summarize estimated R_0 of Omicron variants in the recent studies. The Omicron variant has an average basic reproduction number of 9.5 and a range from 5.5 to 24. For population composition, our calibration yields a 4.1% of social infection rate at stationary equilibrium. The value matches the UK observation after 2023 when the pandemic is stabilized. However, it is hard to find statistics on recovery rate. We find the recovered group in our calibration is close to proportion of adults with antibodies over 800 ng/ml.[21] We will vary the parameters in the coming section of comparative studies.

Table I. Calibration

	Model		Data
	Mean	Median	
Basic Rep. Num. R_0	9.236		9.5 ave., range 5.5-24
Days to Infection	19.183	18.833	-
Days to Recover	7.241	7.244	around 7 to 15
Days to Lose Immunity	150		around 90 to 240
Fraction $\mathcal{S}$	10.8%		-
Fraction $\mathcal{I}$	4.1%		2%-5% after 2023 (UK)
Fraction $\mathcal{R}$	85.1%		77%-80% Feb 2023 (UK)

Notes: (a) Data source: R_0 Liu and Rocklöv (2022) etc.; Days to recover UK Health Security Agency (2023); Days to lose immunity Cagigi et al. (2021); Gilboa et al. (2022) etc.; UK data ONS (2023a). (b) The data of recovery population is proxied by fraction of population with antibody more than 800 ng/ml

V. Stationary Equilibrium

A. *Baseline Results*

In the stationary equilibrium, the value function and distribution are not changing overtime. That is, $\partial_t \mathbf{V} = 0, \partial_t \bar{\mathbf{g}} = 0$, where $\bar{\mathbf{g}}$ is the stationary distribution. Hence, we can re-write conditions in Definition 2. A fixed-point iteration algorithm is applied to solve the system. We present the detail in Appendix E.

[21] ONS (2023b) estimates that 800 ng/ml is the highest level which can produce a historic back-series and enables enhanced monitoring of antibody levels and waning.

$$\begin{aligned} \rho \mathbf{V} &= u(\mathbf{V}) + \mathcal{A}\mathbf{V}, \\ \mathbf{0} &= \mathcal{A}^{*}\bar{\mathbf{g}}, \\ \mathcal{F}(\bar{\mathbf{g}}) &= 0. \end{aligned} \tag{20}$$

In the baseline model, we choose $\chi = 0.3$. Figure 5 presents the stationary equilibrium of the baseline model. In each panel, the horizontal is wealth and curves of different colours represent different health status. The health expenditure is increasing with individual wealth.[22] While we find the main part of the health policy functions being close to linear, the extreme poor individuals near the borrowing constraint behave differently. We observe that they substitute treatment health expenditure and consumption for prevention, with an upward turn in the preventive policy function. This is because their assets cannot go further down when getting close to the borrowing constraint. Individuals would keep their preventive expenditure to be high enough to prevent further income loss from future infection. When boundary individuals accumulate assets, that is, a moving marginally away from the borrowing constraint, they would substitute prevention expenditure for treatment expenditure.

The first two Panels in the first row of Figure 5 plots the value and consumption policy functions for each health status. Qualitatively similar to the health policies, the value and consumption also show momentum on wealth. When it comes the comparison among different health status, we observe the value and consumption for recovered individuals are higher than the other two types in level. This is because they gain temporal immunity after went through infection. The recovered people hence don't need to spend on either prevention or treatment as implied by the F.O.C. we derived in the previous section. Infected individuals have the lowest value and consumption policy among health groups because they are incapacitated with the lowest labour income, and they also spend extra money on treatment.

The disparity in optimal policies generates heterogeneity in savings and wealth. For savings, as shown in the last Panel in the first row of Figure 5, we observe that the infected individuals consume their assets with a negative saving rate, while the other two types of individuals have higher savings. The last panel in the second row of Figure 5 plots the stationary wealth distribution for each epidemiological compartments. We find the wealth distribution in stationary equilibrium is positive skewed for all health statuses. We also plot the wealth share in each percentile (Lorenz Curve) in Appendix Figure A2. The Gini Index for wealth in our model is

[22] The wealth effect of health expenditure our model captures is also found in the model by Hall and Jones (2007) and specially, for preventive expenditure, Ozkan (2014). Life expectancy and survival probability are the key mechanism in these literatures. Our model generates similar observations via incapacitation of infection.

Figure 5. Baseline Model ($\chi = 0.3$)

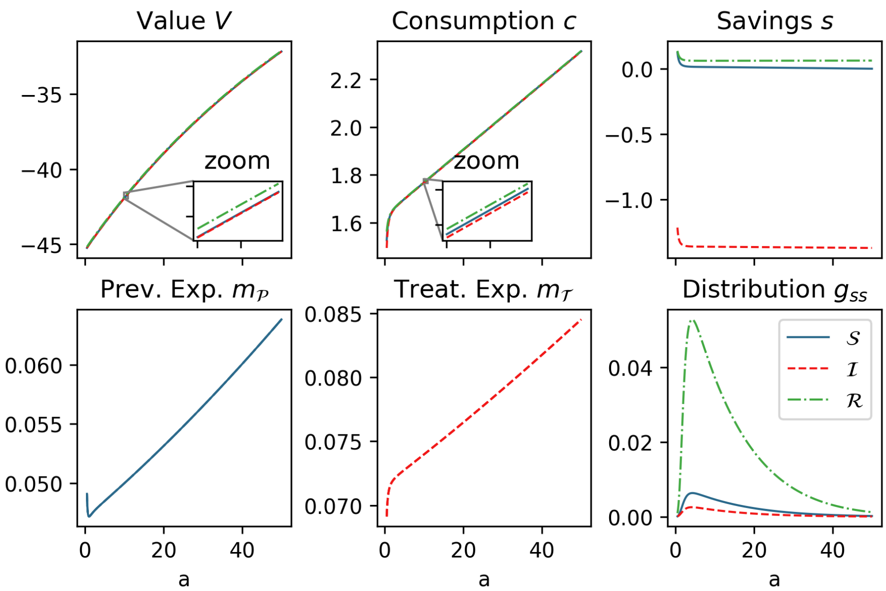

Notes: (a) This Figure plots the baseline results ($\chi = 0.3$) at the stationary equilibrium. The subfigures plot the value function; policy function for consumption, savings and health expenditure; distribution. (b) The horizontal axis is the individual wealth. The blue, orange and green lines denote health status susceptible $\mathcal{S}$,infective $\mathcal{I}$ and recovered $\mathcal{R}$ respectively.

around 0.412, which is much lower than the empirical observations by survey data (around 0.7 for UK; around 0.85 for US.) (CreditSuisse, 2023). This is due to the nature of Aiyagari model that heterogeneity from idiosyncratic shock is not enough to characterize large skewness of wealth distribution.[23]

However, we notice that the wealth Gini index in our model is still higher than the basic Aiyagari model with uninsured shock, which is roughly 0.32.[24] We believe the insurance mechanism of health expenditure worsens the wealth equality. Too see this, we compare the outcomes of different models in Table II. In the second row, we shut down both preventive and treatment expenditure that the idiosyncratic risk is now uninsured. We find the disease is more transmissive with higher basic reproduction number R_0. However, the model with uninsured risk brings lower wealth Gini index (0.365). When we only enable one of the health expenditure, as in the third and fourth rows, the wealth Gini slightly increases, but is still lower than the baseline case. This is because the rich people are unable or less able to migrate the negative impact using more health expenditure. The risk of income loss is identical regardless of individuals' wealth, while being lower for the wealthy in the baseline.

[23]see e.g. Krueger, Mitman and Perri (2016); Stachurski and Toda (2019)
[24]The last row of Table II shows the Gini index of a standard Aiyagari model, where possible productivity are $\{0.2, 1\}$ in lined with our baseline model. The Poisson intensities are $\{0.5, 0.5\}$.

Table II. Model Comparison

Model	R_0	agg.Capital	agg.Income	Wealth Gini
Baseline	9.236	14.447	1.838	0.412
Exog. Disease	216.0	13.869	1.763	0.365
$m_{\mathcal{P}}$ only	10.427	13.966	1.775	0.37
$m_{\mathcal{T}}$ only	104.282	14.393	1.831	0.407
Aiyagari	-	43.981	2.376	0.319

Notes: This table compares the stationary equilibria of different models. The first row is the baseline model in our paper. The second row we assume the exogenous disease dynamics. The third and forth rows assume that individuals optimize only one health expenditure. The final row shows the results for a standard Aiyagari model of two types of productivity $\{0.2, 1\}$ with the same Poisson intensity.

Table III. Income Distribution in the Baseline Model

(a) Low Income Group

	$\mathcal{I}$	$\mathcal{S}$	$\mathcal{R}$
Low a	0.042	0.089	0.748
Mid a	0.081	0.0	0.0
High a	0.04	0.0	0.0

(b) Middle Income Group

	$\mathcal{I}$	$\mathcal{S}$	$\mathcal{R}$
Low a	0.0	0.007	0.056
Mid a	0.0	0.104	0.833
High a	b	0.0	0.0

(c) High Income Group

	$\mathcal{I}$	$\mathcal{S}$	$\mathcal{R}$
Low a	0.0	0.0	0.0
Mid a	0.0	0.005	0.039
High a	b	0.117	0.839

Notes: 0<b<1e-5

To provide some more insights to the wealth and income inequality, we tabulate the income distribution against wealth and health in Table III. We split the total population by the 1^{st} and 3^{rd} quantile of wealth and income distribution. The entries in the table denote the share of population in each income group. In Panel (a), we can see that the largest component in the low income group is the people below the first quantile of the wealth distribution, which takes up more than 80%. Some people of the wealthiest 25% could also fall into low income when they are infected and lose labour income. They only share around 4% in the group. Panel (b) and (c) show the distribution for middle and high income group respectively. The middle and high income group mainly consist of those healthy individuals (susceptible and recovered). Only few infected people of the wealthiest 25% could remain middle or high income. This is due to their low labour income share.[25] The impact from disease-induced labour loss is insignificant when capital income is high enough.

[25]In Appendix Figure A3, we plot the share of labour income in total income for the infected and uninfected group. The labour income share is decreasing with wealth. When individuals get infected, the labour income share reduce that people rely more on capital income.

B. Income Elasticity of Health Expenditure

Figure 5 shows the policy function for health expenditure. To further disentangle the implication on individual's health policy from wealth heterogeneity, we solve for the income elasticity of health expenditure. Instead of using the instantaneous policy functions directly, we consider the expenditure over a certain period (0 to τ) in the stationary equilibrium (Achdou et al., 2022; Laibson, Maxted and Moll, 2022) as follows

$$\begin{aligned} M_{\mathcal{P}}(a_0,h_0) &= \mathbb{E}\left[\int_0^\tau m_{\mathcal{P}}(a_t,h_t)dt\middle| a_0,h_0\right], \\ M_{\mathcal{T}}(a_0,h_0) &= \mathbb{E}\left[\int_0^\tau m_{\mathcal{T}}(a_t,h_t)dt\middle| a_0,h_0\right]. \end{aligned} \tag{21}$$

$M_{\mathcal{P}}$ and $M_{\mathcal{T}}$ sum up the health expenditure from time 0 to τ for individuals starts with state (a_0, h_0). These expressions are important complementations to the instantaneous policy functions as they additionally capture the information at the dimension of time. In our model, health expenditure are restricted to individuals who are infected or susceptible. However, the health status is stochastic. The duration for each health status varies along the wealth space, and thus differs the cumulative health spending in a certain period. This means that whether the riches spend more on health over time in our model is not intuitively explicit. For example, although wealthier individual spend more on prevention and treatment, they consequently experience fewer shots and shorter duration of infection. The second advantage of using expenditure over time is that for most survey data, we mainly observe individuals' time-aggregated variables at some specific frequency.

We apply the new measurement to solve for the Income Elasticity of Health Expenditure as Equation 22, where we assume there is a windfall income Δ on individuals' asset. These expressions measure the fractional change on health expenditure over τ periods, if the wealth endowment is increased by $\Delta/a_0 \times 100\%$. In Appendix D, we show how Equation 21 is computed by the Feynman-Kac Formula.

$$\begin{aligned} \varepsilon_{M_h,y} &= \frac{\partial M_h(a_0,h_0)}{\partial y}\frac{y}{M_h} \\ &= \frac{M_h(a_0+\Delta,h_0)-M_h(a_0,h_0)}{\Delta}\frac{a_0}{M_h(a_0,h_0)} \\ h &= \{\mathcal{P},\mathcal{T}\} \end{aligned} \tag{22}$$

We set the time period τ to one-year duration and presents the computational results at Figure 6. The surface represents the estimated elasticities corresponding to income realization Δ and wealth percentile. We focus on the baseline case where

Figure 6. Health Expenditure Elasticity of Income

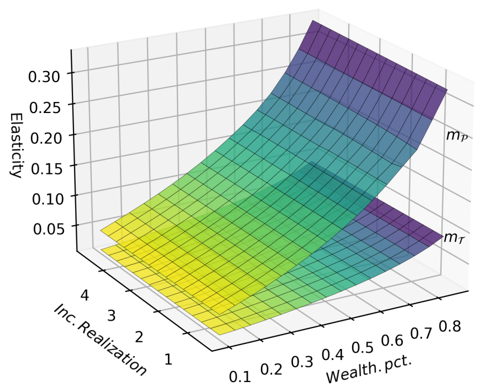

Notes: (a) This Figure plots the health expenditure elasticity of income when the health punishment is 0.3. (b) The x-axis denotes the percentiles in the wealth distribution. The y-axis denotes the realization of windfall income Δ.

$\chi = 0.3$. We find that the income elasticity is positive but lower than unity[26] for both types of health expenditure. Preventive expenditure is more elastic than the treatment expenditure, with its surface lying well above. We also find the elasticity is increasing with wealth level. Individuals at the top wealth decile exhibit elasticity around 5 times more than those at the lowest decile. However, we find the estimated elasticity is not sensitive to the rate of windfall income Δ.

C. Comparative statics

To the study long-run implication of the model, we solve the stationary equilibria under different parameters for comparative statics. Specifically, we conduct the experiment by varying disutility χ. Figure 7 presents health policy function with varying degrees of disutility from being infected. When lowering the level of disutility, health expenditure become less sensitive to wealth. This is because when χ decreases, the extra punishment of being infected is lowered. Therefore, the value of infection $v(a, \mathcal{I})$ increases and changes the denominator in F.O.C. Equation 15. For the special case of $\chi = 0$, the mechanism via direct loss of being ill is shut down. Infection is therefore a pure income shock. However, temporary income drop of being infection is trivial for the wealthier individuals. Hence, we observe very small heterogeneity in health expenditure along the wealth distribution as the blue

[26] This is consistent with the empirical evidence that health expenditure is a necessary good rather than luxury good (Di Matteo, 2003; Freeman, 2003; Moscone and Tosetti, 2010).

Figure 7. Health Policy Function

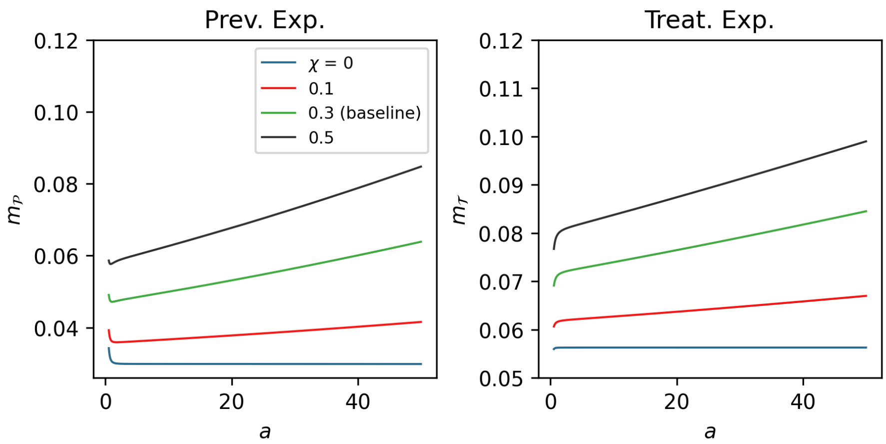

Notes: The first and second Panel of this Figure plot the health policy functions varying health punishment χ. The slope is higher when the punishment increases.

line. The corresponding income elasticity of health expenditure also gets smaller as shown in Appendix Figure A4.

Table V provides more details on how variables change in response to change in disutility. Panel (a) compares the aggregate variables. Overall, the infection rate for the rich (top 25%) is smaller. When the disutility increase, the gap in infection rate is widened. The richer are getting less likely to be infected, related to the poor. The disparity of infection outcomes among wealth groups matches our the empirical observation in UK. ONS (2022a) documents a statistically significant 1.8% gap on infection risk[27], 2.8% gap on self-reported hospital admission rate between people living in the most and least deprived area.

The infection rate gap generated in the model is due to the optimal policy that the rich spend more on prevention, as shown in Panel (b) and in lined with our observation in Figure 7. Price (w, r) do not changed too much. This is because aggregate capital and labour move at the same direction. Capital is increased. Labour is also increased because of less infection. The influence on pricing is then cancelled out in the long run. However, as we will show in the later session, the prices would change in the short run when converging to the stationary equilibrium or being subjected to shocks.

The next few blocks in the Panel (a) compare the wealth and income inequality. We observe the Gini index for wealth and inequality moves in opposite directions as punishment χ increases. On the one hand, income equality is improved with higher χ. This is due to the property that infection harms labour productivity such

[27] For Delta variant, the difference was 1.9pp (most deprived: 7.3%, 95% CI: 6.9 to 7.7; least deprived: 5.4%, 95% CI: 5.2 to 5.6). While for Omicron the difference was 1.8pp (most deprived: 6.7%, 95% CI: 6.2 to 7.1; least deprived: 4.9%, 95% CI: 4.6 to 5.1)

Table V. Comparative Study

(a) Aggregate Variables

χ	0	**0.3**	0.5
Infection Rate			
Aggregate	4.344	4.107	3.97
Bottom 25%	4.444	4.235	4.115
Top 25%	4.307	4.023	3.862
diff.	-0.137	-0.212	-0.253
Capital	14.418	14.447	14.463
Prices			
Wage Rate	1.694	1.694	1.694
Interest Rate	0.014	0.014	0.014
Inequality			
Wealth Gini	0.41	0.412	0.423
Income Gini	0.072	0.071	0.07
Wealth Share			
Bottom 25%	6.72	6.67	6.49
Top 25%	52.89	53.03	54.08
diff.	46.18	46.36	47.59

(b) Contol Variables

χ	0	**0.3**	0.5
Consumption			
Aggregate	1.83	1.829	1.827
Bottom 25%	1.682	1.681	1.678
Top 25%	2.052	2.053	2.059
diff.	0.37	0.372	0.38
Preventive Exp.			
Aggregate	0.03	0.052	0.066
Bottom 25%	0.03	0.048	0.06
Top 25%	0.03	0.057	0.074
diff.	-0.0	0.009	0.015
Treatment Exp.			
Aggregate	0.056	0.075	0.085
Bottom 25%	0.056	0.072	0.081
Top 25%	0.056	0.079	0.092
diff.	0.0	0.007	0.01

Notes: (a) This table compares the stationary results of models with different health punishment $\chi \in \{0, 0.3, 0.5\}$, where $\chi = 0.3$ is used as the baseline. For the special case $\chi = 0$, infectious disease is a pure income shock. (b) Panel (a) compares the aggregate outcome of price, inequality measures, and infection rate. Panel (b) compares the optimal controls at bottom and top wealth quantile.

that the majority of infected individuals has the instantaneous income under the 25% percentile of the income distribution (see Table III). Therefore, the reduction of overall infection rate implies smaller size of low income group, and thus a more equal income distribution. On the other hand, the wealth inequality becomes more profound with the wealth Gini index and the wealth shared by the wealthiest 25% increase slightly.

We provide a possible explanation in Table VII, where we use Feynman-Kac Formula[28] to calculate the expected income and savings over a 3-years window. In the first block, we find that expected income increases for both poor and rich, while their income gap is widened when χ goes up. This is because the richer spend more on prevention. Hence, they are less likely to be infected and thus experience smaller productivity loss in a given period. When breaking the income into categories, we find both labour and capital income gap expand.

The change of income stream affects the savings choice. When it comes to the expected savings in the second block of Table VII, we find the savings for the poor is generally higher. As χ increases, savings is reduced for the poor, but increased

[28] We would like to calculate the expected variables (income, expenditure, savings) over a period τ for each individual with state (a_0, h_0), i.e. $\mathbb{E}[\int_0^\tau y(a_t, h_t)dt | a_0, h_0]$.

Table VII. Comparative Study (cont.)

χ	0	**0.3**	0.5
Expected Income in 3-yr duration			
Bottom 25%	20.5	20.532	20.534
Top 25%	25.0	25.07	25.204
diff.	4.5	4.539	4.669
Labour Income diff.	0.0	0.013	0.02
Capital Income diff.	4.461	4.488	4.612
Expected Savings in 3-yr duration			
Bottom 25%	2.793	2.701	2.755
Top 25%	-1.029	-0.991	-0.916
diff.	-3.822	-3.692	-3.672

Notes: This table uses the Feynman-Kac formula to calculate the expected value within a 3-years duration. We compare the expected income and savings for models with different punishment χ.

for the rich. The saving gap between the poor and rich gets smaller. Therefore, the richer accumulate more capital and implies a more unequal wealth distribution.

We also implement the same exercise by varying the infectiousness of the disease. Appendix B Table B2 presents the corresponding results where we change the coefficient ϵ_0 in the contact rate function. In the Appendix B Table B5 and Table B8, we conduct another two experiments by raising the effectivity of health expenditure. Specifically, we increase ϵ_1 and η_1 to allow more curvature on $\alpha(m_{\mathcal{P}}), \gamma(m_{\mathcal{T}})$.

VI. Transitional Dynamics

In this section, we move on from the discussion on the long-run stationary equilibrium to the short-run dynamics. Specifically, we consider two practices on the transitional dynamics of the model: (1) Given the arbitrary initial distribution of individual states, solve for the convergence path towards the stationary equilibrium; (2) Given that the economy is initially at the stationary equilibrium, impose a temporary unanticipated shock (MIT shock) to the model.

A. Transition Path

We would like to find a full dynamic sequence of distribution $\{g(a, h)\}_t$ and value function $\{v(a, h)\}_t$ satisfying the Nash equilibria in Definition 1 for $t \in [0, \infty)$. To give a bird's eye view, we solve the HJB (Equation 17) backwards knowing the stationary solution $v^*(a, h)$; solve the KFP (Equation 18) forward given a specific initial distribution. We show the full algorithm in Appendix E.

We inherit the value function from the baseline stationary equilibrium solved in section V.. Then, we construct several initial distributions for individual states. For simplicity, we only disturb the distribution of health status in the following steps.

Firstly, we let the marginal distributions of wealth and productivity be identical to that in the stationary equilibrium. Then for the simplex of epidemiological compartment (s_0, i_0, r_0), we assign 0.5% of initial infection rate and vary the initial recovery rate in $\{0, 34\%, 68\%\}$, while the rest are susceptible to disease. We use the different sizes of initial recovered group to give insights on vaccination. One could interpret that higher initial recovery size implies higher vaccination rate. This is because the recovered group consists of individual with temporal immunity to infection, essentially shares the same characteristics with vaccinated group. Vaccination policy in fact brings individuals from $\mathcal{S}$ to $\mathcal{R}$ without going through group $\mathcal{I}$ (Federico, Ferrari and Torrente, 2022)[29], and hence expands the size of pre-pandemic recovered group.

The third case with 68% of pre-existing recovery matches the fully-vaccinated rate in UK before the outbreak of Omicron B.A.1 variant. Figure 8 shows how the simulation match the empirical data of this wave of outbreak. We set the date when infection case began to increase as the reference. In Panel A, we match the social infection rate to the data of positive testing rate. The simulation well matches the data except that we underestimate the infection rate at the beginning phase of the outbreak. This is because our simulation does not incorporate infection from other variants like Delta variant before the outbreak.[30] Panel B matches population flow from susceptible group to infected group, i.e. $\int \alpha(m_{\mathcal{P}})\zeta \mathbb{1}(h = \mathcal{S}) d\mu$, to the data of new infection case. For comparison, we standardize the data at the referenced date to 1. We find the simulated dynamics roughly fits the data.

Figure 9 plots the transitional dynamics towards the stationary equilibrium given multiple initial distributions. Throughout the simulation period[31], there would be outbreak that the social infection rate peaks in the first month. We find the infection rate converges to the same value for all simulations. However, with smaller initial pre-existing recovered group, the pandemic is worse with larger strike of infection. Correspondingly, labour supply drops significantly during the pandemic and recovers to its steady state. The temporary loss of labour productivity affects wealth accumulation that aggregate capital also sees a subsequent decrease in the first month. Although both capital and labour are negatively shocked, it shows dif-

[29]Another possible approach is to introduce a new compartment for vaccinated group like e.g. Sun and Yang (2010); Safan, Kretzschmar and Hadeler (2013); Garriga, Manuelli and Sanghi (2022) (another health status in our model). The vaccinated group is mostly similar to the recovered group as they both carries temporary immunity. The only difference is on their reinfection probability. Clinical evidence shows immunity from previous infection lasts longer than from primary series or first booster of vaccination. But the gap is not pronounced (Bobrovitz et al., 2023).

[30]Clinical evidence shows that infection could take place at different variants of virus. Infection cannot provide effective immunity to the new variant (ONS, 2023a).

[31]We let the simulated period to be long enough to ensure convergence to the stationary equilibrium. Here we only plot the first 3 months to visualize the short-run dynamics. Same for other simulations in this session.

Figure 8. Simulation and Empirical Data

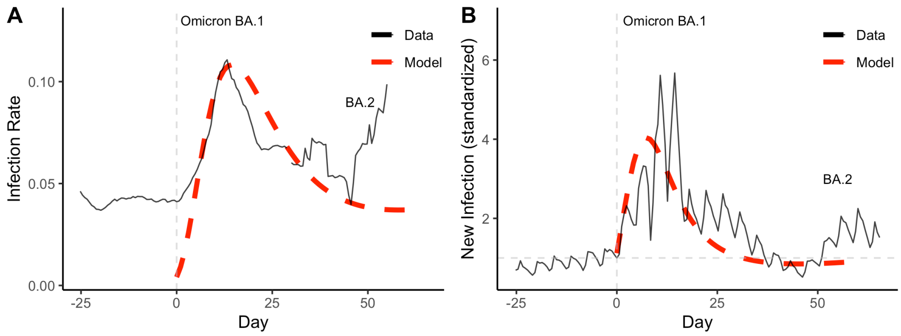

Notes: (a) The red dash lines and black solid lines in this Figure shows dynamics of infection in the model and data respectively. We match the empirical data of the wave of Omicron B.A.1 variant in UK. (b) We set the date when infection began to climb as the reference. (c) In Panel A, we match the social infection rate in the model to the data of positive testing rate. (d) In Panel B, we match the new infection rate to the data. We standardize the observation at the reference date to 1.

ference in their timing of adjustment. Aggregate labour bounces back very quickly within 2 months as the infected people overcoming illness and obtain immunity. The capital accumulates very slowly and remains in low level for a longer period.

The gap on convergence speed induces factor price fluctuation unlike that in our long-run comparative statics (Table V) where the effect from aggregate K and L offset each other. The change of prices largely follows the motion of infection rate, and is more dynamic with smaller pre-existing recovered group. We observe labour wage is increased while capital interest rate is decreased during the pandemic. The rising wage is due to the shortage of workers, especially in some labour-intensive industries like restaurant, delivery, express etc.. The UK data by ONS (2022b) shows similar pattern during the pandemic. The unit labour cost for firms is significantly increased in Q1 - Q3 of 2020.[32] The data also reveals a drop in average weekly earning and average output per workers. This observation is also explained by our model that the productivity drop overwhelms the effect of rising labour price in aggregate level. The motion of interest rate also matches our empirical observation during pandemic that average sharecite-keyholder returns declines for most sectors in the first 3 seasons (see e.g. Bradley and Stumpner (2021); Bai et al. (2023) etc.).

One of the key advantages of our HACT setup is that we can track the evolution of the joint distribution $g_t(a, h)$ by the Kolmogolov Forward Equation. This allows us to measure the inequality dynamics by calculating Gini index overtime. In the third row of Figure 9, we find that both income inequality and wealth inequality rise during the outbreak, and are worse for the simulations initiated with smaller recovered group. Specifically, the income Gini index is largely procyclical to the

[32]The largest component of total nominal employment costs is compensation of employees which grew by 11.1% between Quarter 4 2019 and Quarter 4 2021

Figure 9. Transitional Dynamics (Convergence Path)

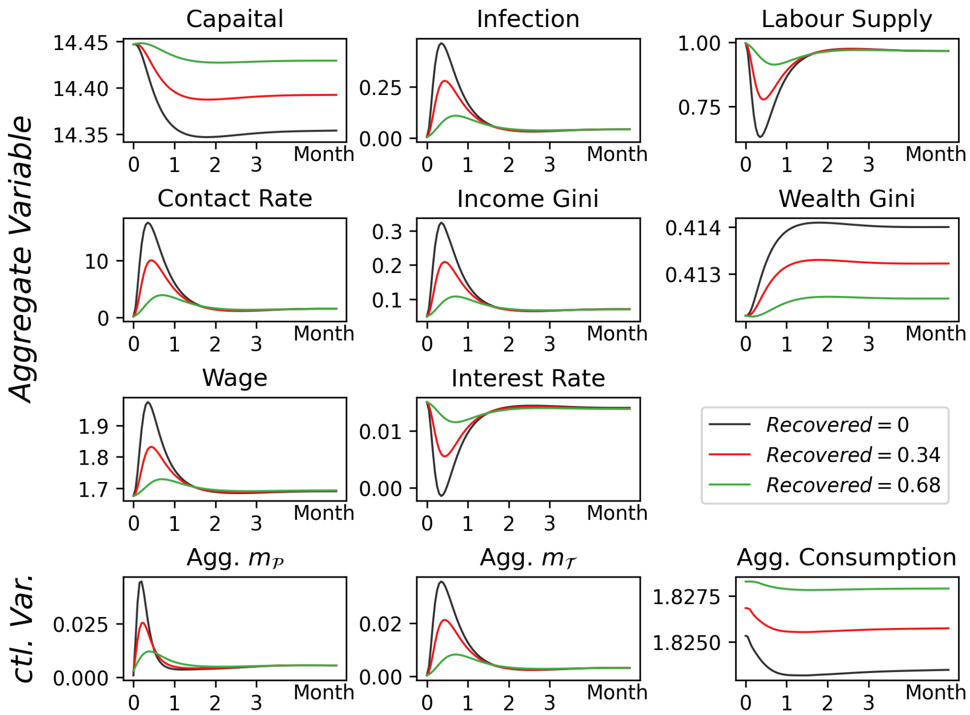

Notes: (a) This Figure plots the transitional dynamics of our baseline model with different initial distributions, where the fraction of pre-existing recovered group are 0 (blue), 16% (yellow) and 32% (green). (b) The first two rows are the dynamics of aggregate variables. The last row shows the control variables aggregated by the time-varying distribution $g_t(a, h)$. (c) The horizontal axis denotes the time (in month) from the simulation.

infection rate dynamics. This is because the growing infection rate implies that more individuals would fall into the low-income group. At the same time, those unaffected people with full productivity benefit from the rising labour wage. The growth of wealth Gini index is the deep consequence of expanding income disparity. Differently, we see that the harm on wealth equality is relatively long-lasting as capital accumulation is a slower process to labour supply recovery.

The rising wealth Gini index is induced by the expanding low wealth group. To show this, we break the aggregate measurement of inequality into the change of population density in each wealth level. In Figure 10, we show the evolution of wealth distribution under the simulation with no initial recovery. The surface represents the change of wealth distribution at marginal time, in expression, $\Delta_{dt} g_t(a) = \sum_h g_t(a, h) - \sum_h g_{t-dt}(a, h)$, corresponding to each wealth grid (y-axis) and time after outbreak (x-axis). The blue stars and the red triangle at the y-axis are the 25%, 50%, 75% percentiles and the mean of the initial wealth distribution.[33] The red lines separate areas with different signs of change. We can see that during

[33]These percentiles would change during the convergence. We only plot the stationary percentiles here as their changes are sufficiently small.

Figure 10. Change in Wealth Distribution

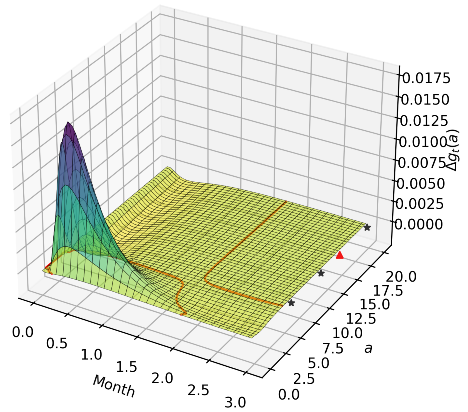

Notes: (a) This Figure shows the change of wealth distribution $\Delta_t g_t(a)$ for the simulation with 16% of pre-existing recovered group, where $g_t(a) = \sum_h g_t(a,h)$. The x-axis is the time after the simulation and the y-axis the wealth level. (b) The blue stars represents the (25%, 0.5%, 0.75%) percentile of wealth distribution. The yellow triangle represents mean of the wealth distribution. (c) The red line is the contour for $\Delta_t g_t(a) = 0$. It separates the increasing and decreasing areas.

the first month of the pandemic, population at lower quantile of wealth distribution increases, while population at middle and higher quantile drops. While the economy consists of more poor people and less middle class, the wealth equality would be worsened.

Our model matches the rising wealth Gini qualitatively. However, we find the magnitude for the rise being small, with the change less than 0.01. We believe this is due to the following reasons: (1) The Gini index is naturally small and less dynamic in the Aiyagari-type models, as they could not capture the thick-tail of the wealth distribution. (2) General equilibrium effect is the main cause for this outcome. The expanding wealth inequality is mainly induced by the disparity in infection rate among wealth levels, which directly affects their labour income. The assets income disparity among wealth, on the other hand, is reduced because of the decreased interest rate. Therefore, the expansion of income disparity is mitigated by reducing assets return. (3) The lost of productivity by infection is temporary (around one week). One wave of pandemic is not enough to generate substantial change of wealth Gini index in our model, while there exist multiple waves due to either seasonal cause or virus mutation in the empirical data. We note that the virus mutation generate multiple waves of infection could amplify the magnitude of increase of wealth Gini index. To model virus mutation, we simply let part

Figure 11. Change in Health Policy

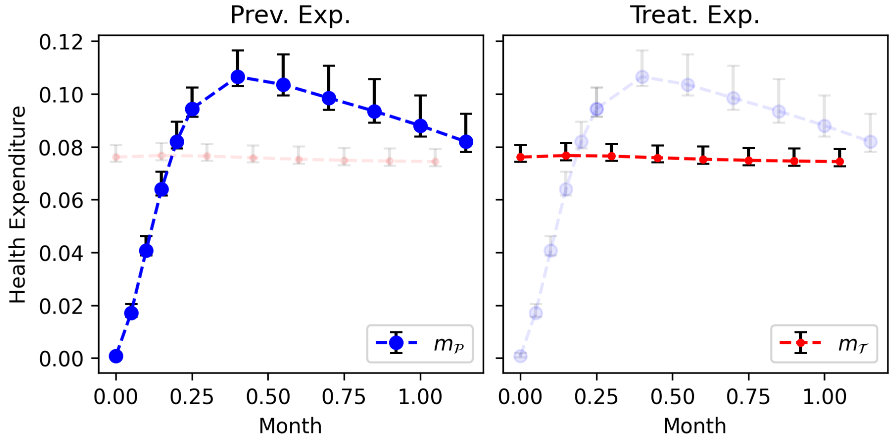

Notes: (a) This Figure plots the dynamics of health policies. Panel A highlights the dynamics of preventive expenditure ($m_{\mathcal{P}}$). Panel B highlights the treatment expenditure ($m_{\mathcal{T}}$). (b) The connected dots are the health expenditure at 50% of wealth distribution. The lower bars and upper bars are the 10% and 90% of wealth distribution.

of recovered people become susceptible when the new variant exist. We show the results in Appendix Figure A5. We firstly match the mutation from Omicron B.A.1 to B.A.2 by letting 25% of recovered people be subjected to the new variant. Then we assume no cross-variant immunity in the next few mutations. We find multiple waves of infection is generated and the increase in wealth Gini index from different waves could be stacked up.

We also study the dynamics of optimal health policy. For the aggregate behaviour, in the last row of Figure 9, we average the individual health expenditure by the sequence of joint distributions $g_t(a, h)$. The dynamics of health expenditure is procyclical with the motion of infection rate in aggregation. We observe substantial increase for both preventive and treatment expenditure in the first month of the pandemic. With slight different between two types of expenditure, the rise of treatment policy is more persistent than preventive one.

When we break the aggregate observations of health expenditure into individual change we find the increase in health expenditure is biased towards higher side of the wealth distribution. As in Figure 11, where we plot the health policy function overtime. Panel A highlights the motion of preventive expenditure. The connected dots, lower and upper bars in the Figure denote the preventive policies at the median, lower 10% and upper 90% of the wealth distribution. We find that the expenditure gap between the rich and poor expands in the first one month of pandemic. The rich people are therefore subjected to lower risk of infection. For treatment policies in Panel B, we still have the observation that the richer have higher expenditure. However, the expenditure gap between the rich and poor does not change too much.

Figure 12. Evolution of Income and Savings in Transition

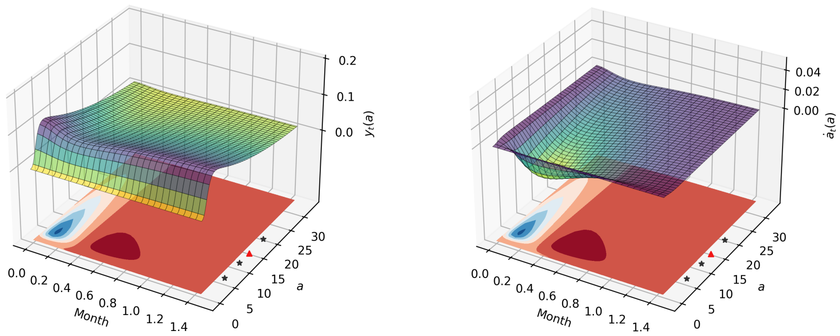

(a) Income Change **(b)** Savings Change

Notes: (a) This Figure plots the change of income and savings along the wealth distribution. The surface denotes the income and savings. (b) We map the change of the income and savings to the x-y plane. The blue area denotes the time and wealth for decreasing income or savings. The red area denotes the time and wealth for increasing income or savings. The notation of blue star and yellow triangle is inherited from Figure 10.

We can now link the transition of distribution (Figure 10) with the motion of optimal policy (Figure 11). The change in wealth is determined by the rate of asset accumulation, that is, savings, which is directly affected by income. In Panel (a) and (b) of Figure 12, the surfaces denote the average income and savings at different wealth level across time.[34] The contour maps at the bottom show the corresponding sign of motion: blue area for decrease; red area for increase. We can see that with decreasing income, the saving rate drops during the first few days of pandemic then slowly goes back. In terms of the change across wealth levels, the decrease in average income and savings is biased towards the lower part of the wealth distribution. This implies that the poor individuals lose more income and spend more net capital on average, and hence get even poorer. Reflected in Figure 10, the population density at lower percentiles increase during the pandemic.

B. The Effect of Income Support Scheme

Support Plan for Infection. We now use our model to explore government's policy. Recall from the empirical evidence in Figure 1 that the wealth Gini index moves differently with or without government subsidy. We add government income support to our framework. We assume that government compensates the infected group by direct transfer. The transfer is lump-sum that government partially cover

[34]The average variables are weighted by distribution $g_t(a,h)$. For example, average value for x with asset a would be $\bar{x}(a) = \sum_h x(a,h)g_t(a,h)$.

Figure 13. Income Support

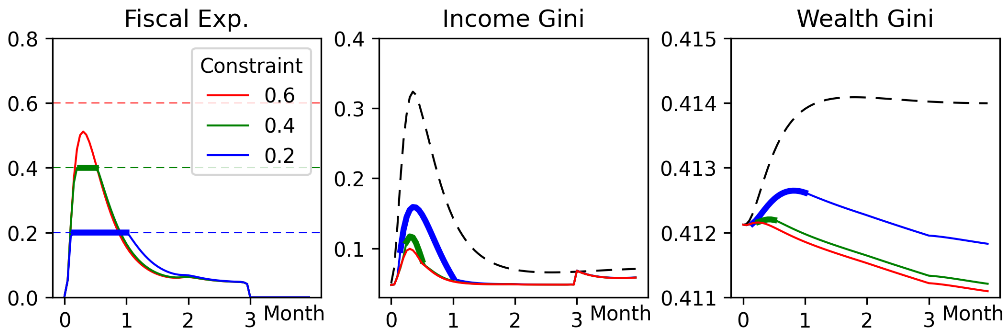

Notes: (a) In this Figure, we study the policy of targeted income support scheme to infected group. This Figure shows the simulated dynamics for fiscal expenditure, aggregate capital, income and wealth Gini index. (b) The red, green and blue lines represent different trajectories that government faces fiscal constraint of 0.6, 0.4 and 0.2. (c) The black dash lines are the referenced dynamics from the baseline results as in Figure 9. The highlighted parts are the time when the fiscal constraints are binding.

the lost of labour income due to infection.[35] In practice, let τ to be the transfer per individual[36], individuals' income becomes

$$ra + wz(h) + \tau \mathbb{1}_{(h=\mathcal{I})}. \tag{23}$$

The income support scheme is financed by government's fiscal expenditure. For simplicity, we abstract from the source of fiscal expenditure.[37] Instead, we assume that government is subjected to an exogenous fiscal constraint $\mathcal{G}_t \leq \bar{\mathcal{B}}$ where $\mathcal{G}_t$ is the aggregate fiscal expenditure

$$\mathcal{G}_t = \int \tau \mathbb{1}_{(h=\mathcal{I})} g_t(a,h) d\mu. \tag{24}$$

During the period when the fiscal budget constraint is binding, government has to lower the transfer τ such that the budget constraint is satisfied. Furthermore, we assume that income support scheme last for 3 months.

We vary $\bar{\mathcal{B}}$ to study the cross-country difference in fiscal constraint. Figure 9 shows the simulation results. The red lines are the results for economies with the highest fiscal constraint, with its expenditure for income support never hitting the

[35]Another way of modelling is by assuming government covers lost of labour income. That is, transfer $\tau = w[z(\mathcal{S}) - z(\mathcal{I})]$. Individuals' total income is hence unrelated to their health status. However, in transitional dynamics, wage rate climbs up during pandemics because of the lack of labour. In this case, government additionally afford the cost of rising price. Thus, transfer could be a more appropriate assumption.

[36]Numerically, we calibrate the transfer τ to be smaller than the wage w, such that the value of infection is always smaller than being healthy.

[37]We don't model taxation in our model as it is not the main source of income support plan during pandemic. Typically, in UK, the income support package came with tax relief policies during the pandemic.

Figure 14. Income Support (cont.)

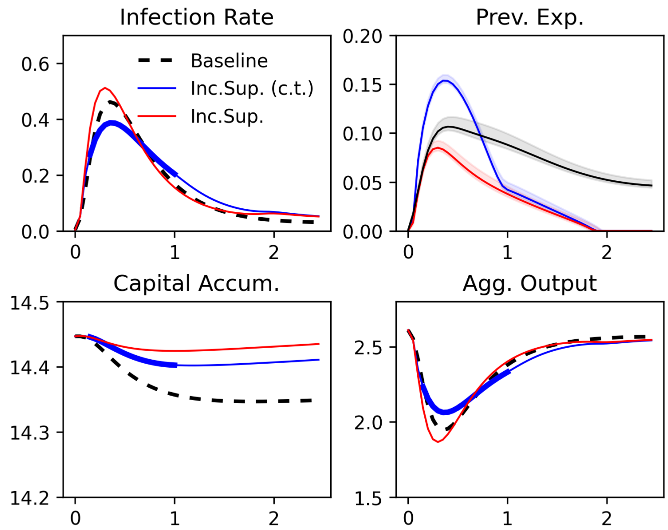

Notes: (a) This Figure shows the infection rate, preventive expenditure, aggregate capital and output under government income support scheme. (b) The red and blue lines denote the simulations under with fiscal constraints of 0.2 and 0.6. The black dash lines are the baseline results without income support. (c) In the top right Panel, the lines denote the preventive expenditure at 50% of the wealth distribution, while the shadowed areas are that at 10%-90% of the wealth distribution.

roof. The green and blue lines are the binding economies with different level of constraints. Compared with the simulation without income support, denoted in black dash lines, the spike of income Gini index during pandemic is largely decreased. This is because the income support is targeted at the infected individuals who partially lose their labour income. As a result, the wealth equality with income support is worsened for a short period then improves subsequently.

When it comes to the comparison of fiscal constraints, we find that economies with tighter constraints are less able to relief the increasing income and wealth inequality, especially during the constrained periods when they have to cut the level of subsidy. Our simulations here match with the empirical evidence that richer countries with stronger income support may conversely improve their wealth equality, even though the income support is temporary.

How the income support affect infection rate? We show two scenarios for illustration. In the first Panel of Figure 14, we find the infection rate is increased when the support doesn't hit the fiscal constraint (red line); is decreased when the support is constrained (blue line). This is because the income support affects individual health expenditure in two different ways. First, the direct transfer increases the wealth level that the susceptible could spend more on prevention. Second, subsidizing the infected group mitigates the value loss of being infected and thus discourages health expenditure. Weather people spend more on health depends on the magnitude of the support. To show this, in the top-right Panel of Figure 14, it could be viewed that the preventive expenditure decreases under the unconstrained support scheme and increases under the constrained support.

For capital accumulation in bottom-left Panel of Figure 14, without any counter-intuitive outcome, we find that capital recovers faster under the unconstrained income support, followed by that under the constrained support and without support. We further analyse the aggregate output $Y = AK^{\beta}L^{1-\beta}$ in the bottom-right Panel. The impact of incapacitated labour (infection rate) dominates the motion of output. We find that the constrained income support increases the aggregate output, but the unconstrained support has the opposite effect. Therefore, for the policymaker, the two-sided effect of income support implies an aggregate trade-off between health and economic equality. The income support by lump-sum transfer could directly improve equality. But it may also induce people to value less on their health and lead to a higher social infection rate, which may reduce aggregate product.

We also discuss other types of support in Appendix Figure A6. Specifically, we evaluate the wealth-targeted support for the poorest 25%[38], i.e. $\tau \mathbb{1}_{(a \leq a_{25\%})}$, and the general support for everyone. They affect equality from different aspects. The infection-targeted support discussed earlier largely improves the income equality. The asset-targeted plan is more effective in improving wealth equality, as it directly rise the income for the poorest 25%. Though asset-targeted and general support plans reduce more wealth Gini index, they put more pressure on fiscal budget as it requires continuous investment.

C. Other Extensions

Weaker Disease. We also explore the convergence path under different calibrations. Specifically, we firstly simulate the dynamics with milder disease. At the later stage of Covid-19 pandemic, the disease mutated towards the variants with lower mortality rate and hospitalized rate. We incorporate this by assuming the infected group are only incapacitated by only 20% while incapacitated by 80% in our previous discussion. The corresponding simulations are shown in Appendix Figure A7. We observe that the infectivity is more severe than the baseline scenario[39] as susceptible people are less precautionary and spend less on health. However, higher infection rate doesn't cut too much aggregate labour supply in this cacse as the disease are weakened. Aggregate capital thus shows smaller decrease and faster recovery. When it comes to inequality measures, both income and wealth

[38]We let the cut-off asset for support to be fixed at the first quantile before the pandemic, i.e. t_0 at the simulation.

[39]We use the simulation with 16% of pre-existing recovered group (yellow lines in Figure 9) as the baseline. Same for the rest of the paper.

Gini index show smaller increase than the baseline because the labour income gap between health group is relatively narrowed.

Long Covid. The second practice in Appendix Figure A8 investigates the effect from Long-Covid, where we lower the productivity of the recovered group that $z(\mathcal{R}) = 0.8$. In this case, individuals' productivity cannot fully recover to the pre-infected stage, thought they still gain immunity. Thus, the value of being infected $v(a, \mathcal{I})$ further reduces as Long Covid cause productivity loss for a longer time. The value for the recovered group $v(a, \mathcal{R})$ also decreases. Consequently, individuals spend more on preventing infection and less on treatment. In aggregation, the peak infection rate is smaller than the baseline. However, as we assume slower productivity recovery process, the decay in aggregate supply of labour and capital is more persistent. Similarly, the income and wealth Gini indices show milder but long-lasting increase.

MIT Shocks. We also study the short-run dynamics of the model by imposing unanticipated temporary shock (MIT shock). We assume the model initiates from the stationary equilibrium in section V.. Then, we impose a temporary increase in infectivity of the disease. As in the first Panel of Appendix Figure A9, the infectivity ϵ_0 is raised by 20%, 40% and 60% respectively then decays back to the initial level. Therefore, the economy will end up with the same stationary equilibrium before the shocks arrived. We find the social infection rate and contact rate increase then adjust back after the shock. Aggregate labour and capital counter the motion of social infection. The magnitude of aggregate capital change is small with only 0.01% to 0.02% deviation from the steady state. But it takes longer for capital to adjust, in lined with our previous observations for convergence paths. The price variables, wage and interest rate, is countercyclical to the motion of labour and capital. For inequality measures, income inequality is procyclical to social infection. Wealth Gini index also increases when infectivity increases. And the impact on wealth inequality is more persistent.

VII. CONCLUSION

Our paper extends the representative agent epidemiological economic model to a heterogeneous agent framework. We explore individuals' optimal policy and aggregate response to infectious disease. We conclude our paper in following remarks: (1) The policy functions for prevention and treatment expenditure are increasing and more elastic with higher wealth. Health expenditure inelastic to wealth if the disutility of being infected is small. (2) In the stationary equilibrium, infection rate for the poor individuals is higher and thus diverges individuals' labour income. (3) In the short-run, there would be pandemic before the stationary equilibrium is reached.

The outbreak is milder with higher level of pre-existing immunity. (4) Income and wealth equality is worsened during the pandemic. The motion of inequality measures are driven by individuals' heterogeneous health policies during the pandemic. (5) Income support scheme can mitigate the negative effect on equality. But it may lead to worse aggregate health outcome.

The heterogeneous agent model in our paper generates increase in income inequality based on optimal policy functions on response to infectious diseases. The wealthy spend more on health because they are endowed with more assets to use. The mechanism is different from Hall and Jones (2007) where health is a superior good with an income elasticity well above one. We abstract from other mechanisms that can also increase inequality including unemployment; sectorial heterogeneity (Chetty et al., 2023); remote working and digital devices (Stantcheva, 2022); mortality (Goenka, Liu and Nguyen, 2022); furlough scheme (Görtz, McGowan and Yeromonahos, 2021) etc.

REFERENCES

Acemoglu, Daron, Victor Chernozhukov, Iván Werning, and Michael D Whinston. 2021. "Optimal targeted lockdowns in a multigroup SIR model." American Economic Review: Insights, 3(4): 487–502.

Achdou, Yves, Guy Barles, Hitoshi Ishii, Grigory L Litvinov, and Yves Achdou. 2013. "Finite difference methods for mean field games." Hamilton-Jacobi Equations: Approximations, Numerical Analysis and Applications: Cetraro, Italy 2011, Editors: Paola Loreti, Nicoletta Anna Tchou, 1–47.

Achdou, Yves, Jiequn Han, Jean-Michel Lasry, Pierre-Louis Lions, and Benjamin Moll. 2022. "Income and wealth distribution in macroeconomics: A continuous-time approach." The review of economic studies, 89(1): 45–86.

Achdou, Yves, Pierre Cardaliaguet, François Delarue, Alessio Porretta, Filippo Santambrogio, Yves Achdou, and Mathieu Laurière. 2020. "Mean field games and applications: Numerical aspects." Mean Field Games: Cetraro, Italy 2019, 249–307.

Adams-Prassl, Abi, Teodora Boneva, Marta Golin, and Christopher Rauh. 2020. "Work tasks that can be done from home: Evidence on variation within & across occupations and industries."

Aiyagari, S Rao. 1994. "Uninsured idiosyncratic risk and aggregate saving." The Quarterly Journal of Economics, 109(3): 659–684.

Alipour, Jean-Victor, Oliver Falck, and Simone Schüller. 2023. "Germany' s capacity to work from home." European Economic Review, 151: 104354.

Alvarez, Fernando, David Argente, and Francesco Lippi. 2021. "A simple planning problem for COVID-19 lock-down, testing, and tracing." American Economic Review: Insights, 3(3): 367–382.

Angelopoulos, Konstantinos, Spyridon Lazarakis, Rebecca Mancy, and Max Schroeder. 2021. "Pandemic-induced wealth and health inequality and risk exposure."

Atkeson, Andrew. 2021. "A parsimonious behavioral SEIR model of the 2020 COVID epidemic in the United States and the United Kingdom." National Bureau of Economic Research.

Bai, Chenjiang, Yuejiao Duan, Xiaoyun Fan, and Shuai Tang. 2023. "Financial market sentiment and stock return during the COVID-19 pandemic." Finance Research Letters, 54: 103709.

Bartik, Alexander W, Zoe B Cullen, Edward L Glaeser, Michael Luca, and Christopher T Stanton. 2020. "What jobs are being done at home during the COVID-19 crisis? Evidence from firm-level surveys." National Bureau of Economic Research.

Beigel, John H, Kay M Tomashek, Lori E Dodd, Aneesh K Mehta, Barry S Zingman, Andre C Kalil, Elizabeth Hohmann, Helen Y Chu, Annie Luetkemeyer, Susan Kline, et al. 2020. "Remdesivir for the treatment of Covid-19." New England Journal of Medicine, 383(19): 1813–1826.

Belot, M, S Choi, JC Jamison, NW Papageorge, E Tripodi, and E Van den Broek-Altenburg. 2020. "Unequal Consequences of Covid 19 Across Age and Income: Representative Evidence from Six Countries: CEPR Discussion Paper No." DP14908.[Google Scholar].

Blundell, Richard, Monica Costa Dias, Robert Joyce, and Xiaowei Xu. 2020. "COVID-19 and Inequalities." Fiscal studies, 41(2): 291–319.

Bobrovitz, Niklas, Harriet Ware, Xiaomeng Ma, Zihan Li, Reza Hosseini, Christian Cao, Anabel Selemon, Mairead Whelan, Zahra Premji, Hanane Issa, et al. 2023. "Protective effectiveness of previous SARS-CoV-2 infection and hybrid immunity against the omicron variant and severe disease: a systematic review and meta-regression." The Lancet Infectious Diseases.

Borgonovi, Francesca, Elodie Andrieu, and SV Subramanian. 2020. "Community level social capital and COVID-19 infections and fatality in the United States." Covid Economics, 32: 110–126.

Bradley, Chris, and Peter Stumpner. 2021. "The impact of COVID-19 on capital markets, one year in." McKinsey & Company.

Brown, Caitlin S, and Martin Ravallion. 2020. "Inequality and the coronavirus: Socioeconomic covariates of behavioral responses and viral outcomes across US counties." national Bureau of economic research.

Cagigi, Alberto, Meng Yu, Björn Österberg, Julia Svensson, Sara Falck-Jones, Sindhu Vangeti, Eric Åhlberg, Lida Azizmohammadi, Anna Warnqvist, Ryan Falck-Jones, et al. 2021. "Airway antibodies emerge according to COVID-19 severity and wane rapidly but reappear after SARS-CoV-2 vaccination." JCI insight, 6(22).

Calvia, Alessandro, Fausto Gozzi, Francesco Lippi, and Giovanni Zanco. 2023. "A simple planning problem for COVID-19 lockdown: a dynamic programming approach." Economic Theory, 1–28.

Cardaliaguet, Pierre, François Delarue, Jean-Michel Lasry, and Pierre-Louis Lions. 2019. The master equation and the convergence problem in mean field games:(ams-201). Princeton University Press.

Carmona, René, François Delarue, et al. 2018. Probabilistic theory of mean field games with applications I-II. Springer.

Chetty, Raj, John N Friedman, Michael Stepner, and Opportunity Insights Team. 2023. "The Economic Impacts of Covid-19: Evidence from a New Public Database Built Using Private Sector Data." The Quarterly Journal of Economics, qjad048.

Coven, Joshua, and Arpit Gupta. 2020. "Disparities in mobility responses to COVID-19." New York Univ, 1.

CreditSuisse. 2023. "Global Wealth Report 2023." Global Wealth Report. https://www.credit-suisse.com/about-us/en/reports-research/global-wealth-report.html.

Di Fusco, Manuela, Xiaowu Sun, Mary M Moran, Henriette Coetzer, Joann M Zamparo, Laura Puzniak, Mary B Alvarez, Ying P Tabak, and Joseph C Cappelleri. 2022. "Impact of COVID-19 and effects of BNT162b2 on patient-reported outcomes: quality of life, symptoms, and work productivity among US adult outpatients." Journal of Patient-Reported Outcomes, 6(1): 123.

Di Matteo, Livio. 2003. "The income elasticity of health care spending: A comparison of parametric and nonparametric approaches." The European Journal of health economics, 4: 20–29.

Dingel, Jonathan I, and Brent Neiman. 2020. "How many jobs can be done at home?" Journal of public economics, 189: 104235.

Fan, Ying, A Yeşim Orhun, and Dana Turjeman. 2020. "Heterogeneous actions, beliefs, constraints and risk tolerance during the COVID-19 pandemic." National Bureau of Economic Research.

Federico, Salvatore, Giorgio Ferrari, and Maria-Laura Torrente. 2022. "Optimal vaccination in a SIRS epidemic model." Economic Theory, 1–26.

Fernández-Villaverde, Jesús, Samuel Hurtado, and Galo Nuno. 2023. "Financial frictions and the wealth distribution." Econometrica, 91(3): 869–901.

Freeman, Donald G. 2003. "Is health care a necessity or a luxury? Pooled estimates of income elasticity from US state-level data." Applied Economics, 35(5): 495–502.

Galasso, Vincenzo, Vincent Pons, Paola Profeta, Michael Becher, Sylvain Brouard, and Martial Foucault. 2020. "Gender differences in COVID-19 attitudes and behavior: Panel evidence from eight countries." Proceedings of the National Academy of Sciences, 117(44): 27285–27291.

Garriga, Carlos, Rody Manuelli, and Siddhartha Sanghi. 2022. "Optimal management of an epidemic: Lockdown, vaccine and value of life." Journal of Economic Dynamics and Control, 140: 104351.

Gersovitz, Mark, and Jeffrey S Hammer. 2004. "The economical control of infectious diseases." The Economic Journal, 114(492): 1–27.

Gilboa, M, G Regev-Yochay, M Mandelboim, V Indenbaum, K Asraf, R Fluss, et al. 2022. "Durability of Immune Response After COVID-19 Booster Vaccination and Association With COVID-19 Omicron Infection. JAMA Netw Open. 2022; 5 (9): e2231778." Epub 2022/09/16. https://doi.org/10.1001/jamanetworkopen. 2022.31778 PMID ···.

Glover, Andrew, Jonathan Heathcote, Dirk Krueger, and José-Víctor Ríos-Rull. 2023. "Health versus wealth: On the distributional effects of controlling a pandemic." Journal of Monetary Economics, 140: 34–59.

Goenka, Aditya, and Lin Liu. 2020. "Infectious diseases, human capital and economic growth." Economic Theory, 70: 1–47.

Goenka, Aditya, Lin Liu, and Manh-Hung Nguyen. 2014. "Infectious diseases and economic growth." Journal of Mathematical Economics, 50: 34–53.

Goenka, Aditya, Lin Liu, and Manh-Hung Nguyen. 2021. "SIR economic epidemiological models with disease induced mortality." Journal of Mathematical Economics, 93: 102476.

Goenka, Aditya, Lin Liu, and Manh-Hung Nguyen. 2022. "Modelling optimal lockdowns with waning immunity." Economic theory, 1–38.

Görtz, Christoph, Danny McGowan, and Mallory Yeromonahos. 2021. "Furlough and Household Financial Distress during the COVID-19 Pandemic." Oxford Bulletin of Economics and Statistics.

Gottlieb, Charles, Jan Grobovšek, Markus Poschke, and Fernando Saltiel. 2021. "Working from home in developing countries." European Economic Review, 133: 103679.

Hakki, Seran, Jie Zhou, Jakob Jonnerby, Anika Singanayagam, Jack L Barnett, Kieran J Madon, Aleksandra Koycheva, Christine Kelly, Hamish Houston, Sean Nevin, et al. 2022. "Onset and window of SARS-CoV-2 infectiousness and temporal correlation with symptom onset: a prospective, longitudinal, community cohort study." The Lancet Respiratory Medicine, 10(11): 1061–1073.

Hale, Thomas, Samuel Webster, Anna Petherick, Toby Phillips, and B Kira. 2022. "Oxford COVID-19 government response tracker (OxCGRT)." Last updated, 8: 30.

Hall, Robert E, and Charles I Jones. 2007. "The value of life and the rise in health spending." The Quarterly Journal of Economics, 122(1): 39–72.

Hensvik, Lena, Thomas Le Barbanchon, and Roland Rathelot. 2020. "Which jobs are done from home? Evidence from the American Time Use Survey."

Hethcote, Herbert W. 2000. "The mathematics of infectious diseases." SIAM review, 42(4): 599–653.

Huang, Minyi, Roland P Malhamé, and Peter E Caines. 2006. "Large population stochastic dynamic games: closed-loop McKean-Vlasov systems and the Nash certainty equivalence principle."

Kaplan, Greg, Benjamin Moll, and Giovanni L Violante. 2020. "The great lockdown and the big stimulus: Tracing the pandemic possibility frontier for the US." National Bureau of Economic Research.

Krueger, Dirk, Kurt Mitman, and Fabrizio Perri. 2016. "Macroeconomics and household heterogeneity." In Handbook of macroeconomics. Vol. 2, 843–921. Elsevier.

Krusell, Per, and Anthony A Smith, Jr. 1998. "Income and wealth heterogeneity in the macroeconomy." Journal of political Economy, 106(5): 867–896.

Laibson, David, Peter Maxted, and Benjamin Moll. 2022. "A simple mapping from mpcs to mpxs." National Bureau of Economic Research.

Lasry, Jean-Michel, and Pierre-Louis Lions. 2007. "Mean field games." Japanese journal of mathematics, 2(1): 229–260.

Lauriere, Mathieu. 2021. "Numerical methods for mean field games and mean field type control." Mean field games, 78: 221.

Lechien, Jerome R, Carlos M Chiesa-Estomba, Sammy Place, Yves Van Laethem, Pierre Cabaraux, Quentin Mat, Kathy Huet, Jan Plzak, Mihaela Horoi, Stéphane Hans, et al. 2020. "Clinical and epidemiological characteristics of 1420 European patients with mild-to-moderate coronavirus disease 2019." Journal of internal medicine, 288(3): 335–344.

Lekfuangfu, Warn N, Suphanit Piyapromdee, Ponpoje Porapakkarm, and Nada Wasi. 2020. "On Covid-19: New implications of job task requirements and spouse's occupational sorting1." Covid Economics, 87.

Lewandowski, Piotr, Katarzyna Lipowska, and Iga Magda. 2021. "The gender dimension of occupational exposure to contagion in Europe." Feminist Economics, 27(1-2): 48–65.

Liu, Ying, and Joacim Rocklöv. 2022. "The effective reproductive number of the Omicron variant of SARS-CoV-2 is several times relative to Delta." Journal of Travel Medicine, 29(3): taac037.

Mongey, Simon, Laura Pilossoph, and Alexander Weinberg. 2021. "Which workers bear the burden of social distancing?" The Journal of Economic Inequality, 19: 509–526.

Moscone, Francesco, and Elisa Tosetti. 2010. "Health expenditure and income in the United States." Health economics, 19(12): 1385–1403.

ONS. 2020. "Deaths involving COVID-19 by local area and socioeconomic deprivation: deaths occurring between 1 March and 31 July 2020."

ONS. 2022a. "Coronavirus (COVID-19) Infection Survey UK funded academic projects, summary results: 2022."

ONS. 2022b. "Labour costs and labour income, UK: 2022."

ONS. 2023a. "Coronavirus (COVID-19) latest insights."

ONS. 2023b. "More information on data sources related to coronavirus (COVID-19)."

Ozkan, Serdar. 2014. "Preventive vs. curative medicine: A macroeconomic analysis of health care over the life cycle." Unpublished. https://sites. google. com/site/serdarozkan/Ozkan_2014. pdf.

Papageorge, Nicholas W, Matthew V Zahn, Michèle Belot, Eline Van den Broek-Altenburg, Syngjoo Choi, Julian C Jamison, and Egon Tripodi. 2021. "Socio-demographic factors associated with self-protecting behavior during the Covid-19 pandemic." Journal of population economics, 34: 691–738.

PHE. 2020. "Disparities in the risk and outcomes of COVID-19 Public Health England."

Safan, Muntaser, Mirjam Kretzschmar, and Karl P Hadeler. 2013. "Vaccination based control of infections in SIRS models with reinfection: special reference to pertussis." Journal of mathematical biology, 67: 1083–1110.

Stachurski, John, and Alexis Akira Toda. 2019. "An impossibility theorem for wealth in heterogeneous-agent models with limited heterogeneity." Journal of Economic Theory, 182: 1–24.

Stantcheva, Stefanie. 2022. "Inequalities in the Times of a Pandemic." Economic Policy, 37(109): 5–41.

Sun, Chengjun, and Wei Yang. 2010. "Global results for an SIRS model with vaccination and isolation." Nonlinear Analysis: Real World Applications, 11(5): 4223–4237.

UK Health Security Agency. 2023. "COVID-19 Omicron variant infectious period and transmission from people with asymptomatic compared with symptomatic infection: a rapid review."

Weill, Joakim A, Matthieu Stigler, Olivier Deschenes, and Michael R Springborn. 2020. "Social distancing responses to COVID-19 emergency declarations strongly differentiated by income." Proceedings of the national academy of sciences, 117(33): 19658–19660.

Yan, Youpei, Amyn A Malik, Jude Bayham, Eli P Fenichel, Chandra Couzens, and Saad B Omer. 2021. "Measuring voluntary and policy-induced social distancing behavior during the COVID-19 pandemic." Proceedings of the National Academy of Sciences, 118(16): e2008814118.

Appendices

A FIGURES

Figure A1. Gini Index from 2012 to 2022

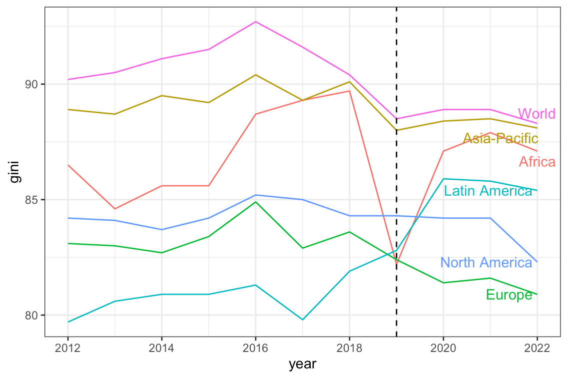

Figure A2. Lorenz Curve

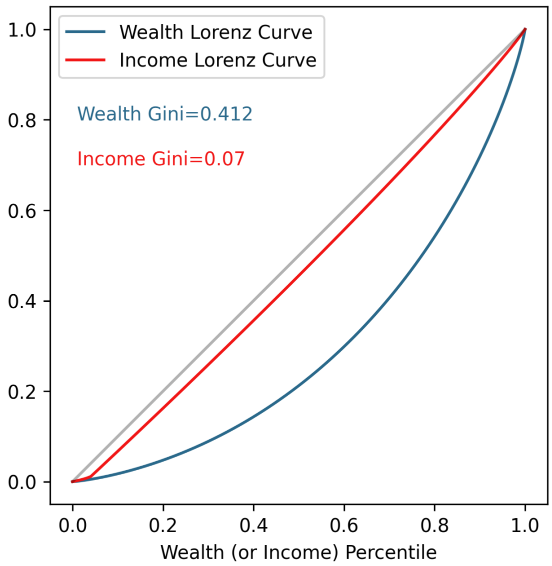

Figure A3. Labour Income Share

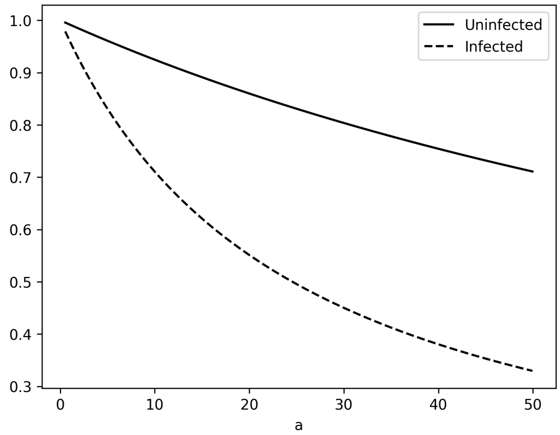

Figure A4. Health Expenditure Elasticity of Income ($\chi = 0$)

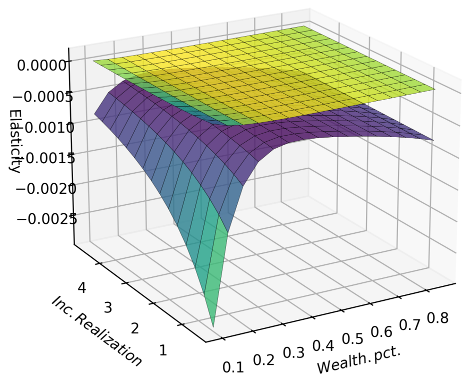

Figure A5. Multiple Waves of Infection

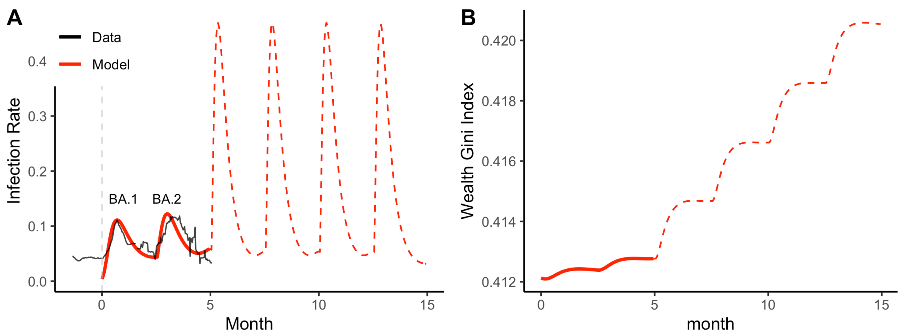

Figure A6. Other Income Support

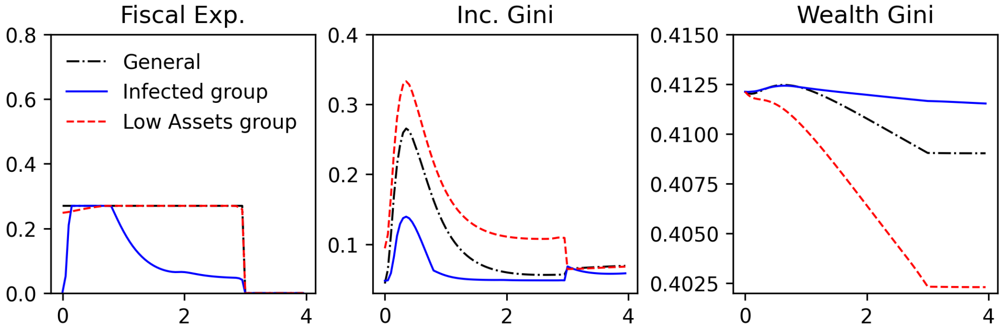

Figure A7. Transitional Dynamics — Lower Productivity Loss

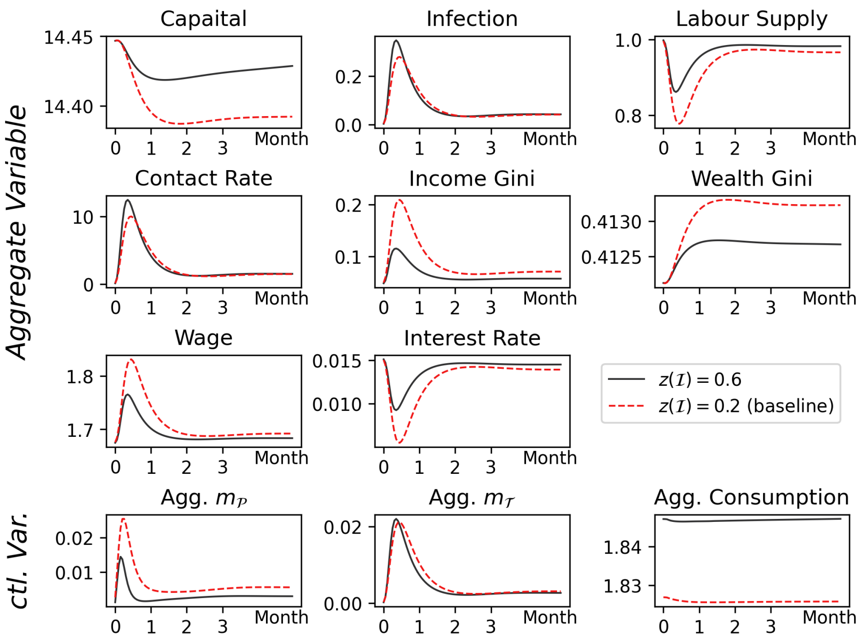

Figure A8. Transitional Dynamics — Long Covid

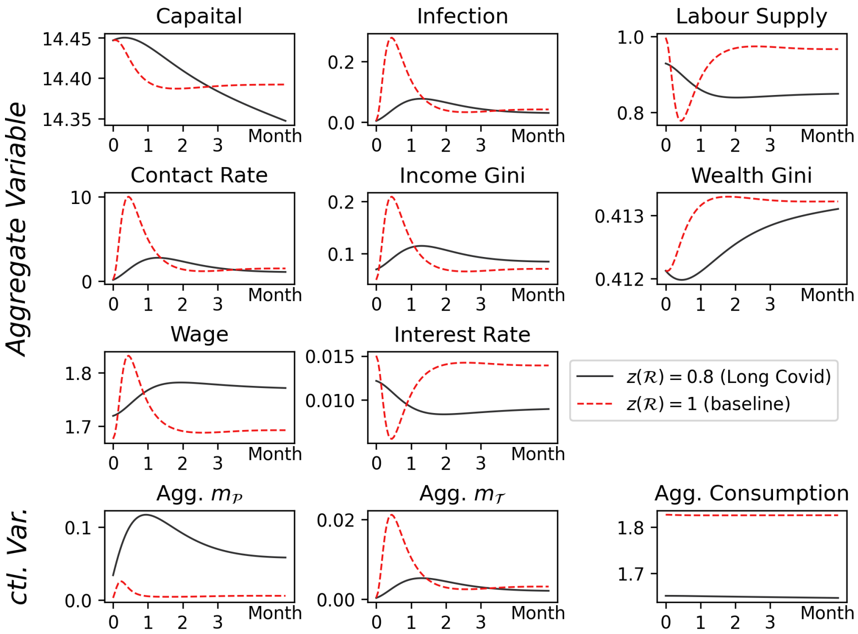

Figure A9. MIT Shock

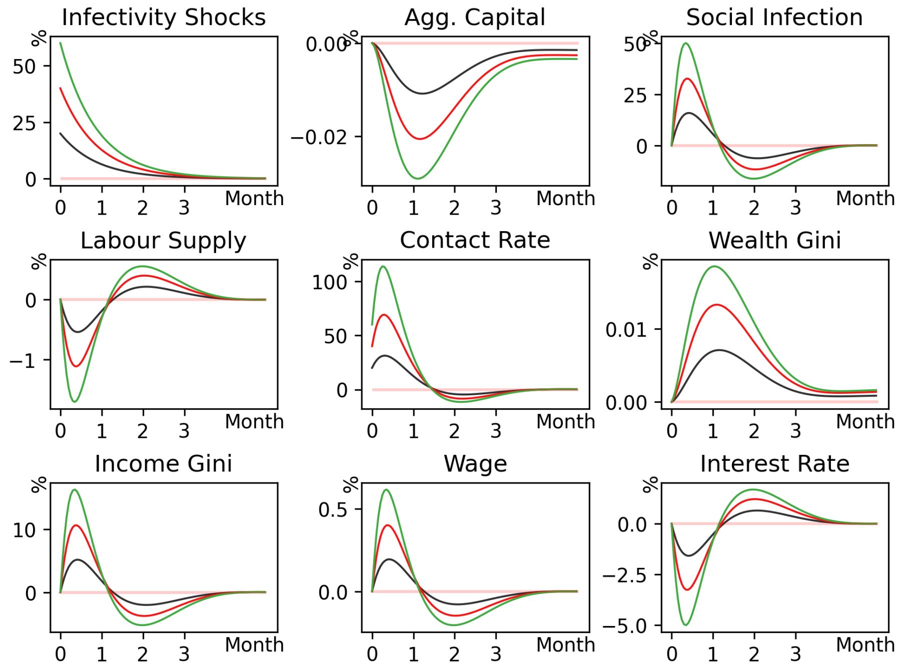

B Table

Table B1. Change of Wealth Gini Index

	gini2016	gini2019	gini2020	gini2022	gini2020	gini2022
(Intercept)	35.5***	7.16	19.2***	22.2***	23.5***	30.8***
	(3.73)	(5.01)	(2.80)	(2.91)	(2.79)	(2.84)
gini2012	0.610***					
	(0.050)					
gini2016		0.849***				
		(0.062)				
gini2019			0.769***	0.730***	0.737***	0.651***
			(0.037)	(0.038)	(0.035)	(0.035)
GovSupp					-2.70***	-4.12***
					(0.546)	(0.580)
Observations	148	158	157	153	148	143
R^2	0.505	0.548	0.738	0.707	0.780	0.789

Table B2. Comparative Study (changing ϵ_0)

(a) Aggregate Variables

ϵ_0	0.162	0.216	0.252
Infection Rate			
Aggregate	3.998	4.253	4.343
Bottom 25%	4.128	4.378	4.467
Top 25%	3.909	4.177	4.274
diff.	-0.219	-0.201	-0.193
Capital	14.459	14.429	14.419
Prices			
Wage Rate	1.694	1.694	1.694
Interest Rate	0.014	0.014	0.014
Inequality			
Wealth Gini	0.413	0.411	0.41
Income Gini	0.07	0.071	0.072
Wealth Share			
Bottom 25%	6.64	6.72	6.75
Top 25%	53.09	52.94	52.87
diff	46.46	46.22	46.12

(b) Contol Variables

ϵ_0	0.162	0.216	0.252
Consumption			
Aggregate	1.83	1.828	1.828
Bottom 25%	1.681	1.681	1.68
Top 25%	2.054	2.051	2.05
diff.	0.372	0.37	0.37
Preventive Exp.			
Aggregate	0.051	0.053	0.053
Bottom 25%	0.047	0.049	0.05
Top 25%	0.056	0.058	0.059
diff.	0.009	0.009	0.009
Treatment Exp.			
Aggregate	0.075	0.075	0.075
Bottom 25%	0.072	0.072	0.072
Top 25%	0.079	0.079	0.079
diff.	0.007	0.007	0.007

Table B4. Comparative Study (changing ϵ_0 cont.)

ϵ_0	0.162	0.216	0.252
Expected Income in 3-yr duration			
Bottom 25%	20.547	20.512	20.5
Top 25%	25.099	25.03	25.003
diff.	4.553	4.518	4.504
Labour Income diff.	0.015	0.01	0.009
Capital Income diff.	4.502	4.469	4.456
Expected Savings in 3-yr duration			
Bottom 25%	2.616	2.816	2.887
Top 25%	-0.958	-1.036	-1.063
diff.	-3.574	-3.852	-3.95

Table B5. Comparative Study (changing ϵ_1)

(a) Aggregate Variables

ϵ_1	-1.1	-1.2	-1.3
Infection Rate			
Aggregate	4.365	4.491	4.551
Bottom 25%	4.49	4.613	4.671
Top 25%	4.295	4.431	4.497
diff.	-0.195	-0.182	-0.174
Capital	14.416	14.401	14.394
Prices			
Wage Rate	1.694	1.694	1.694
Interest Rate	0.014	0.014	0.014
Inequality			
Wealth Gini	0.41	0.409	0.408
Income Gini	0.072	0.072	0.073
Wealth Share			
Bottom 25%	6.75	6.8	6.83
Top 25%	52.92	52.81	52.73
diff	46.16	46.01	45.9

(b) Contol Variables

ϵ_1	-1.1	-1.2	-1.3
Consumption			
Aggregate	1.827	1.827	1.827
Bottom 25%	1.68	1.68	1.68
Top 25%	2.05	2.049	2.048
diff.	0.37	0.369	0.368
Preventive Exp.			
Aggregate	0.056	0.06	0.063
Bottom 25%	0.052	0.056	0.058
Top 25%	0.062	0.066	0.069
diff.	0.01	0.011	0.011
Treatment Exp.			
Aggregate	0.075	0.075	0.075
Bottom 25%	0.072	0.072	0.072
Top 25%	0.079	0.079	0.079
diff.	0.007	0.007	0.007

Table B7. Comparative Study (changing ϵ_1 cont.)

ϵ_1	-1.1	-1.2	-1.3
Expected Income in 3-yr duration			
Bottom 25%	20.496	20.479	20.472
Top 25%	25.003	24.966	24.944
diff.	4.508	4.486	4.472
Labour Income diff.	0.009	0.006	0.004
Capital Income diff.	4.459	4.44	4.426
Expected Savings in 3-yr duration			
Bottom 25%	2.914	3.013	3.056
Top 25%	-1.071	-1.108	-1.126
diff.	-3.985	-4.121	-4.182

Table B8. Comparative Study (changing η_1)

(a) Aggregate Variables

η_1	-1.1	-1.2	-1.3
Infection Rate			
Aggregate	4.086	4.069	4.057
Bottom 25%	4.211	4.193	4.179
Top 25%	4.003	3.988	3.976
diff.	-0.208	-0.205	-0.203
Capital	14.449	14.451	14.452
Prices			
Wage Rate	1.694	1.694	1.694
Interest Rate	0.014	0.014	0.014
Inequality			
Wealth Gini	0.413	0.413	0.414
Income Gini	0.07	0.07	0.07
Wealth Share			
Bottom 25%	6.65	6.63	6.61
Top 25%	53.09	53.13	53.17
diff	46.44	46.5	46.56

(b) Contol Variables

η_1	-1.1	-1.2	-1.3
Consumption			
Aggregate	1.83	1.83	1.831
Bottom 25%	1.681	1.682	1.682
Top 25%	2.054	2.055	2.055
diff.	0.372	0.373	0.373
Preventive Exp.			
Aggregate	0.051	0.051	0.051
Bottom 25%	0.048	0.047	0.047
Top 25%	0.057	0.056	0.056
diff.	0.009	0.009	0.009
Treatment Exp.			
Aggregate	0.068	0.062	0.057
Bottom 25%	0.066	0.06	0.055
Top 25%	0.072	0.065	0.06
diff.	0.006	0.005	0.005

Table B10. Comparative Study (changing η_1 cont.)

η_1	-1.1	-1.2	-1.3
Expected Income in 3-yr duration			
Bottom 25%	20.534	20.535	20.536
Top 25%	25.08	25.087	25.093
diff.	4.546	4.552	4.557
Labour Income diff.	0.013	0.013	0.013
Capital Income diff.	4.497	4.504	4.509
Expected Savings in 3-yr duration			
Bottom 25%	2.657	2.622	2.593
Top 25%	-0.974	-0.96	-0.949
diff.	-3.631	-3.582	-3.541

C R_0 in Heterogeneous Agent Model

Basic reproduction number R_0 is defined as the average number of secondary infections that occur when one infective is introduced into a completely susceptible host population. The replacement number R (Effective reproduction number) is defined to be the average number of secondary infections produced by a typical infective during the entire period of infectiousness.

In a simple epidemiological model with SIRS dynamics, the motion of infection rate can be written as

$$\begin{aligned} \dot{i} &= \alpha s i - \gamma i \\ &= \gamma i\left(\frac{\alpha s}{\gamma} - 1\right) \end{aligned} \tag{25}$$

where α and γ is the contact and recovery rate. This sign of this expression is governed by $\frac{\alpha s}{\gamma} - 1$. Therefore, the varying ratio $\frac{\alpha s_t}{\gamma}$ is the effective reproduction number R. If R is positive, $\dot{i} > 0$ that infection rate increases. Given a complete host population with $s_0 = 1$, the basic reproduction number is

$$R_0 = \frac{\alpha s_0}{\gamma} = \frac{\alpha}{\gamma} \tag{26}$$

Morover, we have the proposition that $R_t = R_0 s_t$

The key difference of solving R_0 in our heterogeneous agent framework is the difficulty that contact rate and recovery rate are endogenized by health expenditure. α, γ vary across the wealth distribution. However, We can find R_0 in a similar way using Kolmogorov Forward Equation. Analogue to Equation 25, the net flow of infectious group in our model is

$$\begin{aligned} \dot{i} &= \int \alpha(m_{\mathcal{P}})\zeta g(a,\mathcal{S})da - \int \gamma(m_{\mathcal{T}})g(a,\mathcal{I})da \\ &= \int \gamma(m_{\mathcal{T}})g(a,\mathcal{I})da \left(\frac{\int \alpha(m_{\mathcal{P}})\zeta g(a,\mathcal{S})da}{\int \gamma(m_{\mathcal{T}})g(a,\mathcal{I})da} - 1\right) \end{aligned} \tag{27}$$

We can similarly define the effective reproduction number and basic reproduction number as

$$\begin{aligned} R_t &= \frac{\int \alpha(m_{\mathcal{P}})\zeta g(a,\mathcal{S})da}{\int \gamma(m_{\mathcal{T}})g(a,\mathcal{I})da} \\ R_0 &= \frac{R_t}{s_t} = \frac{\int \alpha(m_{\mathcal{P}})\zeta g(a,\mathcal{S})da}{\int \gamma(m_{\mathcal{T}})g(a,\mathcal{I})da \int \mathbb{1}(h=\mathcal{S})g(a,h)d\mu} \end{aligned} \tag{28}$$

D Finite Differencing Method

To solve the following HJB-KF system
(Optimal HJB)

$$\begin{aligned}\rho v(a,h) = u(c^*) + \partial_a v(a,h)[wz^h(h) + ra - c^* - m^*_{\mathcal{P}} - m^*_{\mathcal{T}}] \\ + \Lambda^{h'}(m^*_{\mathcal{S}}, m^*_{\mathcal{I}}, h)[v(a,h') - v(a,h)] + \partial_t v(a,h)\end{aligned} \tag{29}$$

where

$$c^* = u'^{-1}(\partial_a v(a,h)) \tag{30}$$

$$m^*_{\mathcal{P}} = \begin{cases} 0; \quad h = \{\mathcal{I}, \mathcal{R}\} \\ \alpha'^{-1}\left(\frac{\partial_a v(a,\mathcal{S})}{\zeta[v(a,\mathcal{I}) - v(a,\mathcal{S})]}\right); \quad h = \mathcal{S}\end{cases} \tag{31}$$

$$m^*_{\mathcal{T}} = \begin{cases} 0; \quad h = \{\mathcal{S}, \mathcal{R}\} \\ \gamma'^{-1}\left(\frac{\partial_a v(a,\mathcal{I})}{v(a,\mathcal{R}) - v(a,\mathcal{I})}\right); \quad h = \mathcal{I}\end{cases} \tag{32}$$

(KF)

$$\begin{aligned}\frac{\partial g(a,h)}{\partial t} = & -\frac{\partial}{\partial a}[s(a,h)g(a,h)] \\ & - \Lambda^{h'}(m^*, h)g(a,h) + \Lambda^h(m^*, h')g(a,h')\end{aligned} \tag{33}$$

(Assets Market Clearing)

$$K = \int a g(a,h) d\mu \tag{34}$$

(Labour Market Clearing)

$$L = \int z(h) g(a,h) d\mu \tag{35}$$

(Rational Expectation)

$$\zeta = \int \alpha(m^*_{\mathcal{P}}) \mathbb{1}(h = \mathcal{I}) g(a,h) d\mu \tag{36}$$

We discretize the state space (a,h) into $na \times 3$ grids, indexed by i, j. Then, we can express the partial differentiation $\partial_a v(a,h)$ by the forward and backward difference as follow

$$\partial_a^F v = \frac{v_{i+1,j} - v_{i,j}}{da}$$
$$\partial_a^B v = \frac{v_{i,j} - v_{i-1,j}}{da} \tag{37}$$

Then, we can obtain the corresponding optimal policies using forward or backward difference by Equation 30 to Equation 32, listed $c_{i,j}^{*F}, c_{i,j}^{*B}, m_{\mathcal{S}i,j}^{*F}, m_{\mathcal{S}i,j}^{*B}, m_{\mathcal{I}i,j}^{*F}, m_{\mathcal{I}i,j}^{*B}$. Let the motion of asset (savings) using forward and backward difference to be $s_{i,j}^F$ and $s_{i,j}^B$ that

$$s_{i,j}^F = wz_{i,j} + ra_{i,j} - c_{i,j}^{*F} - m_{\mathcal{P}i,j}^{*F} - m_{\mathcal{T}i,j}^{*F}$$
$$s_{i,j}^B = wz_{i,j} + ra_{i,j} - c_{i,j}^{*B} - m_{\mathcal{P}i,j}^{*B} - m_{\mathcal{T}i,j}^{*B} \tag{38}$$

The Finite Differencing Method uses the forward difference if $s_{i,j}^F > 0$, backward difference if $s_{i,j}^B < 0$. By this principal, the Equation 29 could be rewritten as

$$\begin{aligned}
\rho v_{i,j} &= u(\tilde{c}_{i,j}) + \partial_a^F v_{i,j} s_{i,j}^+ + \partial_a^B v_{i,j} s_{i,j}^- + \tilde{\Lambda}_{i,j}[v_{i,j'} - v_{i,j}] + \partial_t v_{i,j} \\
&= u(\tilde{c}_{i,j}) + (\frac{v_{i+1,j} - v_{i,j}}{da}) s_{i,j}^+ + (\frac{v_{i,j} - v_{i-1,j}}{da}) s_{i,j}^- + \tilde{\Lambda}_{i,j}[v_{i,j'} - v_{i,j}] + \partial_t v_{i,j} \\
&= u(\tilde{c}_{i,j}) + \left(\frac{s_{i,j}^+}{da}\right) v_{i+1,j} + \left(\frac{s_{i,j}^- - s_{i,j}^+}{da}\right) v_{i,j} - \left(\frac{s_{i,j}^-}{da}\right) v_{i-1,j} + \tilde{\Lambda}_{i,j}[v_{i,j'} - v_{i,j}] + \partial_t v_{i,j}
\end{aligned} \tag{39}$$

where $s_{i,j}^+ \equiv s_{i,j}^F \mathbb{1}(s_{i,j}^F > 0)$, $s_{i,j}^- \equiv s_{i,j}^B \mathbb{1}(s_{i,j}^B < 0)$. $\tilde{c}_{i,j}$ is the optimal consumption under FDM scheme, that $\tilde{c}_{i,j} \equiv c_{i,j}^{*F} \mathbb{1}(s_{i,j}^F > 0) + c_{i,j}^{*B} \mathbb{1}(s_{i,j}^B < 0)$. $\tilde{\Lambda}_{i,j}$ is the transition probability under optimal health expenditure defined in the similar way. Let $\tilde{m}_{\mathcal{S}i,j} \equiv m_{\mathcal{S}i,j} \mathbb{1}(s_{i,j}^F > 0) + m_{\mathcal{S}i,j} \mathbb{1}(s_{i,j}^B < 0)$ and $\tilde{m}_{\mathcal{I}i,j} \equiv m_{\mathcal{I}i,j} \mathbb{1}(s_{i,j}^F > 0) + m_{\mathcal{I}i,j} \mathbb{1}(s_{i,j}^B < 0)$, $\tilde{\Lambda}_{i,j}$ could be expressed as.

$$\begin{aligned}
\tilde{\Lambda}_{i,1} &= \alpha(\tilde{m}_{\mathcal{P}i,1})\zeta \quad \text{Infection Probability} \\
\tilde{\Lambda}_{i,2} &= \gamma(\tilde{m}_{\mathcal{T}i,2}) \quad \text{Recovery Probability} \\
\tilde{\Lambda}_{i,3} &= \psi \quad \text{Reinfection Probability}
\end{aligned} \tag{40}$$

Boundary Conditoins. Our model assumes wealth $a \in [\underline{a}, \bar{a}]$. In the boundaries of the distribution, wealth cannot go further down or up. Hence, the savings must be non-negative at the lower bound; non-positive at the upper bound. Hence, if we have $s_{na,j}^F > 0$ with $a_{na} = \bar{a}$ or $s_{1,j}^B < 0$ with $a_1 = \underline{a}$, we need to activate the boundary conditions.

We use the lower bound as an example. We make use of the F.O.C. and the boundary condition $s_{1,j}^B = 0$. We can write

$$\begin{cases} wz(\mathcal{S}) + r\underline{a} - c_{1,1}^{*B} - m_{\mathcal{S}_{1,1}}^{*B} = 0 \\ wz(\mathcal{I}) + r\underline{a} - c_{1,2}^{*B} - m_{\mathcal{I}_{1,2}}^{*B} = 0 \\ wz(\mathcal{R}) + r\underline{a} - c_{1,3}^{*B} = 0 \end{cases} \tag{41}$$

that is

$$\begin{cases} wz(\mathcal{S}) + r\underline{a} - u'^{-1}(\partial_a^B v_{1,1}) - \alpha'^{-1}\left(\frac{\partial_a v_{1,1}}{\zeta[v_{1,2}-v_{1,1}]}\right) = 0 \\ wz(\mathcal{I}) + r\underline{a} - u'^{-1}(\partial_a^B v_{1,2}) - \gamma'^{-1}\left(\frac{\partial_a v_{1,2}}{v_{1,1}-v_{1,2}}\right) = 0 \\ wz(\mathcal{R}) + r\underline{a} - u'^{-1}(\partial_a^B v_{1,3}) = 0 \end{cases} \tag{42}$$

where we make use of the F.O.C. Equation 31 and Equation 32. Equation 42 are equations for $\partial_a^B v(a,h)$. We can thus solve out backward differentiation at the lower bound of a. Finally, we use these solutions and F.O.C.s to update the value of choice variables and savings at the boundary. Similar strategy could be applied to the upper bound.

Matrix Notation for HJB. We could further express Equation 39 as

$$\begin{aligned} \rho v_{i,1} &= u(\tilde{c}_{i,1}) + \left(\frac{s_{i,1}^+}{da}\right) v_{i+1,1} + \left(\frac{s_{i,1}^- - s_{i,1}^+}{da}\right) v_{i,1} - \left(\frac{s_{i,j}^-}{da}\right) v_{i-1,1} + \tilde{\Lambda}_{i,1}[v_{i,2} - v_{i,1}] + \partial_t v_{i,1} \\ \rho v_{i,2} &= u(\tilde{c}_{i,2}) + \left(\frac{s_{i,2}^+}{da}\right) v_{i+1,2} + \left(\frac{s_{i,2}^- - s_{i,2}^+}{da}\right) v_{i,2} - \left(\frac{s_{i,2}^-}{da}\right) v_{i-1,2} + \tilde{\Lambda}_{i,2}[v_{i,3} - v_{i,2}] + \partial_t v_{i,2} \\ \rho v_{i,3} &= u(\tilde{c}_{i,3}) + \left(\frac{s_{i,3}^+}{da}\right) v_{i+1,3} + \left(\frac{s_{i,3}^- - s_{i,3}^+}{da}\right) v_{i,3} - \left(\frac{s_{i,3}^-}{da}\right) v_{i-1,3} + \tilde{\Lambda}_{i,3}[v_{i,1} - v_{i,3}] + \partial_t v_{i,3} \end{aligned} \tag{43}$$

Next, we stack $v_{i,1}, v_{i,2}, v_{i,3}, i = 1, 2, \ldots na$ into one long vector

$$\mathbf{V} = \begin{bmatrix} v_{1,1} \\ v_{2,1} \\ \cdots \\ v_{na,1} \\ v_{1,2} \\ v_{2,2} \\ \cdots \\ v_{na,2} \\ \cdots \\ v_{na,3} \end{bmatrix} \tag{44}$$

Then, Equation 43 could be written into matrix form as

$$\rho \mathbf{V} = \mathbf{u} + \mathbf{A}\mathbf{V} + \mathbf{B}\mathbf{V} + \partial_t \mathbf{V} \tag{45}$$

$$\mathbf{A} \equiv \begin{bmatrix} \frac{s^-_{1,1}-s^+_{1,1}}{da} & \frac{s^+_{1,1}}{da} & 0 & 0 & \cdots & 0 \\ -\frac{s^-_{2,1}}{da} & \frac{s^-_{2,1}-s^+_{2,1}}{da} & \frac{s^+_{2,1}}{da} & 0 & \cdots & 0 \\ 0 & -\frac{s^-_{3,1}}{da} & \frac{s^-_{3,1}-s^+_{3,1}}{da} & \frac{s^+_{3,1}}{da} & \cdots & 0 \\ 0 & 0 & -\frac{s^-_{4,1}}{da} & \frac{s^-_{4,1}-s^+_{4,1}}{da} & \cdots & 0 \\ \cdots & \cdots & \cdots & \cdots & \cdots & \cdots \\ 0 & 0 & 0 & 0 & 0 & \frac{s^-_{na,3}-s^+_{na,3}}{da} \end{bmatrix} \tag{46}$$

$$\mathbf{B} = \begin{bmatrix} -\mathbf{L}_1 & \mathbf{L}_1 & \mathbf{0} \\ \mathbf{0} & -\mathbf{L}_2 & \mathbf{L}_2 \\ \mathbf{L}_3 & \mathbf{0} & -\mathbf{L}_3 \end{bmatrix} \tag{47}$$

where

$$\begin{aligned} \mathbf{L}_1 &= Diag(\Lambda_{1,1}, \Lambda_{2,1}, \ldots \Lambda_{na,1})_{na \times na} \\ \mathbf{L}_2 &= Diag(\Lambda_{1,2}, \Lambda_{2,2}, \ldots \Lambda_{na,2})_{na \times na} \\ \mathbf{L}_3 &= Diag(\Lambda_{1,3}, \Lambda_{2,3}, \ldots \Lambda_{na,3})_{na \times na} \end{aligned} \tag{48}$$

Thus, define $\mathcal{A} = \mathbf{A} + \mathbf{B}$, the HJB equation could be written as

$$\rho \mathbf{V} = \mathbf{u} + \mathcal{A}\mathbf{V} + \partial_t \mathbf{V} \tag{49}$$

Expressing $\partial_t \mathbf{V} = \frac{V_{t+1}-V_t}{\Delta}$ and using the implicit update method, we can have

$$\begin{aligned} \frac{\mathbf{V}_{t+1} - \mathbf{V}_t}{\Delta} + \rho \mathbf{V}_{t+1} &= \mathbf{u} + \mathcal{A}\mathbf{V}_{t+1} \\ \left((\rho + \frac{1}{\Delta})I - \mathcal{A} \right) \mathbf{V}_{t+1} &= \mathbf{u} + \frac{\mathbf{V}_t}{\Delta} \\ \mathbf{V}_{t+1} &= \left((\rho + \frac{1}{\Delta})I - \mathcal{A} \right)^{-1} \frac{\mathbf{V}_t}{\Delta} \end{aligned} \tag{50}$$

The Kolmogorov Forward Equation Equation 33 can be then expressed asset

$$\dot{\mathbf{g}}_t = \mathcal{A}^* \mathbf{g}_t \tag{51}$$

where $\mathcal{A}^*$ is the adjoint matrix for $\mathcal{A}$ defined before.

E Stationary Equilibrium and Transitional Dynamics

A. Stationary Equilibrium

Solving the Stationary Equilibrium

In the stationary equilibrium, we have the joint distribution $g(a, h)$ and value function $v(a, h)$ being unchanged over time. That is $\dot{\mathbf{g}}_t = 0$ and $\dot{\mathbf{V}}_t = 0$

Thus, given any initial value function $\mathbf{V}^0$ and price (w, r) [40], we can iterate Equation 50 until $abs(\mathbf{V}_{t+1} - \mathbf{V}_t)$ is sufficiently small. The corresponding value function $\mathbf{V}^*$ would be value function at the stationary equilibrium. Then, we can solve out the corresponding stationary distribution $\mathbf{g}$ by $0 = \mathcal{A}^*\mathbf{g}$.

Next, we calculate the aggregate supply by

$$\begin{aligned} K_S &= \int a g^*(a, h) d\mu \\ i_S &= \int \mathbb{1}(h = \mathcal{I}) g^*(a, h) d\mu \\ \zeta_S &= \int \alpha(m^*_{\mathcal{P}}) \mathbb{1}(h = \mathcal{I}) g^*(a, h) d\mu \end{aligned} \tag{52}$$

We update the aggregate demand and repeat the steps until the aggregate supply and aggregate demand are sufficiently close. The following bullet points summarize the Algorithm

- (i) Given (K_D, i_D, ζ_D), calculate (r, w)
- (ii) Loop the HJB Equation 50 to find $\mathcal{A}$ and $\mathbf{V}^*$
- (iii) Solve out the corresponding stationary equilibrium by $0 = \mathcal{A}^*\mathbf{g}$
- (iv) Use $\mathbf{g}$ to calculate aggregate supply using Equation 52
- Repeat step (i) to (iv) until the gap between aggregate supply and aggregate demand is sufficient small

Income Elasticity of Health Expenditure

The Income Elasticity of Health Expenditure is defined as follow

$$\begin{aligned} \varepsilon_{M_h, y} &= \frac{\partial M_h(a_0, h_0)}{\partial y} \frac{y}{M_h} \\ &= \frac{M_h(a_0 + \Delta, h_0) - M_h(a_0, h_0)}{\Delta} \frac{a_0}{M_h(a_0, h_0)} \\ h &= \{\mathcal{P}, \mathcal{T}\} \end{aligned} \tag{53}$$

[40] The price determined by the aggregate supply (K_D, L_D, ζ_D)

where

$$
\begin{aligned}
M_{\mathcal{P}}(a_0,h_0) &= \mathbb{E}\left[\int_0^{\tau} m_{\mathcal{P}}(a_t,h_t)dt \middle| a_0,h_0\right] \\
M_{\mathcal{T}}(a_0,h_0) &= \mathbb{E}\left[\int_0^{\tau} m_{\mathcal{T}}(a_t,h_t)dt \middle| a_0,h_0\right]
\end{aligned} \tag{54}
$$

To solve the cumulative health expenditure over the period of τ, we apply the Feynman-Kac Formula

Lemma (Feynman-Kac Formula): *Define a time varying function $\Gamma(a,h,t)$ satisfying PDE*

$$
0 = m_{\mathcal{P}}(a,h) + \partial_a\Gamma(a,h,t)\dot{a}(a,h) + \Lambda^{h'}(h)[\Gamma(a,h',t) - \Gamma(a,h,t)] + \partial_t\Gamma(a,h,t) \tag{55}
$$

with terminal condition $\Gamma(a,h,\tau) = 0$, where $h = \{\mathcal{S},\mathcal{I},\mathcal{R}\}$. Then, $M_{\mathcal{P}}(a_0,h_0) = \Gamma(a,h,0)$.
Similarly, $M_{\mathcal{T}}(a_0,h_0)$ can be computed as $\Gamma(a,h,0)$, where $\Gamma(a,h,t)$ satisfies

$$
0 = m_{\mathcal{T}}(a,h) + \partial_a\Gamma(a,h,t)\dot{a}(a,h) + \Lambda^{h'}(h)[\Gamma(a,h',t) - \Gamma(a,h,t)] + \partial_t\Gamma(a,h,t) \tag{56}
$$

Corollary: *The second part of Feynman-Kac Formula is exactly $\mathcal{A}$ matrix in the FDM algorithm. Thus, the PDE could be written as*

$$
0 = x(a,h) + \mathcal{A}\Gamma(a,h,t) + \partial_t\Gamma(a,h,t) \tag{57}
$$

where $x(a,h) = \{c(a,h), ra + wz^h(h)\}$

Computation: We know the terminal condition $\Gamma(a,h,\tau) = 0$, we can solve $\Gamma(a,h,t)$ backward recursively and obtain $\Gamma(a,h,0)$ by

$$
\begin{aligned}
0 &= x(a,h) + \mathcal{A}\Gamma(a,h,t-1) + \frac{\Gamma(a,h,t) - \Gamma(a,h,t-1)}{\Delta t} \\
\left(\frac{1}{\Delta t}I - \mathcal{A}\right)\Gamma(a,h,t-1) &= x(a,h) + \frac{\Gamma(a,h,t)}{\Delta t}
\end{aligned} \tag{58}
$$

B. Transitional Dynamics

We now simulate the transitional dynamics given initial distribution $g_0(a,h)$ and terminal value function $v_T(a,h)$. Assume an initial path of aggregate demand $\{K_t^D\}, \{i_t^D\}, \{\zeta_t^D\}$, where $t = \{0,1,...N\}$ with time interval dt. Using the paths of aggregate variables, we can compute the paths for price $\{w_t\}$ and $\{r_t\}$.

Then, we can solve the HJB backward by

$$\rho \mathbf{V}_t = u(\mathbf{V}_{t+1}) + \mathcal{A}(\mathbf{V}_{t+1}; r_t, w_t, \zeta_t)\mathbf{V}_t + \frac{\mathbf{V}_{t+1} - \mathbf{V}_t}{dt} \tag{59}$$

where we could obtain $\{\mathbf{V}_t\}$. Then, we can solve KF forward by

$$\frac{\mathbf{g}_{t+1} - \mathbf{g}_t}{dt} = \mathcal{A}^*(\mathbf{V}_t; r_t, w_t, \zeta_t)\mathbf{g}_{t+1} \tag{60}$$

to obtain $\{\mathbf{g}_t\}$. Using the sequence of distribution, we can solve out sequence of aggregate supply $\{K_t^S\}, \{i_t^S\}, \{\zeta_t^S\}$. Finally, we repeat the steps above until the aggregate supply sequence and aggregate demand sequence are sufficiently close to each other. The following bullet points summarize the Algorithm for transitional dynamics

- (i) Given sequence of demand $(\{K_t^D\}, \{i_t^D\}, \{\zeta_t^D\})$, calculate sequence $(\{r_t\}, \{w_t\})$
- (ii) Solve HJB backward from stationary equilibrium $\mathbf{V}^*$ by Equation 59 to find sequence $\{\mathbf{V}_t\}$
- (iii) Solve KF forward from the initial distribution $\{\mathbf{g}_0\}$ by Equation 60 and obtain distribution sequence $\{\mathbf{g}_t\}$
- (iv) Use sequence $\{\mathbf{g}_t\}$ to calculate sequences for aggregate supply $(\{K_t^S\}, \{i_t^S\}, \{\zeta_t^S\})$
- Repeat step (i) to (iv) until the gap between aggregate supply and aggregate demand is sufficient small

For the MIT shock, we can also solve the transitional dynamics using the algorithm above. In the case of MIT shock, the terminal equilibrium is identical to the equilibrium before the shock arrives. Hence, we can just use $v^*(a, h)$ as the terminal value function and $g^*(a, h)$ as the initial distribution.